

“Capillary Suspensions with Polymeric Bridges”

zur Erlangung des akademischen Grades einer
DOKTORIN DER INGENIEURWISSENSCHAFTEN (DR.-ING.)

von der KIT-Fakultät für Chemieingenieurwesen und Verfahrenstechnik des
Karlsruher Instituts für Technologie (KIT)
genehmigte

DISSERTATION

von

M. Sc. Katharina Hauf-Hartung
aus Georgiewsk (Russland)

Erstgutachterin: Prof. Dr. Erin Koos

Zweitgutachter: Prof. Dr.-Ing. Matthias Kind

Tag der mündlichen Prüfung: 17. September 2019

Preface

The present dissertation is based on three peer-reviewed articles published in scientific journals and one additional chapter, written in the form of a paper to be submitted. They compose in a multi-scale research of porous polymeric composite materials made from capillary suspensions, which was investigated at the Karlsruhe Institute of Technology (KIT), Institute of Mechanical Process Engineering and Mechanics in the group of Applied Mechanics between June 2015 and December 2018.

After a general introduction into the state of the art in capillary suspensions and their applications fields, this dissertation comprises the following adapted publications:

1. Structure of capillary suspensions and their versatile applications in the creation of smart materials (MRS Communications, 8(2): 332-342 (2018))
2. Radical polymerization of capillary bridges between micron-sized particles in liquid bulk phase as a low-temperature route to produce porous solid materials (Colloid & Polymer Science, 10: 1773-1785 (2017))
3. Lightweight porous glass composite materials based on capillary suspensions (MDPI Materials, 12, 619: 1-14 (2019))

The thesis concludes with a summary and an outlook as well as a bibliography.

Acknowledgements

I would like to take the opportunity to thank all people who contributed to my dissertation by providing experimental help, fruitful and creative discussions or general support in all cases during my time at the Karlsruhe Institute of Technology.

First of all I would like to thank Prof. Dr. Erin Koos and Prof. Dr. Norbert Willenbacher for giving me the chance to write and finish my dissertation at the Institute for Mechanical Process Engineering and Mechanics in the group of Applied Mechanics. The fruitful discussions gave me the opportunity to see things from different perspectives and outgrow myself.

Furthermore, I would like to thank Prof. Dr.-Ing. Matthias Kind for being my second referee.

I would like to thank Dr. Bernhard Hochstein for helping me on technical and overall questions as well as mental support during my time at the group of Applied Mechanics.

Special thanks to all my colleagues at the AME. It was great to work with all of you and especially thanks for the amusing lunch breaks.

It was a pleasure for me to work with my students Carolyn Benner, Philipp Quarz, Philipp Menesclou, and Moaaz Rauf Nizami, who gave their best contributions for my work.

Furthermore, I would like to thank the technical staff at the AME including Thomas Lebe, Klaus Hirsch, Astrid Huber, for help with technical analysis and Regina Mall for the pleasant cooperation in the practical course of “falling sphere viscosimeter”. Also special thanks to Volker Zibat, from the Laboratory for Electron Microscopy, for professional SEM images and fruitful discussions.

For the nice and productive collaboration in the field of polymer chemistry, I would like to thank Prof. Dr. Manfred Wilhelm from the Karlsruhe Institute of Technology (KIT), Institute for Chemical Technology and Polymer Chemistry, group for Polymeric Materials and his staff Christopher Klein, Kamran Riazi, Jonas Keller and Christoph Pfeifer.

Furthermore, great thanks to Dr. Hendrik Hölscher, Richard Thelen and Christian Lutz from the Institute of Microstructure Technology at the KIT for the great support with the AFM measurements and creative discussions. It was a pleasure to work with you.

Last, but not least, I would like to thank my parents, Swetlana and Wladimir, as well as my wise grandparents and my husband Knud Hartung for supporting me over all the years of my studies and research.

Abstract

Porous materials are used in a wide field of applications, such as separation and filtering techniques, as well as thermal insulation materials and catalytic materials, depending on their pore size. These porous materials are additionally classified by their porosity, the ratio of the void volume to the total volume of a material. The structure of the material is also important, since it influences the mechanical properties in addition to the porosity. Porous materials can be found in natural materials, e.g. rocks or wood, or they can be produced using different artificial techniques, like foaming sacrificial templating or via particle networks. These particle network routes can be realized through some well-known states and classes, like the granular media, spherical agglomeration, Pickering emulsions and dispersions that can be created by varying the amount of the solid phase and the two liquid phases, a material class called capillary suspensions.

Capillary suspensions are three-phase systems, containing a dispersion of micron-sized solid particles in a bulk liquid and a fractional amount of second immiscible liquid phase, which modifies the rheological properties of the suspension. The changes can be identified by, e.g., a strong increase of the yield stress, which is caused by a transition from fluid-like to gel-like behavior due to structure formation within the suspension. In recent years, many different application fields for capillary suspensions, like in food technology, slurries for battery electrodes or printable electronics, crack-free films, bio-slurries for renewable energy processes and dense as well as cellular ceramics have been explored and investigated. These capillary suspensions were classified by Koos and Willenbacher (2011) in two general forms: the capillary state, where the three-phase-contact angle $\theta_{S,B}$, which the secondary phase (S) forms between the particles when surrounded by the bulk fluid (B), is higher than 90° ; and the pendular state with a three-phase contact angle lower than 90° . This small amount of secondary liquid phase is distributed as capillary bridges between the micron-sized particles, leading to a particle network stabilized via capillary attraction. This percolating network of particles and capillary bridges was directly visualized using confocal microscopy by Bossler and Koos (2016). Both the pendular and capillary states lead to a sample-spanning network, but with significant differences in the overall structure. The pendular state is characterized by individual capillary bridges between the particles (binary interactions), while the capillary state often appears in multibody particle clusters. The structure of these networks can be used to define porosity, pore size and pore structure in a resulting solidified porous material, which has been realized via sintering techniques. While there are advantages in the physical and mechanical properties of these products over traditional bulk manufacturing, the high sintering temperatures and long processing time over preparation, debinding and sintering are clear drawbacks. Therefore, a simpler and more energy efficient processing route should be explored. One possible route is the solidification of capillary bridges in the molded suspension.

The direct bonding of particles via polymeric bridges using the capillary suspension processing route is described in this thesis, where I focus on macroporous materials that are made from glass and polymers. The aim of this work is to create a porous, multifunctional, lightweight and strong material for different application fields, e.g. filtering or insulation materials, in an environmentally friendly manner using cost-effective, simple materials and straightforward methods. Therefore, low density hollow glass spheres and polymeric bridge materials, like methyl methacrylate, hydroxyl-ethyl methacrylate or epoxy, were used to realize highly porous, lightweight and sufficiently strong bodies. The following questions are investigated and discussed in this thesis:

- Can a bulk-immiscible monomer or cross-linking liquid be placed between microspheres to create a capillary suspension?
- Can a monomer be polymerized directly within the capillary bridges and what influence do the process parameters have on the molecular weight of the polymeric bridges?
- Can the capillary force between two spheres be directly measured along with the breaking force of a solidified bridge?
- Can potential commercially applicable materials be produced by using local bonding of micron-sized particles?

The requirements for an appropriate material are:

- Micron-sized particles with non-reactive surface properties
- A secondary liquid that is able to polymerize or crosslink without contact to air
- A bulk fluid that is insoluble with the bridging fluid and non-reactive to the particles. Furthermore, the bulk fluid must provide a sufficient droplet break up with the second liquid to realize enough small droplets between the particles to form a sample-spanning network.

The thesis starts in **chapter 2** with an introduction to the method of using capillary suspensions as precursors for local bonding of particles, giving an overview of research and applications in this field to demonstrate their versatility. This summary of the state of the art is provided by the first publication “Structure of capillary suspensions and their versatile applications in the creation of smart materials”, where a review of similar research is presented. Starting from the investigative work on capillary suspensions from Bossler (2018), the focus in this publication was on the different methods to bond particles. The work of Das et al. (2017), using hydrogels as the bridging phase, and the PDMS-like samples of Roh et al. (2017) are described. Furthermore, various control and tuning parameters are demonstrated.

Chapter 3 concentrates on capillary suspensions with polymerized bridges with a focus on the nanoscale chemical properties. A proof of concept for direct polymerization within the capillary bridges, where a simple method for direct polymerization in the bridges, at temperatures below 100 °C and requiring less time and effort than existing methods, is presented. The first model system with the aforementioned requirements was realized in this second publication “Radical polymerization of capillary bridges between micron-sized particles in liquid bulk phase as a low-temperature route to produce porous solid materials”. Here, micron-sized glass hollow spheres are used in a suspension with water and a small amount of methyl methacrylate, which is radically polymerized with benzoyl peroxide under thermal treatment. In this paper, I investigated the chemistry, including the chemical composition and molecular weight distribution of poly(methyl methacrylate) (PMMA) capillary bridges between glass particles to demonstrate how the bridge structure and the resulting porous body properties can be tuned. It is possible to place the monomer between the particles via the capillary suspension preparation method and to polymerize it in situ. This is possible under 100 °C and with a polymerization time of less than 5 h. The chemical composition of the polymerized bridging phase and the molecular weight distribution are influenced by the amount of monomer, the concentration of the initiator as well as the experimental conditions namely the polymerization temperature and time. An unexpected phenomenon is the almost 3x higher molecular weight of the bridge polymer compared to the bulk polymer, which is explained by the more efficient heat transfer and the large

surface-to-volume-ratio of the small monomer bridges surrounded by glass and bulk fluid. Additionally, another model is presented with glass particles in paraffin oil with hydroxyethyl methacrylate and the application of other particles, like graphite, using this material system and processing route. This shows the versatility of the idea of placing and polymerizing a monomer droplet between particles to create a sample-spanning particle network which results in a porous material.

In **chapter 4**, an advanced AFM set-up, which enables the micromechanical properties of the capillary bridges to be investigated, is presented. The advanced setup combines an atomic force microscope (AFM) with an additional camera, written in the form of a scientific paper for further investigation and better understanding of the inter-particulate forces that the bridging phase creates between the particles. With this arrangement, it is possible to transfer picoliters of a bridging fluid between two micron-sized spheres to determine the capillary forces of the unpolymerized bridges where every step has simultaneously visual observation of the bridge. Special features of this system are shown to be the direct observation of the behavior of capillary bridges while ramping as well as the easy calculation of the wetting contact angle between the liquid bridge and the spherical shaped particles from the capillary force data. A further remarkable improvement is the comparison of the theoretically calculated and experimentally determined Hamaker constant via force-distance measurements between micron-sized glass particles in air and in glycerol. Additionally, an example force-time experiment is shown for the breaking of a crosslinked epoxy bridge between two microparticles.

Chapter 5 discusses the macroscale properties of materials made from capillary suspensions with cross-linked bridges between glass hollow spheres having different surface properties. In the paper “Lightweight porous glass composite materials based on capillary suspensions”, an advanced method using capillary suspensions to create self-organized porous bodies with open porosities of up to 67% at an apparent density of only 200 kg/m^3 and a compressive strength of 0.6 MPa is presented. These samples are made of micron-sized hollow glass spheres that are locally connected by two-component epoxy bridges. The cross-linking in glycerol provides the preservation of the network structure from liquid into the solid state. The density of the glass-epoxy materials approach that of balsa wood and are comparable to common insulation materials, like foamed poly(styrene), but they have superior resistance against chemicals, solvents, or thermal exposure, in addition to the easy surface modification. Furthermore, the process route is very simple, low cost, consumes little energy, and is environmentally friendly. Using hydrophilic and hydrophobically modified glass hollow spheres, two different particle networks with different physical properties could be created. The tuning vehicle was the contact angle, which determines the bridge shape between the particles as well as the resulting network.

Finally, **chapter 6** summarizes the publications and their main results. This chapter also provides an outlook for other possible applications and future work. The benefits of porous materials made of interconnected particle networks are evident in a broad field of applications, like materials for heat-exchange-interphases, flexible and conductive membranes for electronics, and a variety of filtering techniques. The processing route of creating porous bodies via capillary suspensions has various variables that can be tuned to influence the properties of the final product, which begins with choosing the appropriate raw materials. The application is defined by the material properties of the particles and the adhering phase. The particles, the secondary phase (adhering material), and appropriate bulk phase are chosen for appropriate handling and the desired rheological behavior for processing the paste. Examples include glass particles, heat exchange particles, graphite particles and stiff or flexible polymers, like epoxy glues or elastomers. The physical properties, like porosity, pore size and, consequently, the mechanical strength, can be controlled by microstructure in the paste, which is deter-

mined by the amount of particles, the particle size, as well as the class and amount of the secondary bridging phase. Capillary suspensions with polymeric bridges, where the chemical and physical characteristics can be tuned, provide an elegant method to produce customer-oriented materials. In addition to the filtering techniques presented in this work, the method is potentially applicable to other product segments like medical tissue engineering, food industries or pharmaceuticals. In each sector where a paste or a particulate network scaffold is needed, capillary suspensions with polymeric bridges could be used. These manifold application fields show the great ability of the capillary suspensions with polymeric bridges for the broad area of life science techniques.

Zusammenfassung

Poröse Materialien werden in einem breiten Anwendungsbereich eingesetzt, wie in der Trenn- und Filtertechnik, sowie als Wärmedämmstoff oder katalytische Materialien je nach ihrer Porengröße. Diese porösen Materialien werden nach ihrer Porosität, d.h. dem Verhältnis des Hohlraumvolumens zum Gesamtvolumen des Materials, klassifiziert. Neben der Porengröße ist außerdem die Struktur des Materials ausschlaggebend, da diese die Porosität und die mechanischen Eigenschaften beeinflusst. Poröse Materialien können in der Natur auftreten, z. B. Gestein oder Holz, oder sie können mit verschiedenen Techniken wie Schäumen, Sacrificial Templating oder über Partikelnetzwerke hergestellt werden. Solche partikulären Netzwerke werden wiederum in verschiedene Materialklassen eingeteilt, wie granulare Medien, sphärische Agglomerate, Pickering-Emulsionen und Dispersionen. Durch Variieren der Menge der festen Phase und zweier flüssiger Phasen in einer Dispersion, kann eine weitere Materialklasse realisiert werden, die sogenannten Kapillarsuspensionen.

Kapillarsuspensionen sind Dreiphasensysteme, die aus einer Dispersion von Feststoffpartikeln in Mikrometergröße in einer Hauptflüssigkeit, sowie einer geringen Menge einer zugefügten zweiten nicht mischbaren flüssigen Phase bestehen. Durch das Verhältnis von Partikelanteil, Hauptphase und Zweitphase können die rheologischen Eigenschaften einer solchen Suspension modifiziert werden. Änderungen können zum Beispiel durch eine deutliche Erhöhung der Fließgrenze identifiziert werden, was durch einen Übergang von flüssigkeitsähnlichem zu gelartigem Verhalten aufgrund von Strukturbildung in der Suspension verursacht wird. In den letzten Jahren wurden viele verschiedene Anwendungsgebiete für Kapillarsuspensionen erforscht und untersucht, wie z. B. in der Lebensmitteltechnologie, als Pasten für Batterieelektroden oder druckbare Elektronik, rissfreie Filme, Bioslurries für erneuerbare Energieprozesse und sowohl dichte als auch zelluläre Keramik.

Diese Kapillarsuspensionen wurden von Koos und Willenbacher (2011) in zwei allgemeine Erscheinungsformen eingeteilt: Der *capillary state*, in dem der Dreiphasenkontaktwinkel $\theta_{S,B}$ größer als 90° ist, welchen die Zweitphase (S) auf der Partikeloberfläche ausbildet, während sie von der Hauptflüssigkeit (B) umgeben ist; und der *pendular state* mit einem Dreiphasenkontaktwinkel von weniger als 90° . Der geringe Anteil der Zweitphase wird in Form von Kapillarbrücken zwischen den mikrometergroßen Partikeln verteilt, was in einem durch Kapillaranziehung stabilisierten Partikelnetzwerk resultiert. Dieses perkolierende Netzwerk aus Partikeln und Kapillarbrücken wurde mittels konfokaler Mikroskopie von Bossler und Koos (2016) visualisiert. Sowohl der *pendular* als auch der *capillary state* führen zu einem probendurchspannenden Netzwerk, jedoch mit deutlichen Unterschieden in der Mikrostruktur. Der *pendular state* ist durch einzelne Kapillarbrücken zwischen den Partikeln (binäre Wechselwirkungen) gekennzeichnet, während der *capillary state* sich häufig durch Mehrkörperpartikelcluster auszeichnet. Die Struktur solcher Netzwerke kann genutzt werden, um Porosität, Porengröße und Porenstruktur in einem resultierenden verfestigten porösen Material zu steuern, was durch Sinter Techniken realisiert werden kann. Während die physikalischen und mechanischen Eigenschaften dieser Produkte gegenüber solchen aus herkömmlicher Massenfertigung Vorteile bieten, sind hohe Sinter temperaturen und eine lange Verarbeitungszeit gegenüber der Vorbereitung, dem Entbindern und dem Sintern eindeutige Nachteile. Daher sollte eine einfachere und energieeffizientere Verarbeitungsrouten untersucht werden. Ein möglicher Weg ist die Verfestigung von Kapillarbrücken in der produzierten Suspension.

In dieser Dissertationsschrift wird die direkte Verbindung von Partikeln über Polymerbrücken unter Verwendung von Kapillarsuspension beschrieben. Der Fokus hierbei liegt auf makroporösen Materia-

lien, die aus Glas und Polymeren hergestellt werden. Das Ziel dieser Arbeit war es, ein poröses, multifunktionales, leichtes und festes Material für verschiedene Anwendungsbereiche, wie beispielsweise für Filter- oder Isoliermaterialien, auf umweltfreundliche Weise zu kreieren unter Verwendung kostengünstiger, einfacher Materialien und unkomplizierter Methoden. Daher wurden hohle Glaspartikel mit niedriger Dichte und polymere Brückenmaterialien wie Methylmethacrylat, Hydroxyethylmethacrylat oder Epoxidharz verwendet, um hochporöse, leichte und ausreichend starke Körper zu realisieren. In dieser Arbeit und den jeweiligen Publikationen werden folgende Fragen untersucht und diskutiert:

- Kann ein mit der Hauptflüssigkeit nicht mischbares Monomer oder eine vernetzbare Flüssigkeit zwischen Mikropartikeln platziert werden, um eine Kapillarsuspension zu erhalten?
- Kann ein Monomer direkt in den Kapillarbrücken polymerisiert werden und welchen Einfluss haben die Prozessparameter auf das Molekulargewicht der Polymerbrücken?
- Kann die Kapillarkraft zwischen zwei Partikeln, zusammen mit der Bruchkraft einer verfestigten Brücke, direkt gemessen werden?
- Können potenziell kommerziell anwendbare Materialien durch lokales Verbinden von Mikropartikeln hergestellt werden?

Die Anforderungen an ein geeignetes Material sind:

- Partikel im Mikrometerbereich mit nicht reaktiven Oberflächeneigenschaften.
- Eine Zweitflüssigkeit, die ohne Kontakt zur Luft polymerisieren oder vernetzen kann.
- Eine Hauptflüssigkeit, welche unlöslich mit der Zweitflüssigkeit und gegenüber den Partikeln nicht reaktiv ist. Diese muss des Weiteren einen ausreichenden Tropfenaufbruch der zweiten Flüssigkeit ermöglichen, um geeignete kleine Tröpfchen zwischen den Partikeln zu erzeugen, welche ein probendurchspannendes Netzwerk bilden.

Die Dissertationsschrift beginnt in **Kapitel 2** mit einer Einführung in die Methode der Verwendung von Kapillarsuspensionen als Präkursor für die lokale Bindung von Partikeln. Das Kapitel gibt einen Überblick über die Forschung und Anwendungen in diesem Bereich, um die Vielseitigkeit der Methode zu demonstrieren. Die Zusammenfassung des Standes der Technik erfolgt in der ersten Veröffentlichung "Structure of capillary suspensions and their versatile applications in the creation of smart materials", in der eine Übersicht über verwandte Forschungsergebnisse präsentiert wird. Ausgehend von den Untersuchungen von Bossler (2018) zu Kapillarsuspensionen, lag der Fokus in dieser Veröffentlichung auf den verschiedenen Methoden zur Verbindung von Partikeln. Die Arbeit von Das et al. (2017), in der Hydrogele als Sekundärphase verwendet werden, und die PDMS-Proben von Roh et al. (2017) werden beschrieben. Darüber hinaus werden verschiedene Steuerungs- und Abstimmungsparameter demonstriert.

Kapitel 3 konzentriert sich auf Kapillarsuspensionen mit polymerisierten Brücken mit einem Fokus auf die nanoskaligen chemischen Eigenschaften. Eine Machbarkeitsstudie für die direkte Polymerisation in den Kapillarbrücken wurde durchgeführt, bei der eine einfache Methode für die direkte Polymerisation in den Brücken bei Temperaturen unter 100 °C vorgestellt wird, die weniger Zeit und Aufwand als die bisherigen Methoden erfordert. Das erste Modellsystem mit den oben genannten Anforderungen wurde in dieser zweiten Veröffentlichung "Radical polymerization of capillary bridges

between micron-sized particles in liquid bulk phase as a low-temperature route to produce porous solid materials" realisiert. Hier werden hohle mikrometergroße Glaspartikel in einer Suspension unter Zugabe von Wasser und einer geringen Menge Methylmethacrylat eingesetzt, welches unter thermischer Behandlung mit Benzoylperoxid radikalisch polymerisiert wird. Hauf et al. (2017) untersuchen die chemischen Eigenschaften, einschließlich der chemischen Zusammensetzung und der Molekulargewichtsverteilung von Kapillarbrücken aus Poly(methylmethacrylat) (PMMA) zwischen den Glaspartikeln, um zu zeigen, wie die Brückenstruktur und die resultierenden Eigenschaften des porösen Körpers eingestellt werden können. Es wird gezeigt, dass es möglich ist, das Monomer durch das Kapillarsuspensionsherstellungsverfahren zwischen den Partikeln anzuordnen und es dort in situ zu polymerisieren. Dies ist unter 100 °C und in einer vergleichsweise kurzen Zeit von weniger als 5 Stunden möglich. Die chemische Zusammensetzung der polymerisierten Brückenphase und die Molekulargewichtsverteilung werden durch die Monomermenge, die Konzentration des Initiators sowie die experimentellen Bedingungen, wie der Polymerisationstemperatur und -zeit, beeinflusst. Ein unerwartetes Phänomen ist das Auftreten eines fast dreimal höheren Molekulargewichts des Brückenpolymers im Vergleich zum Massepolymer, was durch die effizientere Wärmeübertragung und das große Verhältnis von Oberfläche zu Volumen der kleinen Monomerbrücken, die von Glas und Hauptflüssigkeit umgeben sind, erklärt wird. Darüber hinaus wird ein weiteres Modell mit Glaspartikeln in Paraffinöl mit Zugabe von Hydroxyethylmethacrylat und der Verwendung anderer Partikel wie Graphit unter Verwendung dieses Materialsystems und dieser Verarbeitungsrouten vorgestellt. Dies zeigt die Vielseitigkeit der Idee, Monomertröpfchen zwischen Partikeln zu platzieren und zu polymerisieren, um ein probennumspannendes partikuläres Netzwerk zu schaffen, welches nach Abzug der Hauptphase in einem porösen Material resultiert.

In **Kapitel 4** wird ein erweitertes AFM-Setup vorgestellt, mit dem die mikromechanischen Eigenschaften von Kapillarbrücken untersucht werden können. Das erweiterte Setup kombiniert ein Atomrasterkraftmikroskop (AFM) mit einer zusätzlichen Kamera, wie in dem in Form einer Veröffentlichung verfassten Kapitel beschrieben wird. Dieses Setup dient zur weiteren Untersuchung und zum besseren Verständnis der interpartikulären Kräfte, die durch die Zweitphase zwischen zwei mikrometergroßen Partikeln auftreten. Mit dieser Anordnung ist es möglich, Pikoliter eines Brückenfluids zwischen zwei Partikeln einzubringen, um die Kapillarkräfte der nicht polymerisierten Brücken zu bestimmen, wobei eine visuelle Beobachtung der Brücke in situ erfolgt. Besondere Merkmale dieses Systems sind die direkte Beobachtung des Verhaltens von Kapillarbrücken während des Auf- und Abbaus der Kapillarbrücke, sowie die einfache Berechnung des Benetzungskontaktwinkels zwischen der Flüssigkeitsbrücke und den kugelförmigen Partikeln aus den Kapillarkraftdaten. Eine weitere bemerkenswerte Verbesserung ist der Vergleich der theoretisch berechneten und experimentell ermittelten Hamaker-Konstante durch Kraft-Abstands-Messungen zwischen mikrometergroßen Glaspartikeln in Luft und in Glycerin. Zusätzlich wird ein exemplarisches Experiment zum Bruchverhalten einer vernetzten Epoxy-Brücke zwischen zwei Mikropartikeln vorgestellt.

In **Kapitel 5** werden die makroskaligen Eigenschaften von Materialien behandelt, die aus Kapillarsuspensionen mit vernetzten Brücken zwischen hohlen Glaspartikeln mit unterschiedlichen Oberflächeneigenschaften hergestellt werden. In der Veröffentlichung "Lightweight porous glass composite materials based on capillary suspensions" handelt es sich um ein fortgeschrittenes Verfahren, bei dem Kapillarsuspensionen verwendet werden, um selbstorganisierte poröse Körper mit offenen Porositäten von bis zu 67% bei einer scheinbaren Dichte von nur 200 kg/m³, sowie einer Druckfestigkeit von 0,6 MPa zu erzeugen. Diese Proben bestehen aus hohlen mikrometergroßen Glaspartikeln, die

lokal durch Zweikomponenten-Epoxybrücken verbunden sind. Die Vernetzung in Glycerin sorgt für die Erhaltung der Netzwerkstruktur vom nassen in den festen Zustand. Die Dichte der Glas-Epoxyd-Materialien reicht an die Dichte von Balsaholz heran und ist vergleichbar mit gängigen Isolationsmaterialien, wie geschäumtem Poly(styrol). Sie weisen jedoch, neben der einfachen Oberflächenmodifizierung, eine Beständigkeit gegen Chemikalien, Lösungsmittel oder thermischer Belastung auf. Darüber hinaus ist der Prozessweg sehr einfach, kostengünstig, verbraucht wenig Energie und ist umweltfreundlich. Mit hydrophilen und hydrophob modifizierten hohlen Glaspartikeln konnten zwei unterschiedliche Partikelnetzwerke mit verschiedenen physikalischen Eigenschaften erzeugt werden. Der variable Parameter war der Kontaktwinkel, der die Brückenform zwischen den Partikeln sowie das resultierende Netzwerk bestimmt.

In **Kapitel 6** werden schließlich die Veröffentlichungen und ihre wichtigsten Forschungsthemen zusammengefasst. Dieses Kapitel bietet des Weiteren einen Ausblick auf andere mögliche Anwendungen und zukünftige Arbeiten. Die Vorteile von porösen Materialien, die aus miteinander verbundenen Partikelnetzwerken bestehen, ermöglichen einen breiten Anwendungsbereich, wie z. B. als Materialien für Wärmeaustauschinterphasen, flexiblen und leitfähigen Membranen für die Elektronik, sowie für eine Vielzahl von Filtertechniken. Der Verarbeitungsweg der Erzeugung poröser Körper über Kapillarsuspensionen weist verschiedene Parameter auf, die variiert werden können, um die Eigenschaften des Endprodukts zu beeinflussen, was mit der Auswahl der geeigneten Rohstoffe beginnt. Die Materialeigenschaften der Partikel und das Brückenmaterial bestimmen die Anwendung. Die Partikel, die Zweitphase (haftendes Brückenmaterial) und eine geeignete Hauptflüssigkeit werden für eine angemessene Handhabung und das gewünschte rheologische Verhalten zur Verarbeitung der Paste ausgewählt. Beispiele umfassen Glaspartikel, Wärmeaustauschpartikel, Graphitpartikel und steife oder flexible Polymere wie Epoxidharze oder Elastomere. Die physikalischen Eigenschaften, wie Porosität, Porengröße und folglich die mechanische Festigkeit können durch die Mikrostruktur in der Paste gesteuert werden, die durch die Menge der Partikel, die Partikelgröße, sowie die Klasse und die Menge der Zweitphase bestimmt werden. Kapillarsuspensionen mit Polymerbrücken, bei denen die chemischen und physikalischen Eigenschaften eingestellt werden können, bieten eine elegante Methode zur Herstellung von kundenorientierten und maßgeschneiderten Materialien. Neben den in dieser Arbeit vorgestellten Filtertechniken, ist das Verfahren möglicherweise auch auf andere Produktsegmente anwendbar, z. B. für medizinisches Tissue Engineering, in der Lebensmittelindustrie oder in Pharmazeutika. In jedem Sektor, in dem eine Paste oder ein Partikelnetzwerk benötigt wird, könnten Kapillarsuspensionen mit Polymerbrücken verwendet werden. Diese vielfältigen Anwendungsgebiete demonstrieren die herausragende Eignung der Kapillarsuspensionen mit Polymerbrücken für den breiten Bereich der Life-Science-Techniken.

Contents

Preface.....	i
Acknowledgements	ii
Abstract	iii
Zusammenfassung.....	vii
Contents	xi
Notations	xiii
Latin symbols.....	xiii
Greek symbols	xiii
Abbreviations	xiv
1. Introduction and motivation	1
2. Structure of capillary suspensions and their versatile applications	3
Abstract	3
2.1 Introduction.....	3
2.2 New materials by solidification of capillary bridges.....	4
2.3 Precursor for sintered materials	7
2.4 Theoretical underpinnings and future pathways	9
2.5 Perspectives and conclusion	13
2.6 Acknowledgments	15
3. Radical polymerization of capillary bridges between micron-sized particles	16
Abstract	16
3.1 Introduction.....	16
3.2 Experimental Section.....	18
3.2.1 Materials.....	18
3.2.2 Sample preparation	19
3.2.3 Polymerization procedure	19
3.2.4 Characterization	20
3.3 Results and discussion.....	21
3.3.1 Rheological behavior	21
3.3.2 Visualization before and after polymerization	22
3.3.3 Chemical composition of polymeric bridges	24
3.3.4 Degree of polymerization in capillary bridges.....	25
3.4 Application routes	28
3.5 Conclusions.....	29
3.6 Acknowledgements	30
3.7 Conflict of interest.....	30

3.8	Supplementary Information	31
4.	Measurement of adhesion and capillary forces between two microparticles	35
	Preface.....	35
	Abstract	35
4.1	Introduction.....	35
4.2	Experimental	36
4.2.1	Materials and sample preparation	37
4.2.2	Setup.....	38
4.3	Results and discussion.....	39
4.3.1	Attractive forces between the particles in air and in glycerol	40
4.3.2	Capillary forces between two microparticles via AFM-measurement.....	41
4.3.3	Comparison between macroscopic and microscopic determined capillary forces...	43
4.3.4	Adhesion force for solidified bridges	44
4.3.5	Conclusion and outlook.....	45
5.	Lightweight porous glass composite materials based on capillary suspensions.....	47
	Abstract	47
5.1	Introduction.....	48
5.2	Experimental Section.....	49
5.2.1	Materials.....	49
5.2.2	Sample Preparation	50
5.2.3	Characterization	50
5.3	Results and Discussion.....	51
5.4	Conclusions.....	59
5.5	Supplementary Information	60
6.	Summary and outlook	64
7.	Bibliography.....	67

Notations

Latin symbols

A_H	Hamaker constant [J]
c_{BPO}	BPO concentration [mg/ml _{MMA or HEMA}]
D	fractal dimension [-]
\mathcal{D}	dispersity [-]
d_{50}	average particle diameter, volume based [μm]
F_c	capillary force [μN]
F_{vdw}	van der Waals force [μN]
G'	shear storage modulus [Pa]
G''	shear loss modulus [Pa]
h	separation distance between two spheres (edge to edge) [μm]
$[I]$	initiator concentration [mg/ml]
k_d	polymerization rate [1/s]
m	slope [-]
M_w	molecular weight [g/mol]
P	pressure [Pa]
p_n	degree of polymerization [-]
R	radius of particle [μm]
R_g	radius of gyration [μm]
T	temperature [$^{\circ}\text{C}$ or K]
$t_{1/2}$	initiator half-life [s]
V_{bridge}	volume of capillary bridge [μm^3]

Greek symbols

δ	chemical shift [ppm]
$\varepsilon, \varepsilon_{\text{total}}$	total porosity [-]
$\varepsilon_{\text{open}}$	open porosity [-]
θ	contact angle [$^{\circ}$]
$\theta_{S,B}$	three-phase contact angle [$^{\circ}$]
Γ	interfacial tension [mN/m]
σ_y	yield stress [Pa]
σ_{failure}	failure strength [MPa]

Notations

$\sigma_{\text{compressive}}$	compressive strength [MPa]
ϕ	volume fraction [-]
$\rho_{\text{material}}, \rho_{\text{particle}}$	density of given material, particle [g/cm^3]
$\rho_{\text{raw}}, \rho_{\text{apparent}}$	raw density [g/cm^3]
$\rho_{\text{skeletal}}, \rho_{\text{true}}$	skeletal density [g/cm^3]

Abbreviations

AFM	atomic force microscope
BPO	benzoyl peroxide
CCT	critical cracking thickness
EDX	energy-dispersive X-ray spectroscopy
ESEM	environmental scanning electron microscope
HEMA	hydroxyethylmethacrylate
HEMATMDI	diurethane dimethacrylate
$^1\text{H-NMR}$	nuclear magnetic resonance spectroscopy
LEM	laboratory for electron microscopy
MMA	methyl methacrylate
PCM	phase change material
PDMS	polydimethylsiloxane
PEO	polyethylene oxide
PIB	polyisobutylene
PMMA	polymethyl methacrylate
PHEMA	polyhydroxyethylmethacrylate
PTFE	polytetrafluoroethylene
rpm	rounds per minute
SEC	size exclusion chromatography
SEM	scanning electron microscope
THF	tetrahydrofuran
UHMWPE	ultra-high-molecular-weight-polyethylene

1. Introduction and motivation

The aim of this work is to create a porous, multifunctional, lightweight and strong material for different application fields, like e.g. filtering or insulation materials, in an environmental friendly manner using cost-effective, simple materials and straightforward methods. Porous materials are established in a wide field of applications depending on their pore size class, such as separation and filtering techniques, as well as thermal insulation materials or catalytic materials [1]. The pore size is categorized as having a micro- (< 2 nm), meso- (50 nm – 2 nm) and macro- (> 50 nm) porous structures [2]. Porosity is defined as the ratio of the void volume to the total volume of a material. It is either naturally formed, e.g. rocks [3] or wood [4], or it can be realized using different artificial techniques, like foaming [5], sacrificial templating [6,7] or via particle networks. These particle network materials comprise a broad field of agglomeration, crystallization and sintering techniques. One special case is the direct bonding of particles via polymeric bridges using the capillary suspension processing route described herein [8].

Capillary suspensions certainly share some similarities with granular media, which consists of particle network bonded though capillary bridges surrounded by air. These particles are typically larger, in the millimeter range, than the microparticles used for capillary suspensions. Furthermore, owing to the change in the Eötvös (Bond) number from $Eo \approx 0.01$ to 0.1 for wet granular media versus $Eo \approx 10^6$ to 10^5 for capillary suspensions [9], the particle loading in granular media is higher, usually close to random close packing. Extensive work on granular media was completed by Rumpf et al. and Schubert [10,11] regarding the adhesion forces, capillary pressure and contact angle of liquid bridges between spherical particles. Additionally, Helmar Schubert [11] investigated the tensile strength of wet particle beds. Even with the differences in bulk liquid and particle loading, the mean coordination number appears to match the prediction made by from Pietsch and Rumpf [10] appears to match the behavior of capillary suspensions (see Bossler [12], figure 6.27). The physical properties of granular media do not perfectly match capillary suspensions, nevertheless, previous research on granular media can provide valuable insight into the capillary suspensions.

Capillary suspensions are three-phase systems, which contain a dispersion of solid particles in a bulk liquid and a fractional amount of second immiscible liquid phase [13]. These capillary suspensions are observed in two general forms: The **capillary** state, where the three-phase-contact angle $\theta_{S,B}$, that the secondary fluid S makes against the solid when surrounded by the bulk fluid B, is higher than 90° and the **pendular** state with a three-phase contact angle of lower than 90° . A further state is the **funicular**, which is an aggregated state at higher secondary fluid content that resembles the capillary state despite a contact angle less than 90° . There are some more well-known states and classes, like the granular media (e.g. sand castles), spherical agglomeration, Pickering emulsions and dispersions that can also be created by varying the amount of the solid phase and the two liquid phases. The properties of capillary suspensions were characterized extensively by Bossler et al. in their research [9,14,15]. It is important to mention that the limit of complete insolubility is physically impossible. In this thesis, we describe immiscible liquids as liquids with very low solubility (e.g. 1.5 g/100 ml for methyl methacrylate in water). The solubility in this case has no influence on the wetting angle, which characterizes the particle network, nor on the polymerization properties in the capillary bridges.

In recent years, many different applications fields for capillary suspensions, like in food technology [16], slurries for battery electrodes or printable electronics [17,18], crack-free films [19], bio-slurries for renewable energy processes [20] and dense [21–23] as well as cellular ceramics [24] have been explored. The choice of the materials used in this thesis and its corresponding publications [8,25,26] distinguishes this work and possible applications from other studies. In this work, low density hollow glass spheres and polymeric bridge materials, like methyl methacrylate, hydroxyl-ethyl methacrylate or epoxy, were used to realize highly porous, lightweight and sufficiently strong bodies. The following questions are investigated and discussed in this thesis:

- Can an immiscible monomer or cross-linking liquid be placed between microspheres to create a capillary suspension?
- Can the monomer be polymerized directly within the capillary bridges and what influence do the process parameters have on the molecular weight of the polymeric bridges?
- Can the capillary force between two spheres be directly measured along with the breaking force of a solidified bridge?
- Can potential commercially applicable materials be produced by using local bonding of micron-sized particles?

These central questions will serve as a guideline for the structure of this thesis and the respective publications. The thesis starts in **chapter 2** with an introduction to the method of using capillary suspensions as precursors for local bonding of particles giving an overview of research and applications in this field to demonstrate their versatility. **Chapter 3** concentrates on capillary suspensions with polymerized bridges, with a focus on the nanoscale chemical properties. In **chapter 4**, an advanced AFM set-up, which enables the microproperties of the capillary bridges to be investigated, will be presented. **Chapter 5** includes the macroscale properties of the resulting material made from capillary suspensions with cross-linked bridges between glass hollow spheres having different surface properties. A schematic overview of the main contents of this thesis is presented in Figure 1.1. Finally, **chapter 6** summarizes the publications and their main research topics. Chapter 6 also provides an outlook for other possible applications and future work.

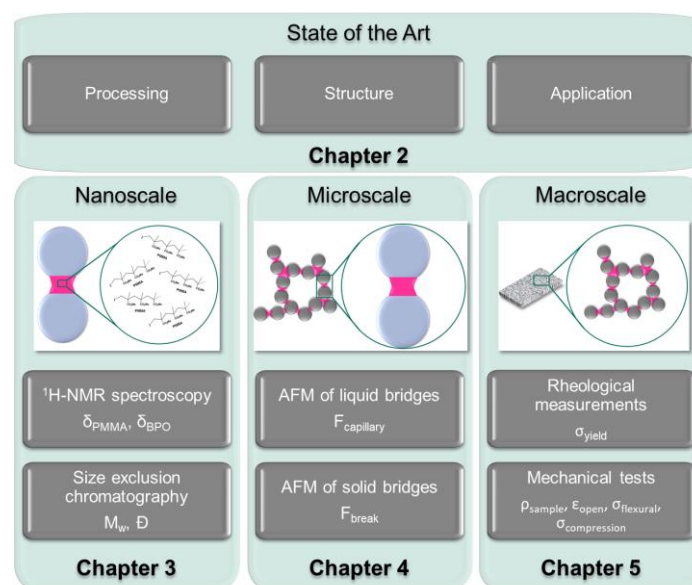


Figure 1.1 Schematic structure of this thesis. The main publications in this dissertation are categorized into nano-, micro-, and macroscale properties of the capillary suspensions with polymeric bridges.

2. Structure of capillary suspensions and their versatile applications

Full title: Structure of capillary suspensions and their versatile applications in the creation of smart materials

Authors: Katharina Hauf, Erin Koos

Status: published

Bibliographic data: MRS Communications, 8(2), 332-342. doi:10.1557/mrc.2018.28

Copyright Materials Research Society 2018, published by Cambridge University Press. Reprinted with permission. The text has been adapted in this thesis to change the citation and figure numbering. Additionally, some symbols have been modified to confirm with the other chapters.

Abstract

In this paper, we reviewed recent research in the field of capillary suspensions and highlight a variety of applications in the field of smart materials. Capillary suspensions are liquid–liquid–solid ternary systems where only one liquid is present in a few percent and induces a strong, capillary-induced particle network. These suspensions have a large potential for exploitation, particularly in the production of porous materials since the paste itself and the properties of the final material can be adapted. We also discussed the rheological properties of the suspension and network structure to highlight the various ways these systems can be tuned.

2.1 Introduction

The field of capillary suspensions is fairly young but has already gained worldwide attention [13,27–32]. This rapidly growing field has shown significant promise in easily creating adaptable pastes to use in a large variety of applications, e.g., heat-stable and low-calorie chocolate spreads [16,33] battery slurries [17,18], highly conductive pastes for solar cells [19,34], stable slurries for biofuels [20], and strong highly porous ceramics [21,23,35]. These different applications illustrate the manifold applicability of capillary suspensions due to the easy way capillary suspensions can be adapted to each desired product. It is important to understand the physical phenomenon of capillary forces to understand how the suspensions can be tuned appropriately to create tailor-made materials. Different particulate networks can be realized when creating capillary suspensions. These differences primarily originate from the wettability of the secondary fluid against the particles, quantified using the three-phase contact angle θ . In the first investigation by Koos and Willenbacher [13], two states were defined. For $\theta < 90^\circ$, the secondary fluid preferentially wets the particles and the system is arranged in the pendular state. The particles are directly connected to each other through pendular bridges, a sample-spanning network is formed. The particulate system is in the capillary state when the contact angle $\theta > 90^\circ$. Here, clusters of particles surrounding secondary fluid droplets are formed [36]. A sample-spanning network is formed in this system through the connections between these polytetrahedral or higher order clusters. These different network structures were first imaged by Bossler and Koos [9], and are shown in Figure 2.1 together with a schematic illustration of the two states.

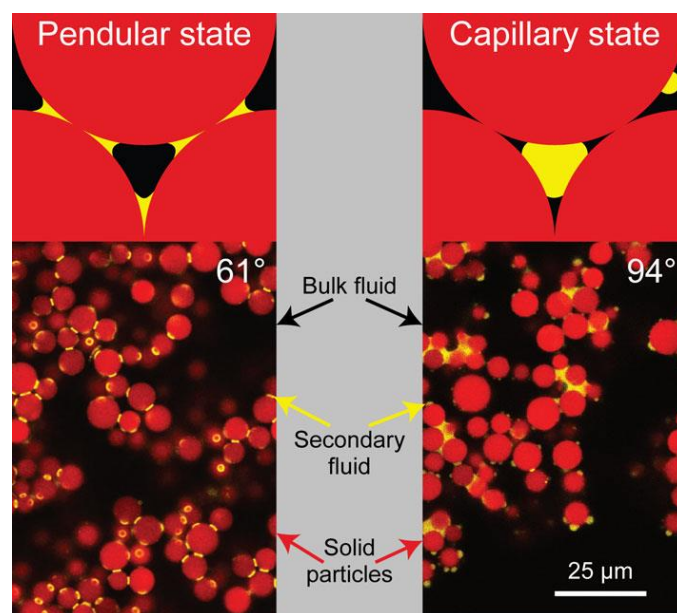


Figure 2.1 Schematic illustration and confocal images of capillary suspensions with silica spheres ($d_{50,3} = 6.40 \pm 0.02 \mu\text{m}$) that are fluorescently dyed with rhodamine B isothiocyanate (shown in red). Their contact angle was chemically modified before sample preparation. A mixture of Hexamoll DINCH and *n*-dodecane was used as a bulk phase, and fluorescently dyed aqueous glycerol (yellow) was used as the secondary fluid. On the left side, the particulate network in the suspension is arranged in the pendular state with a contact angle of 61° and the system on the right side is in the capillary state with 94° . Images reprinted with permission from Bossler and Koos [9]. Copyright 2016 American Chemical Society.

They used a system containing fluorescently labeled silica microspheres ($d_{50} = 6.4 \mu\text{m}$) dispersed in a mixture of Hexamoll DINCH and *n*-dodecane with fluorescently dyed aqueous glycerol as the secondary fluid [9]. Two different microstructures are visible depending on the surface treatment of the particles, given by the three-phase contact angle θ . The drops in the pendular state have a narrow volume distribution between 2% and 5% of the average particle volume. In the capillary state, the drop sizes have a much wider distribution, ranging from the small, singly connected drops on the particle surface to larger drops connecting many particles. In both cases, a clear sample-spanning network is visible. Various types of structured materials can be created if the structure of this sample-spanning network is preserved.

2.2 New materials by solidification of capillary bridges

The first class of materials is created by preserving the capillary bridges connecting particles through bridge solidification. This can be accomplished through gelation or crystallization of the bridging fluid, or by carrying out a chemical reaction, e.g., polymerization, within the fluid. The structure of these materials should be closely related to the structure of the capillary suspension precursor. Using systems with a hydrogel bridging fluid, Das et al. recently showed that the properties of the capillary suspensions could be reversibly controlled [37]. Aqueous solutions with hydrogel-forming polymers (Methocel A4M and SeaPrep agarose) were used as the immiscible secondary phase binding together pre-hydrophobized calcium carbonate particles in silicone oil, as shown in Figure 2.2. For both secondary phase compositions, they observed the reproducible reaction of the capillary suspension upon external thermal changes using rheological measurements. The gelation of the secondary fluid bridges could be accomplished by either raising or lowering the sample temperature [37]. Samples with aqueous Methocel A4M gelled at higher temperatures and an increase in the complex shear modulus by several orders of magnitude was observed for the capillary suspension.

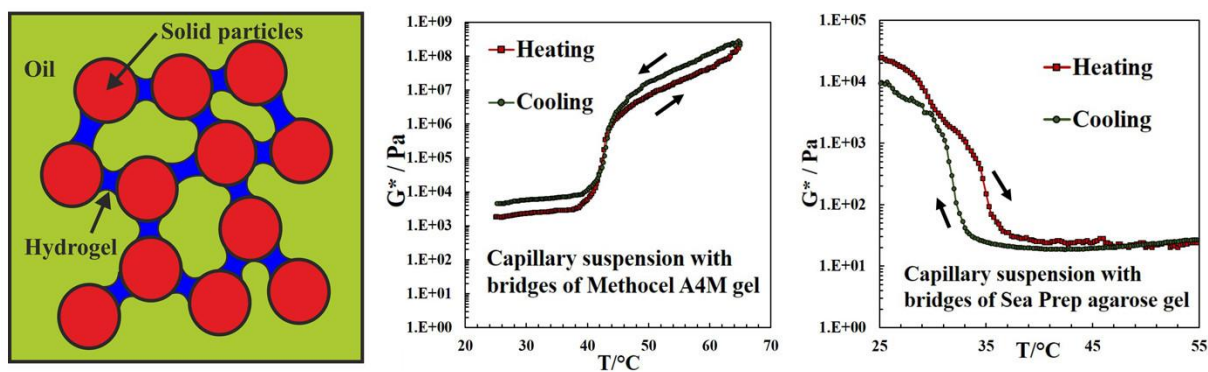


Figure 2.2 (left) Scheme for capillary suspensions made of pre-hydrophobized calcium carbonate in silicone oil with a hydrogel-forming secondary phase. (right) Complex shear modulus as a function of sample temperature. Reprinted with permission from Das et al. [37]. Copyright 2017 American Chemical Society.

The reverse effect was observed using Sea Prep agarose, where the complex shear modulus decreases with increasing temperature. In both cases, a hysteresis was observed at heating and cooling rates of 1 °C/min or faster, but the effect was highly reproducible. These thermally responsive capillary suspensions could potentially be used in personal care or home products. Domenech and Velankar used a multiphase solution consisting of silica particles in a bulk polyisobutylene (PIB, $M_w \sim 2200$ g/mol) with small amounts of added polyethylene oxide (PEO, $M_w \sim 20,000$ g/mol) [27]. The system was mixed at an elevated temperature of 80 °C, above the melting temperature of the PEO, and then were rapidly cooled to 5 °C whereupon the bridges would crystallize. This system was used to study the structure of the capillary bridges and morphologic changes with the addition of increasing amounts of secondary fluid [27,38]. In several papers, Velankar and coworkers described the various morphologic changes that were possible in this system and even described bicontinuous structures when larger amounts of secondary fluid are added and the interface becomes jammed by the particles [28,31,39–41]. Velankar and coworkers used this system primarily to investigate the structure, removing the liquid PIB from the solidified structure produced solid bodies. Presumably, this method can be used to design porous materials.

Hauf et al. proved that direct polymerization within the capillary bridges can be used to control the physical and chemical properties of the bridges to create porous materials [8]. This publication is fully described in chapter 3. They primarily used two material systems made of micron-sized hollow glass spheres with monomers as the secondary phases. One system was hydrophobic glass spheres dispersed in water and methyl methacrylate (MMA) as the bridging fluid, as shown in Figure 2.3(a). The other system was made of hydrophilic glass hollow spheres in low-viscosity paraffin oil as bulk fluid and hydroxyethylmethacrylate (HEMA) as secondary fluid, as shown in Figure 2.3(c). The capillary bridges, which are shown in red, keep their shape after polymerization. The corresponding polymerized porous bodies, without any remaining bulk fluid, are imaged using ESEM as shown in Figure 2.3(b) and in Figure 2.3(d), respectively. Hauf et al. determined that it is possible to polymerize the capillary bridges in the wet state, at moderate temperatures below 100 °C, without losing volume and by preserving the structure of the material [8]. Therefore, the volume and the shape of the capillary/polymeric bridges can be controlled from the wet to the solid state. By varying the initiator concentration during the radical bulk polymerization process, it is possible to control the molecular weight of the polymeric bridges and thus to tune the properties of the final material [8]. Porosities of $\epsilon_{open} = 65\%$ were reached for samples that are made of 40 vol% hydrophilic glass spheres with 6 vol% HEMA. These samples have a failure strength under four-point-bending of 0.1 MPa. For the

other material system, made of 40 vol% hydrophobic glass spheres with 6 vol% MMA, the porosity was $\varepsilon_{open} = 60\%$ and the failure strength was 0.05 MPa. Hauf et al. also demonstrated that this process can be used with other particles or other combinations of particles [8].

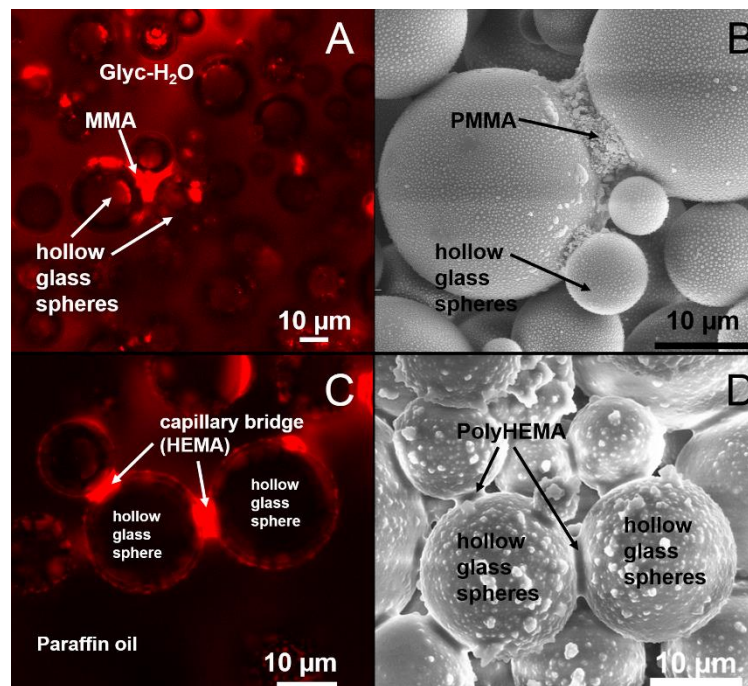


Figure 2.3 (a) Confocal image slice for capillary suspensions made of 40 vol% hydrophobic hollow glass spheres in a glycerin/water mixture (61/39 wt%) with 6 vol% added MMA. The MMA is dyed (red), and the other components are undyed. (b) Corresponding ESEM images of a fractured section of the porous body and the polymeric bridges. (c) Confocal image slice for the 40 vol% hydrophilic hollow glass spheres in paraffin oil with 4 vol% added HEMA. The HEMA here is dyed (red), and the other components are undyed. (d) Corresponding porous solid samples with visible poly(HEMA)-bridges, which interconnect the particles. The samples were polymerized in the bulk fluid for 2.5 h at 82 °C, and the BPO content was 15 mg/mL [8]. The samples in paraffin oil were washed in diethyl ether and soaked on paper towels after polymerization. Figure adapted from Hauf et al. [8], reprinted with permission from Springer (Colloid and Polymer Science), copyright 2017.

Roh et al. have recently shown the application of capillary suspensions to form complex and flexible structures by using the elastomeric polydimethylsiloxane (PDMS), which has important implications for biomedical applications [42]. In this study, the capillary suspensions contained 50% (v/v) precured PDMS microbeads dispersed in water and 10–40 vol% uncured liquid PDMS as the bridging fluid. The suspensions had paste-like behavior and could be three-dimensional (3D) printed in several structures in air and under water. They were then heat-cured at 85 °C to crosslink the liquid silicone bridges between the microbeads, which lead to solidified 3D shapes [42]. The rheological behavior of these capillary suspensions showed an increase in yield stresses and storage moduli, but a reduction as the amount of PDMS increased above 20 vol%. The cured 3D structures showed increasing tensile strength flexibility with increasing amounts of the secondary phase, up to 0.9 MPa at a strain of 1.4 for samples with 30% secondary phase. Depending on the amount of secondary phase, the porosity and the mechanical properties could be controlled, which is useful for creating self-supporting, highly extensive and elastic bodies. These structures feature shape memory effects. An example was shown by bringing a water droplet in contact with a printed mesh, the structure wraps around the droplet and keeps it like a grid-like shell. The biocompatibility of the silicone-based pastes is advantageous for 3D printed biomedical products, or in the field of tissue engineering such as direct printing of bio-scaffolds [42].

2.3 Precursor for sintered materials

A similar way to use capillary suspensions as precursors to create porous materials with beneficial properties is to use them for producing highly porous and strong ceramic bodies with pore sizes $<10\ \mu\text{m}$ and porosities $>50\%$. Dittmann et al. investigated a processing route for tailor-made macroporous ceramics by sintering green bodies made of capillary suspensions following debinding of the bulk phase [22]. Therefore, a particulate system with 15–20 vol% raw ceramic powder, made of calcined $\alpha\text{-Al}_2\text{O}_3$, dispersed in paraffin oil and a water sucrose solution was used as a secondary phase with a varying amount of 0–4 vol%. The water sucrose solution is important because the removal of the bulk phase and water during the debinding process leads to a network collapse if a stabilizing agent is not used. The sucrose crystallizes, and therefore, preserves the structure. Another alternative is to use paraffin wax as the bulk fluid, which also creates a processable paste that is ideal for extrusion and provides an adequate shape accuracy of the porous bodies. The capillary suspensions showed an increase in yield stress with higher particle fractions and with increasing amount of secondary phase over several decades up to 200 Pa. Dittmann and coworkers determined that with the addition of only small fractions of the bridging fluid, from 0 to 1 vol%, the rheological behavior changes dramatically. With more secondary phase, the yield stress reaches a plateau. The amount of secondary fluid also affects the material properties of the sintered bodies. Increasing amounts of secondary phase increase the porosity from 50% to almost 65%. This was also observed in the average pore size of the porous media. The pore sizes are larger for higher porosity samples, but their distribution increases, which means a heterogeneous pore network [22]. Increasing particle fractions naturally lead to a decrease in the porosity. These porous bodies are interesting for the rapid production of porous ceramics that can be used as lightweight building materials or filter membranes and in applications such as catalytic carriers. Further microstructural investigations of these macroporous ceramic materials were completed by Dittmann and Willenbacher, with special attention to the influence of the induced structural properties on the mechanical performance, as shown in Figure 2.4 [35]. The structure of these materials can be controlled using the amount of the secondary phase from the van der Waals particle network in regime I at 0.0 vol%, to a homogeneous flocculated and sample-spanning pendular state particle network stabilized with capillary liquid bridges in regime II at 2.5 vol%, and finally to strong aggregation and inhomogeneous structure formation due to spherical agglomeration in regime III at 8.0 vol% secondary phase. These changes are also apparent in the rheological behavior of the corresponding capillary suspensions. The sample-spanning particle network stabilized by capillary liquid bridges in regime II (pendular state) leads to an open, porous structure. This transitions to a body with a strong increase in porosity and the formation of a bimodal pore size distribution with higher average pore size upon increasing amounts of liquid (funicular state). Further increases of the bridging fluid induce the formation of large aggregates (regime III, agglomeration). The body has a similar porosity, but a broad multimodal pore size distribution and an increase of the average pore size were observed due to coarsening of the microstructure. This also affects the mechanical properties of sintered bodies. For regimes I and II, the mechanical strength depends only on porosity, not on pore size. With increasing porosity, the mechanical strength decreases [35]. These properties of capillary suspensions as precursors can also be used to produce highly porous glass filters with porosities over 50% at average pore sizes between 1 and 50 μm and high gas permeability, as Maurath et al. showed in their study [43].

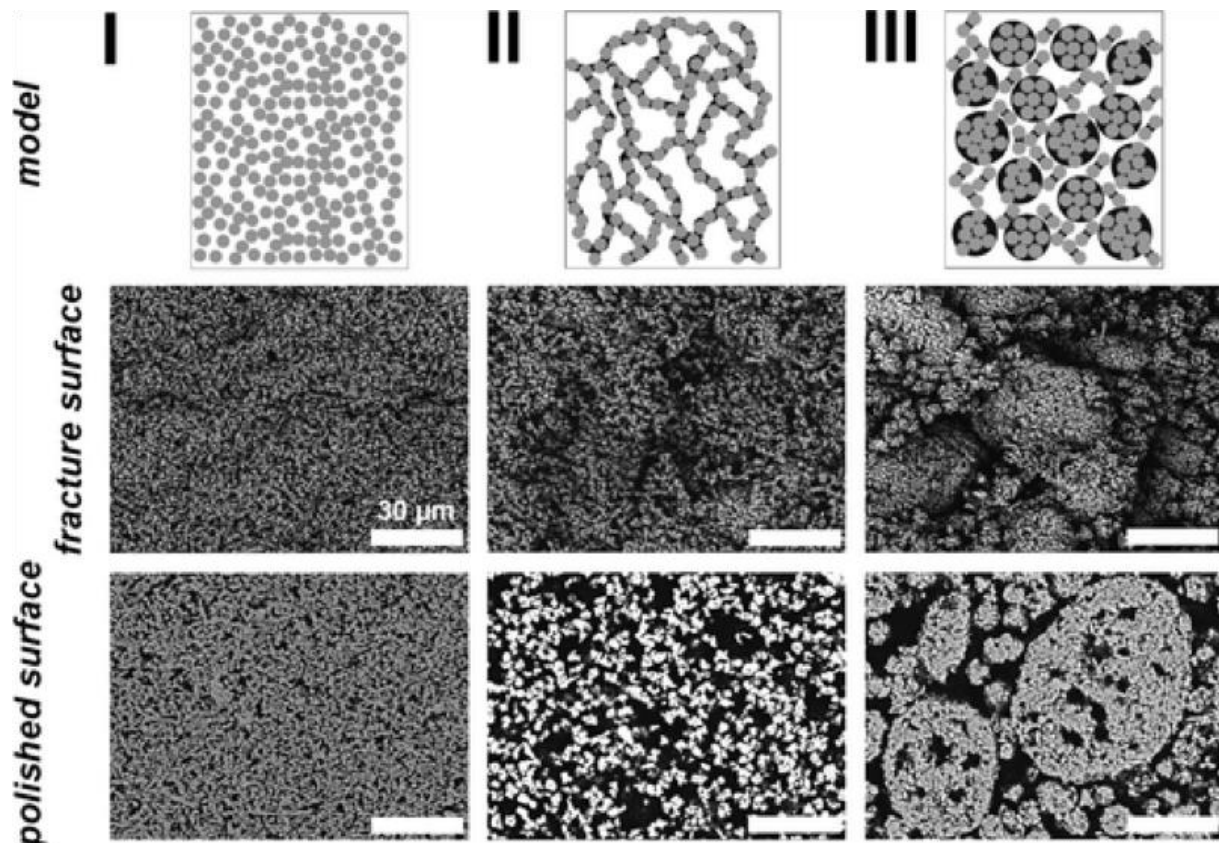


Figure 2.4 Model for capillary suspensions in the pendular state and corresponding SEM images of the fractured and polished surfaces of sintered parts. The images show the particle network in regime I with 0.0 vol% sucrose solution, 2.5 vol% in regime II (pendular state), and 8.0 vol% in regime III (spherical agglomeration). The suspensions have a solid loading of 20 vol% α - Al_2O_3 in paraffin oil and the ceramics were sintered at 1650 °C for 2 h. Figure from Dittmann and Willenbacher [35], reprinted with permission. Copyright 2014 John Wiley & Sons, Inc.

An extended field is the 3D printing of capillary suspensions, which was investigated by Maurath and Willenbacher for highly open porous, hierarchically structured ceramics [24]. They produced cellular and honeycomb bodies with porosities up to 88% and an open-porous struts with porosities between 45% and 60% and pore sizes smaller than 6 μm using capillary suspensions. The materials have a high specific compressive strength. They found that the density could be decreased by 2–3 times without any decrease of the mechanical strength. The manufacturing of 3D honeycomb structures showed anisotropic behavior under compression depending on if the applied force was perpendicular to or in-line with the cell orientation. The largest advantage in 3D printing is the hierarchical structure of the samples, whose shrinkage can be appropriately controlled by adapting the sintering temperature. The 3D printing offers different parameters for the body shape, structure, and the printed pore sizes, as well as the paste properties, which determine the smaller pore sizes. Tailor-made products can, therefore, be realized for specific applications such as separation and filtration processes, or as microfluidic crossflow filters for hot gas filtration. Another possible field is in catalyst supports with smart flow channels for fast chemical reactions requiring high internal surface [24]. The effect of preserving the structure using capillary suspensions was adapted by Schneider et al. to enhance crack-free drying of films [19]. Here, particle systems in n-octanol and water, but also with paraffin oil as bulk phase and a water–sucrose solution as secondary phase were used. The capillary bridges prevent particle motion during drying and the uniform network limits variations in the capillary pressure as the solvent evaporates. This increases the critical cracking thickness (CCT) and decreases the extent of cracking for films above the CCT. Without the use of a stabilizing agent, the network collapses

and dense films are created. This research can be applied to a large range of materials, such as suspensions of metals, semiconductors, and glassy polymeric particles. A particular area of interest is in printed electronic devices where cracks reduce the conductivity [19]. This work also demonstrated that a stabilizing agent such as sucrose preserved the porosity of ceramic films, and a reduction in cracking, which even persisted after debinding and sintering, was observed. This allows thin, active ceramic films to be printed onto a scaffold. Superior filtration efficiency was demonstrated in these films. Finally, Dittmann et al. demonstrated that suspensions with a bimodal particle size distribution can be used to reinforce ceramic and polymeric porous bodies [23]. Ceramics with coarse and fine Al_2O_3 were produced and the addition of these fine particles increased the compressive strength doubled from 15 to 30 MPa for bodies with the same porosity of 55%. The flexural strength also increased, but this effect was less pronounced. Dittmann and coworkers also used fine particles made of tetragonal stabilized (3 mol% Y_2O_3) $t\text{-ZrO}_2$. The stronger zirconium toughened alumina bodies show an approximately threefold increase in both the compressive and flexural strength [23]. Presumably, this method can also be combined with other methods such as 3D printing to form porous bodies with a further decrease in density without a loss in strength.

2.4 Theoretical underpinnings and future pathways

In order to design the next generation of smart materials, we must have a clear idea of how the properties of the component materials, their ratios, and the processing of these materials affect the network and microstructure. Understanding these inter-relations allows the properties of the final material to be tuned from existing formulations as well as the directed design of new materials, such as hierarchically structured materials with a multimodal, custom-designed pore size distribution and combined strength properties resulting from different raw materials such as glass, ceramics, polymers, etc., which could have strong, but flexible structures at the same time. The general and proven way to create capillary suspensions is to add a small amount of an immiscible secondary fluid to a particulate suspension [13]. The rheological behavior of this suspension can be tuned and controlled by the following factors: wettability [9] and amount of secondary fluid [21], particle fraction [35], particle size [35], and particle shape [44] within the suspension and the overall mixing conditions [14]. Hence, all these parameters are also important for the resulting materials, which are produced with capillary suspensions as precursors. The capillary force F_c is the most decisive factor for understanding capillary suspensions and depends on several key parameters. For a small toroidal bridge between equally sized spheres with radius R , separated by a distance h is

$$F_c = f(V_{bridge}, h) 2\pi\Gamma R \cos\theta = \frac{1}{1+1.05h\sqrt{(R/V_{bridge})+2.5h^2(R/V_{bridge})}} 2\pi\Gamma R \cos\theta \quad (1)$$

where V_{bridge} is the capillary bridge volume and Γ describes the interfacial tension between the two fluids [10,45–47]. The interfacial tension is regarded as the force required to change the interfacial area between two immiscible fluids. The contact angle, formed by the liquid–liquid interface on the particles, is θ . For particles in contact with the function, $f(V_{bridge}, h)$ becomes zero [9]. From Equation (1), it is clear that the capillary forces increase with increasing interfacial tension and increasing particle radius, but decreasing contact angle and decreasing particles separation. This equation should hold for particles in the range $0.5 \mu\text{m} < R < 50 \mu\text{m}$, described in the previous sections. It does not, however, include the influence of the particle volume fraction and network structure on the bulk material stresses, originally described in a simplified model by Pietsch and Rumpf [10]. The yield

stress σ_y is given by the capillary force divided by the contact area R^2 with a correction for these factors. Bossler et al. [14] found a correlation, shown in Equation (2), between the solid volume fraction, particle size, and the yield stress,

$$\sigma_y = f(\phi_{solid}, \phi_{sec}) \frac{F_c}{R^2} = f(\phi_{solid}, \phi_{sec}) g\left(\frac{V_{bridge}}{R^3}\right) \frac{2\pi\Gamma \cos\theta}{R} \quad (2)$$

where $f(\phi_{solid}, \phi_{sec})$ is a function of particle and second fluid volume fractions and $g(V_{bridge}/R^3)$ is a function of the bridge volume relative to the particle volume [14]. The influence of the particle size on the yield stress was investigated by Koos et al. for spherical, glass particles, where the dependence on the reciprocal radius was reproduced [48]. The influence of the shape on the rheology was investigated by Maurath et al. using application-oriented particles [44]. They used spherical, scalenohedral-, plate-, and needle-shaped particles made from precipitated calcium carbonate and aluminum flakes. All suspensions were prepared in the pendular state with a particle fraction of $\phi = 7$ and 10 vol%. The impact of particle shape on the yield stress is shown in Figure 2.5(a). The yield stress strongly increases with increasing amount of secondary phase for each of the shapes tested, with a maximum between $\phi_{solid}/\phi_{sec} \approx 0.1$ and 0.2. The yield stress for spherical particles is almost one decade lower than the other particle shapes at the 1 vol% secondary phase peak. The differences in this rheological behavior for these differently shaped particles are assumed to be related to the shape of the capillary bridges formed in the suspensions [44]. For example, the contact area and corresponding capillary force are lower in spheres than for equally sized plates. This trend is clearly shown in Figure 2.5(b), where data from two different aspect ratios as a function of ϕ_{solid}/ϕ_{sec} are shown. The capillary suspensions with flakes with the larger flat area result in higher yield stress values for the same ratio of secondary phase amount to a solid fraction. The particle shape also influences the aggregation of particles caused by oversaturated bridges.

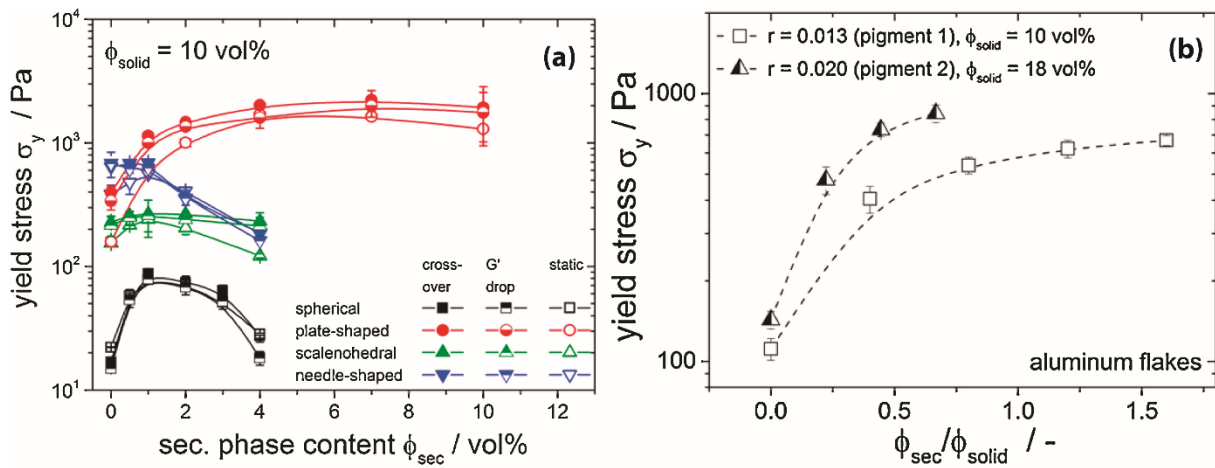


Figure 2.5 (a) Yield stress σ_y versus secondary phase content ϕ_{sec} for capillary suspensions made of calcium carbonate particles with varying particle shapes. Yield stress was determined by oscillatory shear experiments (crossover of G' and G'' in amplitude sweep; drop of G') and with steady shear experiments (vane geometry). (b) Yield stress σ_y versus ϕ_{solid}/ϕ_{sec} for suspensions made of aluminum flakes with varying aspect ratio (r) in a mixture of paraffin oil and mineral spirit and pure water as the secondary fluid. Figure from Maurath et al. [44], reprinted with permission. Copyright 2016 Elsevier.

The saturation of the bridges and the aggregation of particles is shown in the location of the yield stress peak. This transition is integrated into the function $g(V_{bridge}/R^3)$ in Equation (2). This transition from a pendular to funicular state was examined in the rheological measurements of Heidlebaugh et al. and Domenech and Velankar and confocal measurements of Bossler and Koos [9,38,39].

By considering the volume needed for a third particle to impinge on a capillary bridge joining two spherical particles, Heidlebaugh et al. calculated a transition at $\phi_{solid}/\phi_{sec} = 0.22$, assuming four contacts per particle. Despite the arbitrary value for the coordination number, this transition points matches quite well with observed yield stress peak in their data [38]. Bossler and Koos directly measured the average bridge size for pendular state samples at 40° and 61° [9]. At the same amount of added secondary fluid, the 61° sample has more binary bridging (pendular state) than the funicular 40° sample. This transition is consistent with the required bridge sizes calculated using the Flemmer criteria [49]. The influence of the secondary and solid volume fractions was investigated by Bossler et al. under the assumption that the yield stress (or other macroscopic property) is power-law function of the solid volume fraction,

$$X(\phi_{solid}) \propto \phi_{solid}^{f(D)} \quad (3)$$

where the constant X is a placeholder for a rheological property, such as the yield stress [50]. In Equation (3), the power exponent is assumed to be a function of the fractal dimension D , which can be calculated from the slope from the solid volume fraction against the yield stress, after Piau et al. [51], as

$$f(D) \equiv m = \frac{4}{3-D} \quad (4)$$

The data for measurements on Al_2O_3 suspensions for ceramics are shown in Figure 2.6. A master curve is shown in Figure 2.6 (a), and the yield stress values at the peak secondary fluid ratio of $\phi_{solid}/\phi_{sec} = 0.12$ are shown in Figure 2.6 (b) as a function of the solid volume fraction. The calculated exponents D indicate an increase in the fractal dimension for the alumina-based capillary suspensions with increasing particle size from $D = 1.86$ to 2.05 . The reason for this change in the dimensionality toward the value of an unstructured value of 3 with increasing particle size is hypothesized to be caused by the relative reduction of capillary force to gravity [50]. The dimensionality was also calculated by Domenech and Velankar for their glass–polymer system as between 1.79 and 1.98 depending on the method used [38].

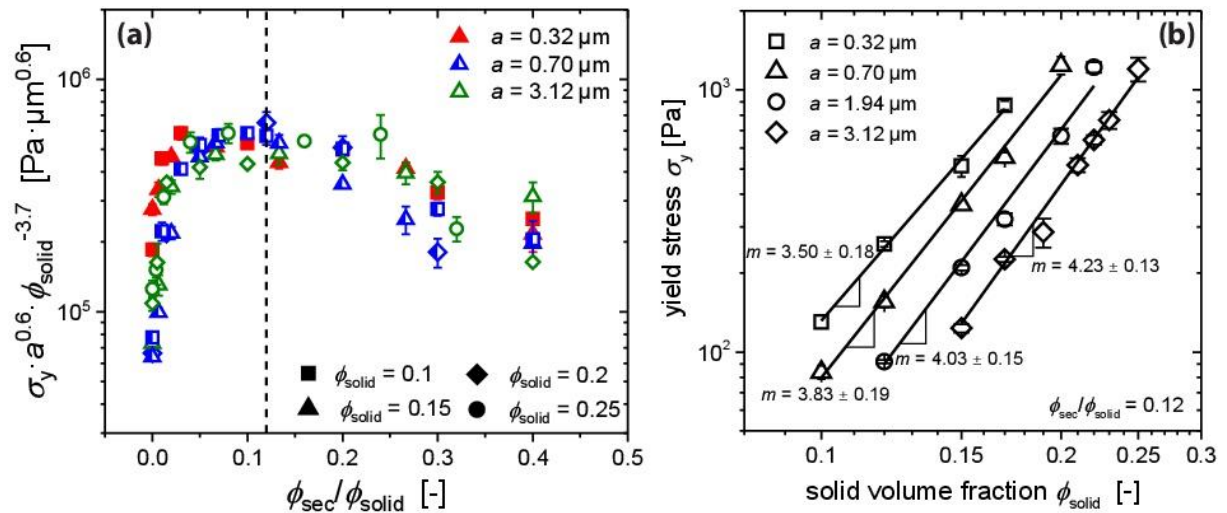


Figure 2.6 (a) Yield stress master curve for Al_2O_3 -based capillary suspensions. Different symbols represent varying solid volume fractions and symbol fillings and color signify different particle sizes. The dashed line defines the position of the yield stress maximum at $\phi_{solid}/\phi_{sec} = 0.12$. (b) Yield stress σ_y of Al_2O_3 -based capillary suspensions as a function of the solid volume fraction ϕ_{solid} at a fixed ratio of $\phi_{solid}/\phi_{sec} = 0.12$ for the four different mean particle radii. Reprinted with permission from Bossler et al. [50] Copyright 2018 AIP Publishing.

This concept of two different dimensions was expanded by Bossler et al., where two different fractal dimensionalities were measured from either yield stress or oscillatory shear data. The network backbone dimensionality of $D = 1.86 - 2.05$ was calculated from the yield stress (as shown above) using the scaling model from Piau et al [51]. An intrafloc dimension with $D = 2.57 - 2.74$ was calculated from the oscillatory data using the scaling model of Wu and Morbidelli [52]. This discrepancy was explained by the inhomogeneity of the microstructure of the capillary suspensions as shown in Figure 2.7 [50]. The fractal dimension calculated with the Piau et al. model is expected to represent the structure of the network backbone, whereas the model from Wu and Morbidelli describes the fractal dimension inside the aggregates. Due to the locally higher particle volume fraction and more compact structure, the floc dimension is much higher than the backbone dimension [50]. This inhomogeneous structure was confirmed with confocal images of the network and flocs [50].

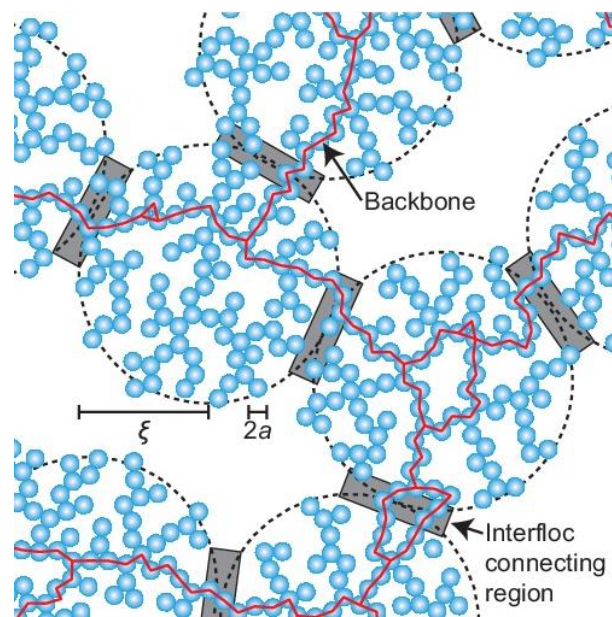


Figure 2.7 Schematic drawing of capillary suspension networks showing the percolation of individual flocs, each with a radius a . The yield stress measurements are dominated by the weak interfloc connecting regions (network backbone), and the shear modulus is dominated by the structure of the flocs themselves. Reprinted with permission from Bossler et al. [50] Copyright 2018 AIP Publishing.

In addition to the parameters described above, which gives us several methods to tune and to control capillary suspensions, we must also consider the preparing and mixing conditions and their influence on the rheological properties of the pastes. Bossler et al. showed that the yield stress and shear moduli depend on the size and distribution of secondary phase droplets created during sample preparation [14]. In this paper, they used different preparation conditions for several different pendular state model systems. Using the dissolver stirrer to turbulently mix the capillary suspensions, the stirring speed and stirring time were varied. For the network in the pendular state, increasing mixing speeds lead to better droplet breakup, but spherical agglomeration was favored at longer times. These changes were monitored by changes in the yield stress with confirmation from microscope images. These suspensions were subsequently mixed with a ball mill where the mixing time was varied. This additional mixing was observed to be beneficial for the resulting sample strength with a plateau in the strength reached after 9.5 h [14]. Pre-emulsification of the secondary fluid in the bulk fluid, before addition of the particles, was also tested. Here, the conditions during emulsification controlled the properties of the final suspensions. This method has also been used by Domenech and Velankar as a way to mix and homogenize their samples [27]. Indeed, both Bossler et al. and

Domenech and Velankar show that enhanced droplet breakup of the secondary fluid leads to stronger particle networks with more homogeneous network structures [14,27]. The structure and strength of the created suspension systems depend strongly on the sample preparation method and the energy input during mixing of the sample [14]. Koos and Willenbacher carried out studies to investigate the configuration of the particulate network and its influence on the rheology of the capillary state suspensions [36]. They determined that the pastes in the capillary state had a sample-spanning network composed of clusters of particles surrounding secondary fluid droplets. The simulation, which varied the three-phase contact angle and assumed spherical particles as well as a monomodal particle size distribution, predicted changes to the yield stress with added secondary fluid. These networks should have a lower yield stress compared with the pendular state because of the decreasing energy of these clusters with increasing contact angle. These clusters form when multiple particles come into contact with a drop and can only relax into the lowest energetically favored state when the drop is completely surrounded by particles. Creating these clusters occurs with increasing energy input during mixing. A strong increase in yield stress was measured with increasing stirring speeds at a single stirring time and at longer times for a single speed using a turbulent dissolver stirrer [14]. The corresponding standard deviation between measurements decreases, indicating a more homogeneous structure, particularly when faster stirring speeds are used. This influence of the stirring speed is stronger for the capillary state than for the pendular suspensions [14]. During mixing, however, existing clusters break leaving drops sitting on the particle surface. These drops, shown in the right-hand image in Figure 2.1, do not move around the droplet and combine with their neighbors due to the wetting angle $> 90^\circ$ [9,36]. They do not take part in the structure formation or contribute to the yield stress. They may, however, cause the aging in capillary state suspensions. This aging was detailed in the work of Koos et al. where a change in the rheological behavior was observed for long time intervals [53]. The droplets may move and cause rearranging of the clusters under oscillatory shear, giving rise to the assisted aging in these capillary suspensions systems [9]. In this review and in the experimental paper with Yang et al., Velankar looked at the various microstructures that could be created with different fractions for particles and liquids [41,54]. They demonstrated that it is possible to produce porous polymer blends with different morphologic structures. These structures ranged from the pendular state suspensions outlined earlier as well as large, interfacially jammed bicontinuous structures. These structures form when the particle loading is above 20% and the contact angle is close to 90° . The amount of wetting fluid should be slightly less than the non-preferentially wetting fluid.

2.5 Perspectives and conclusion

Capillary suspensions have been demonstrated to be beneficial for the creation of smart materials. It is possible to create a porous material with either polymeric or sintered bridges where the desired properties, such as porosity and pore sizes, can be adapted for specific applications. The incorporation of a hydrogel can even be used to tune these properties with temperature. Capillary suspension pastes can be used as precursors in capillary foams [55], glass filters [43], and sintered ceramics [22,23,35]. These porous materials are produced by using a binding secondary fluid, like PEO or a sucrose solution. The secondary fluid crystallizes during the subsequent debinding process and serves as a local sintering assistant. It keeps the particles close to each other and provides and improves the sintering between the particles. The final material properties of the porous bodies can be controlled very easily by varying the amount of the secondary fluid. With increasing amounts of the secondary phase in the region $\phi_{sec} = 0 - 2.5$ vol%, the porosity can be increased from 43% to 55%. Meanwhile, the pore size distribution in this region becomes broader from the monomodal distribu-

tion at small pores around 10 μm to a broad size distribution larger pores up to 40 μm . This implies that using capillary suspensions, the structure of ceramic materials can be tuned and adapted for desired application only by variation of the amount of secondary fluid. It should be possible to further tune the structure of these porous bodies, decoupling the pore size from the porosity, by adapting the mixing conditions, contact angles, and particle shapes. While these properties are so far superior to the porous bodies created using monomers or polymeric solutions, the structure of the bridges and the resulting porous material can be preserved during the solidifying process in the polymeric route. Shrinkage during processing still causes problems for sintered materials. While the general wet network structure is preserved in these sintered bodies, the solid material shrinks during debinding and sintering [24]. This is a drawback, which needs more investigation at this moment. A further push toward systems that can be tuned with external stimuli, such as the hydrogel bridging fluid of Das et al. [37], is expected in the future. A new way to create extraordinary properties was recently investigated by Bharti et al., where they used the capillary bridging between magnetic nanoparticles coated with a liquid lipid shell to create the assembly of ultraflexible microfilaments and network structures [56]. The capillary and magnetic forces allowed these systems to be restructured after external stimuli, which could be perfectly applied in micromanipulators, microbots with ultrasoft joints, or even magnetically self-repairing gels [56]. This push toward the use of new materials must be combined with an increased flexibility in the choice of the bulk and bridging fluids. Dunstan et al. [30] found a way to tune the wetting effects by mixing a hydrophobizing agent into the bridging fluid during the formation of capillary suspensions, as shown in Figure 2.8.

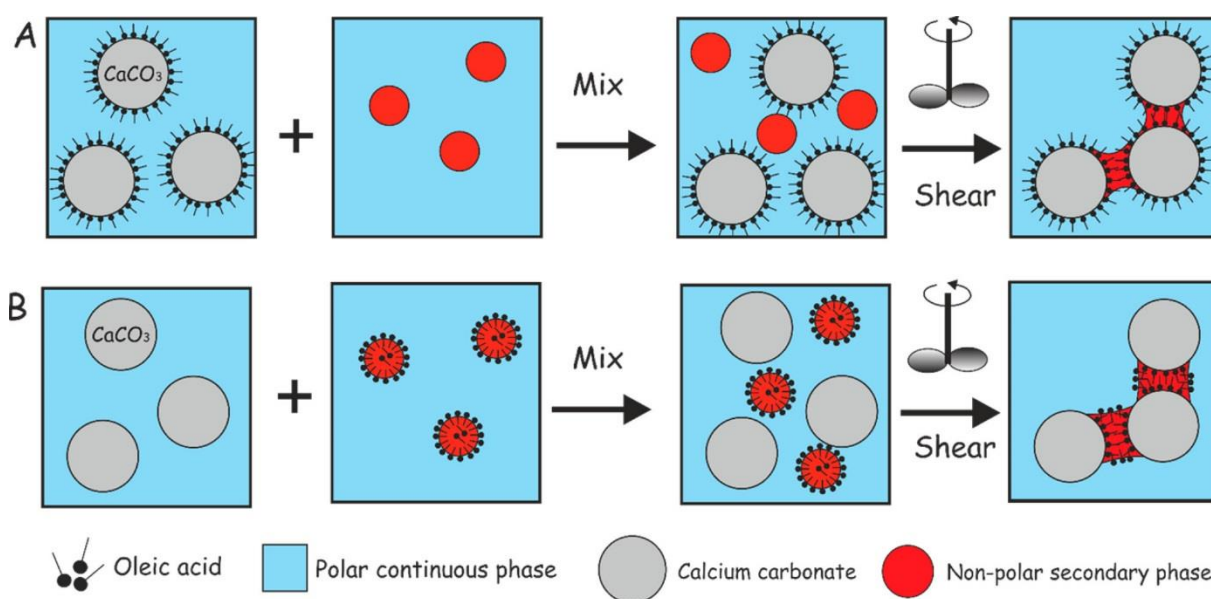


Figure 2.8 In situ hydrophobization of calcium carbonate particles in a capillary suspension. Processing route to create capillary suspensions using (a) pre-hydrophobized calcium carbonate with unmodified non-polar secondary phase and (b) in situ hydrophobization of calcium carbonate using modified non-polar secondary phase. Reprinted with permission from Dunstan et al. [30] Copyright 2018 American Chemical Society.

Dunstan et al. demonstrated two processes to form capillary suspensions from calcium carbonate particles dispersed in a polar liquid phase (e.g., glycerol or water). In the more traditional method, the non-polar secondary fluid is to add to the calcium carbonate, which was pre-hydrophobized by oleic acid, suspended in a polar continuous phase [Figure 2.8 (a)]. As shown in Figure 2.8 (b), the oleic acid can be mixed into the non-polar secondary phase, which is then added to the suspension of untreated particles in the polar solvent. In both cases, the oleic acid transforms changes in the contact

angle and wetting properties [30]. This method opens up possibilities for increasing the number of particle–fluid combinations, particularly to create capillary suspensions where water is used as the bulk fluid, opening up new possibilities for environmentally friendly materials. This in situ hydrophobization can also be used to create more capillary state suspensions. Up until now, suspensions, where the secondary fluid does not preferentially wet the particles, have not been used in the material design. The unique structure of these capillary state particle networks and the drops on the surface, which give rise to the observed aging behavior, may open up new areas and these structures should be incorporated into future designs of smart materials.

2.6 Acknowledgments

The authors would like to acknowledge the financial support from the European Research Council under the European Union’s Seventh Framework Program (FP/2007–2013)/ERC Grant Agreement no. 335380.

3. Radical polymerization of capillary bridges between micron-sized particles

- Full title:** Radical polymerization of capillary bridges between micron-sized particles in liquid bulk phase as a low temperature route to produce porous solid materials
- Authors:** Katharina Hauf, Kamran Riaz, Norbert Willenbacher, Erin Koos
- Status:** published
- Bibliographic data:** Colloid Polym Sci (2017) 295: 1773. <https://doi.org/10.1007/s00396-017-4149-y>

Copyright 2017, Springer-Verlag GmbH Germany. Reproduced with permission. The text has been adapted in this thesis to change the citation and figure numbering. Additionally, some symbols have been modified to confirm with the other chapters.

Abstract

We present a generic and versatile low temperature route to produce macro-porous bodies with porosity and pore size distribution that are adjustable in a wide range. Capillary suspensions, where the minor fluid is a monomer, are used as pre-cursors. The monomer is preferentially located between the particles, creating capillary bridges, resulting in a strong, percolating network. Thermally induced polymerization of these bridges at temperatures below 100 °C for less than 5 hours and subsequent removal of the bulk fluid yields macroscopic, self-supporting solid bodies with high porosity. This process is demonstrated using methyl methacrylate and hydroxyethylmethacrylate with glass particles as a model system. The produced PMMA had a molecular weight of about 500.000 g/mol and dispersity about three. Application specific porous bodies, including PMMA particles connected by PMMA bridges, micron-sized capsules containing phase change material with high inner surface, and porous graphite membranes with high electrical conductivity, are also shown.

3.1 Introduction

Solid porous media are found in a wide range of applications such as in building materials, e.g. porous cement and concrete that are lighter and allow airflow [57], as well as porous pills [58] and pellets with a high surface area [59,60]. Controlled porosity is also very important in separation devices such as filters, membranes and microsieves. Depending on the requirements for the separation process, such as micro-, ultra-, nanofiltration, pervaporation, reverse osmosis or gas separation, there is a huge variety of membrane types made from different materials [61]. Producing highly porous media can be realized utilizing different techniques depending on the materials. Glass and other inorganic materials can be directly sintered using particle network formation [22,43] or solution casting [62]. While sintering is also employed in thermoplastics, like ultra-high-molecular-weight-polyethylene (UHMWPE) and polytetrafluoroethylene (PTFE) for polymeric membranes [63], other methods can also be used such as stretched films [64–66], nucleation track [67], phase inversion [61,63,67–69], extrusion [70], interfacial [71–73] and plasma polymerization [69,74] or emulsion-templated porous polymers [75]. Each method can produce a range of pore sizes and porosities. Stretching produces bodies with porosities of 90% and very small pore sizes of 0.11 μm [64]. Thermal

sintering can yield bodies with pore sizes up to 25 μm and a porosity of 77% [23]. Unfortunately, these methods can only be employed for a limited range of materials, e.g. PTFE for filter media, may require a high temperature, e.g. sintering, or require large amounts of organic solvent, e.g. phase inversion. Nearly every method also needs numerous processing steps and may be time consuming. An alternative way to produce porous polymeric media is to use foams and emulsions stabilized by colloidal particles [76], or particles as sacrificial templates. This method can produce membranes with a very high porosity and narrow pore size distributions of approximately 310 nm [77]. In the work of Feng and Goedel [77], a method is presented where silica particles are used to create porous materials by dissolving the particles with hydrofluoric acid to keep only the polymeric scaffold [77]. A major disadvantage of this method, and sacrificial templates in general, is the additional step to remove the particles, which is done here using an acid that has a significant health risk and may not be completely removed from the membrane. Additionally, a porous and hybrid material made with reactive particles cannot be manufactured with this method. A processing time of almost two days is also a disadvantage of this method is to be adapted to an industrial scale. There have been other investigations using particles as a wall material to produce porous membranes, for example with wet granular media as a precursor. Hemmerle et al. [78] used this method for local agglutination of micron-sized particles where glass beads (diameter 55 to 2040 μm) were mixed with polydimethylsiloxane (PDMS) and a curing agent in a mortar with a pestle and afterwards compressed into a desired shape. To crosslink the PDMS between the particles, samples were heated for 14 hours at 75 $^{\circ}\text{C}$. While Hemmerle et al. showed very nicely how the bulk material properties could be varied by changing the number and size of particles and bridging material, they were only able to produce samples with a narrow range of porosities between 41% and 47%. Another example was presented by Kiesow et al., where bicontinuous composite membranes were made out of a zeolite monolayer and diurethane dimethacrylate (HEMATMDI) as monomer [79]. Capillary forces between the zeolite particles at the air-monomer-water-interface kept the particles together. However, the porosity in this system only results from the porous structure of zeolite with pore sizes 4 to 5 \AA . This method does not offer a clear way to control the pore size, porosity or associated physical properties. Furthermore, the porous layer of these membranes can be only a single particle layer thick.

Therefore, we present a new method using capillary suspensions as a precursor for porous media with a defined porosity and pore size that can be manufactured at a temperature below 100 $^{\circ}\text{C}$ with less time and effort than existing methods. Capillary suspensions are formed by adding a small amount of a secondary fluid that is immiscible with the bulk fluid phase to a particle suspension [13]. The rheological properties can be tuned in a wide range. E.g., the yield stress can be increased by several decades as the mixture transforms from fluid-like to gel-like behavior or from a weak to a strong gel. The change in the strength of these capillary suspensions arises due to the capillary forces between micron-sized particles, which lead to the formation of a percolating particle network. This network and the bridges between the particles have previously been directly visualized with a confocal microscope [9]. There are two extrema for the shape of the capillary bridges between the particles in the suspension depending on the three-phase contact angle $\theta_{S,B} > 90^{\circ}$, that the secondary fluid S makes against the solid when surrounded by the bulk fluid B. If the secondary fluid preferentially wets the particles ($\theta_{S,B} < 90^{\circ}$), the system is arranged in the pendular state and the particles are directly connected by capillary bridges, which lead to a sample-spanning network. In contrast, the system is in the capillary state with contact angles $\theta_{S,B} > 90^{\circ}$, where particle clusters are formed. The particle networks in the pendular state tend to be stronger than in the capillary state with the same solid-liquid-liquid-system [9,14]. This method has already been used to produce porous materials

where the particles are either sintered or a reactive epoxy resin is used as the secondary fluid, finally resulting in a solid porous body [23]. In this latter case, a porous (60 – 75% porosity), lightweight and conductive graphite-based material with a narrow pore size distribution ($d_{50} = 15 \mu\text{m}$) was produced. A similar method was shown by Domenech et al. using a ternary mixture of polyisobutylene, polyethylene oxide and silica particles [40]. A drawback of using epoxy or PEO are the limited options regarding control of mechanical as well as other physical or chemical properties. This paper presents an optimized way to solidify capillary bridges between micron-sized particles in a liquid bulk using a monomer as the bridging fluid. The capillary suspension is then heated under defined conditions to polymerize the bridges. A porous body, with porosity > 50%, remains after the bulk fluid is removed. The resulting network consists of particles that are interconnected by polymeric bridges and has been demonstrated here for several fluid combinations. The characteristic dimension of these bridges is on the order of microns, i.e. approximately 100 times larger than the radius of gyration R_g of the produced polymer molecule. Therefore, the polymer is not confined and the resulting polymer is equivalent to bulk polymerization [80,81]. However, as in suspension polymerization, the heat transfer should be different from bulk polymerization. In this paper, a proof of concept was made using glass spheres as solid phase. This enabled an easy extraction of polymeric bridges needed for further analysis. A general chemical characterization of the polymeric bridges, made from poly(methyl methacrylate) (PMMA) with benzoyl peroxide (BPO) as initiator at temperatures below 100 °C and polymerization times below 5 h was completed. Chemical composition and molecular weight distributions of the polymeric bridges as well as reference PMMA samples are compared and discussed. Finally, simplified application-specific bodies using different particles and monomers are shown.

3.2 Experimental Section

3.2.1 Materials

Hollow glass spheres (iM16K and iM16K OTES) were provided by 3M Deutschland GmbH (Neuss, Germany) with a diameter $d_{50} = 20 \mu\text{m}$ (with $d_{3,10} = 12 \mu\text{m}$ and $d_{3,90} = 30 \mu\text{m}$) and a density of 0.46 g/cm³. They had a hydrophilic (iM16K) or hydrophobic (iM16K OTES) surface (see Figure S3.1 and S3.2 in the supplementary information). The choice of fluids was made to enable simple handling, the possibility of direct polymerization in the capillary bridges and simple chemical analysis of PMMA. The other material systems were chosen to verify the method and to demonstrate the applicability to different materials. The focus of this publication lay on the polymerization and chemical analysis. Further experiments with other material systems were carried out by other researchers from our working group, i.e. on the influence of interfacial tension ([82], Figure 49) and three-phase borderlines [9]. The monomers were methyl methacrylate (MMA) ($\geq 99\%$, Carl Roth) with a density of 0.94 g/cm³ and hydroxyethylmethacrylate (HEMA) ($\geq 99\%$, Sigma-Aldrich) with a density of 1.07 g/cm³. Both monomers were used as secondary phases. The initiator for both monomers was benzoyl peroxide (BPO) (75% water remaining Luperox A75, Sigma-Aldrich). Distilled water and paraffin oil (low viscosity, Carl Roth) were used as bulk fluids. All items were used as received. For the application routes, we used: a) poly(methyl methacrylate) particles (Altuglas BS 130) from Altuglas International (Arkema Group, La Garenne-Colombes, France) with a $d_{50} = 20 \mu\text{m}$ and a density of 1.19 g/cm³; b) Phase change material capsules (Micronal DS 5038 X), consisting of a PMMA shell and a core filled with paraffin wax, provided by BASF SE (Ludwigshafen, Germany) with $d_{50} = 5.2 \mu\text{m}$ particles and a density of 0.98 g/cm³; and c) graphite particles provided by China Steel Corporation (Kaohsiung, China) with a primary particle diameter $d_{50} = 7.8 \mu\text{m}$ and a density of 2.27 g/cm³.

3.2.2 Sample preparation

The solid-liquid-liquid combinations we used are shown in Table 1.

Table 1 Composition of capillary suspensions used in this paper. Copyright 2017, Springer-Verlag GmbH Germany. Reproduced with permission.

Solid phase	Bulk fluid	Secondary fluid	Initiator
hydrophobic glass (iM16K OTES)	dist. water	MMA	BPO
hydrophilic glass (iM16K)	paraffin oil	HEMA	BPO
PMMA (Altuglas BS130)	dist. water	MMA	BPO
paraffin wax, acrylate shell (Micronal DS)	dist. water	MMA	BPO
graphite	paraffin oil	HEMA	BPO

To prepare the capillary suspensions, the particles were dispersed in the bulk fluid with a high-shear dissolver stirrer (35 mm diameter for confocal microscopy and 60 mm diameter for the polymerized samples) at 1200 rpm for 10 min with a solid volume fraction $\phi_{glass\ spheres} = 40\ vol\%$, $\phi_{PMMA} = 25\ vol\%$, $\phi_{Micronal} = 35\ vol\%$ and $\phi_{Graphite} = 20\ vol\%$. The monomer and initiator were premixed with a magnetic stirrer at 500 rpm for 5 minutes where the concentration of initiator in monomer was varied between 5, 10 and 15 mg/ml. This secondary liquid phase was added to the suspension and mixed first at 2000 rpm for two minutes. Then the speed was decreased to 800 rpm for 5 minutes of additional mixing. The amount of secondary fluid was 0, 1, 2, 4 or 6% (12% for graphite/HEMA) by volume (ϕ_{sec}). This procedure and the subsequent polymerization are shown in Figure 3.1.

3.2.3 Polymerization procedure

The prepared capillary suspensions were filled in silicone baking molds (35 mm diameter, 5 mm height). They were then polymerized in the mold, which was placed inside a preheated desiccator set in a laboratory oven.

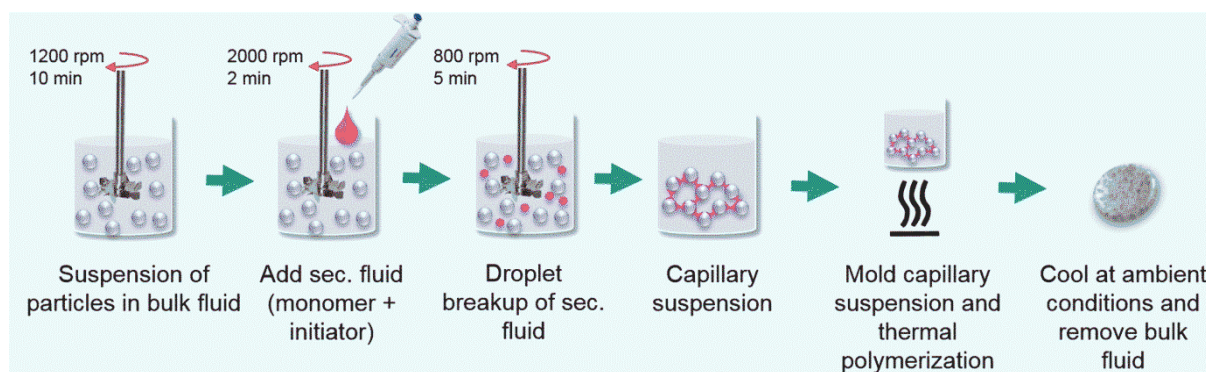


Figure 3.1 Processing route for preparation of capillary suspensions and solid porous materials. Figure reprinted with permission from Springer (Colloid and Polymer Science), copyright 2017.

The samples were placed in the desiccator at a starting temperature close to the desired polymerization temperature. The temperature was confirmed with a thermometer inside the oven. Polymerization was done at temperatures of 60 °C, 85 °C and 120 °C and polymerization times of 1.5, 2.5, 3.5, and 5 hours were employed. The solid samples with MMA as secondary phase were cooled overnight at room temperature under the hood to interrupt the polymerization and dried afterwards at 74 °C in an oven for 4 h. Any residual BPO and MMA is expected to be unaffected by this drying step due to the low diffusion within the solidified sample. Samples with HEMA were cooled overnight at room temperature and placed on a paper towel for 1 day to remove most of the paraffin oil. Then, the remaining paraffin oil was extracted for 4 h with n-hexane (VWR Chemicals). For each sample, references were prepared using the same amount of monomer and initiator in an open glass vial, which was added to the oven with the other samples for polymerization under identical polymerization conditions.

3.2.4 Characterization

Yield stress measurements were performed with the stress-controlled rheometer Haake Mars II (Thermo Scientific, Karlsruhe, Germany) using a plate–plate geometry (35 mm diameter, 0.2 mm gap height) by increasing the shear stress stepwise in a range from 0.1–1000 Pa. The temperature for all measurements was $T = 20 \pm 0.5$ °C. A sandblasted lower steel plate and a sandblasted upper titanium plate (surface roughness for both plates ~ 1.2 μm) were applied to reduce wall slip during the measurements. The yield stress was defined using the tangential method [43].

The capillary bridges between the glass spheres in the wet state prior to polymerization were imaged using a confocal microscope (TCS SP8, Leica Microsystems) with a 552 nm laser. These samples were prepared without the initiator and a fluorescence dye was added to the monomer. Nile red (Sigma-Aldrich, Steinheim, Germany) was used for MMA samples and rhodamine B (Sigma-Aldrich, Steinheim, Germany) for the HEMA system. Glycerin was added in a ratio of 61/39 %wt. (glycerin/water) to adapt the refractive index of MMA and water.

The samples were also inspected after polymerization using an environmental scanning electron microscope (ESEM-mode at $p = 70$ Pa, Quanta 650 FEG, FEI, Hillsboro, Oregon, USA) and images were taken from a fractured section of the solid samples. The samples were sputtered with a mixture of platinum and palladium. Energy-dispersive X-ray spectroscopy (EDX) was also carried out on the fractured samples. Micro-tomography was performed at Freudenberg SE (Weinheim, Germany) with a computer tomography device (General Electric, Phoenix X-Ray VTOME|X 240 D) using a 240 kV direct X-ray.

The samples made with PMMA as polymeric bridges and the corresponding reference samples were characterized to determine the effect of varying polymerization conditions using size exclusion chromatography (SEC) and nuclear magnetic resonance spectroscopy ($^1\text{H-NMR}$). The samples were prepared by dissolving the solid porous material in tetrahydrofuran (THF, Sigma-Aldrich) in an ultrasonic bath for 1 h. The medium was filtered (1.6 μm pore size, Por. 4/5) to separate the glass spheres, and then the THF was evaporated in a rotation evaporator (Büchi) at 55 °C and 385 mbar. Afterwards, the remaining polymer was dried overnight in a laboratory oven at 70 °C and then redissolved in a solvent at a specific concentration depending on the following measurement.

The molecular weight distribution of the polymeric bridges and reference polymers were measured using size exclusion chromatography (SEC), which was operated with THF (Scharlan, SEC-grade) as

solvent and calibrated with linear PMMA standards. The instrument consists of an Agilent 1100 pump and the sample separation was achieved via two linear columns provided by PSS (SDV-Lux -103 Å and 105 Å and 5 µm). It was equipped with an Agilent 1200 differential refractive index (DRI) detector. Measurements were performed at 25 °C with a flow rate of 1 ml/min. The polymer concentration was approximately 2 mg/ml and the injection volume was 100 µl. The functional groups were determined with ¹H-NMR (400MHz, CDCl₃) carried out using a Bruker Avance III Microbay 400 MHz (typically 1024 scans). Chloroform (Deutero, 99.8%) was used as a solvent at a polymer concentration of approximately 15 mg/ml.

The porosity ε of the solid bodies was calculated using the ratio of the raw density of the sample and the skeletal density.

$$\varepsilon = 1 - \frac{\rho_{raw}}{\rho_{skeletal}} \quad (5)$$

The raw density of the sample was calculated as the ratio of sample weight and volume. The skeletal density was measured using a Multivolume gas pycnometer (Modell MP 1305 with Helium) at 20 °C. The flexural strength characterizing the mechanical strength of the solid porous materials was measured using a 4-point bending test on a custom-made device following DIN EN 843-1.

3.3 Results and discussion

3.3.1 Rheological behavior

The prepared suspensions showed a nearly two decade increase in yield stress with increasing secondary phase content as shown in Figure 3.2.

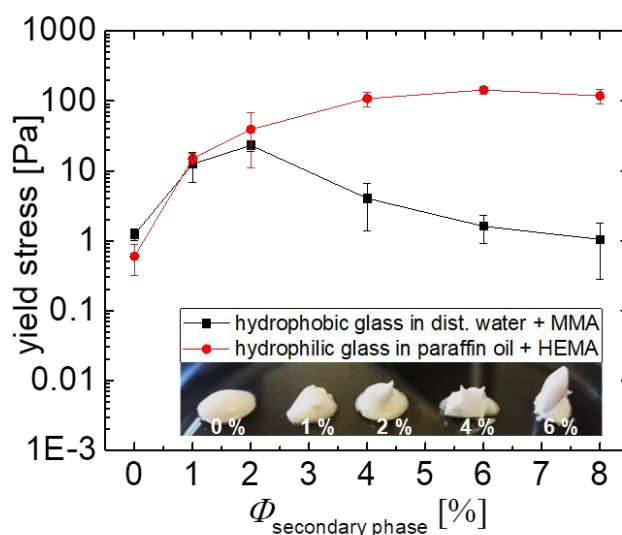


Figure 3.2 Yield stress of capillary suspensions made from hydrophobic glass spheres ($\phi_{solid} = 40$ vol%) in distilled water with MMA as secondary phase (black squares) and hydrophilic glass spheres ($\phi_{solid} = 40$ vol%) in paraffin oil with added HEMA (red circles). The inset images show the consistency of the HEMA sample. Lines are to guide the eye. Figure reprinted with permission from Springer (Colloid and Polymer Science), copyright 2017.

This increase indicates the creation of a sample-spanning network caused by the strong attractive capillary forces between particles. The high yield stress implies the existence of a percolated particulate network, which should be strong enough to resist destruction during molding and polymeriza-

tion so that a body with high open porosity can be formed. Furthermore, the high yield stress implies the presence of a network backbone, which can transmit forces so that the final porous body should also have a high Young's modulus [83]. The sample with hydrophilic glass spheres shows a continuously increasing yield stress with increasing amount of added HEMA. The sample with added MMA, however, has a maximum yield stress at $\phi_{sec} = 2$ vol%. The existence of such a maximum can indicate the transition from the pendular to the funicular state as larger agglomerates are formed with increasing amounts of secondary liquid [9,84]. This transition typically occurs at $\phi_{sec}/\phi_{solid} \approx 0.1 - 0.2$ depending on the contact angle and coordination number [9,27,54,62]. Our results for the glass/MMA system are consistent with these earlier findings. The capillary suspensions made from hydrophilic glass spheres with paraffin oil as the bulk liquid and HEMA as secondary fluid were stable and homogeneous for more than 5 days. This stability is typical for a capillary suspension. However, phase separation was observed after 10 minutes for the system with hydrophobic glass spheres, water as bulk fluid, and MMA as secondary fluid phase. For this MMA sample, the particles with the dyed MMA showed creaming behavior.

3.3.2 Visualization before and after polymerization

To confirm if the increasing yield stress was caused by the capillary force and to determine if such agglomeration might occur, the microscopic configuration was imaged to visualize the existence of capillary bridges and their shape between the particles. A capillary suspension with MMA as secondary fluid in the wet, unpolymerized state as obtained from confocal microscopy is shown in Figure 3.3.

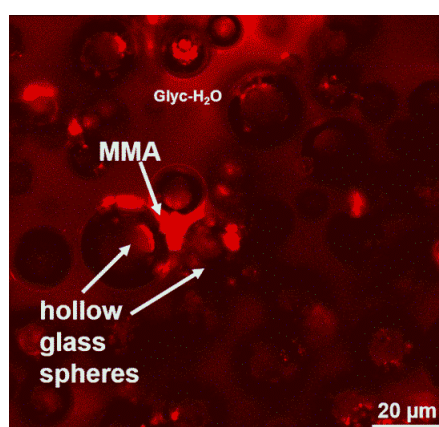


Figure 3.3 Confocal image slice for the hydrophobic hollow glass spheres in glycerin/water mixtures (61/39 %wt.) with 6 vol% added MMA. The MMA is dyed (red) and the other components are undyed. Figure reprinted with permission from Springer (*Colloid and Polymer Science*), copyright 2017.

This sample used a water/glycerine mixture as a bulk fluid to match the refractive indices and 6 vol% dyed MMA as the secondary phase. The sample with 2% MMA was not visible because of the low fraction of secondary phase reducing the overall amount of fluorescent dye. The particles in this image are visible as dark circles because of their hollow character. The MMA (red) is located in between the particles and creates bridges. Most of these bridges appear to join more than two particles, forming a funicular network. While there may be a large number of binary interactions, which can be more difficult to image due to their smaller volume, a small number of these funicular clusters can monopolize a large fraction of the available secondary fluid [9]. The general shape of the specimen can be preserved during the polymerization process as is presented in Figure 4a. Particle distribution within the polymerized samples and shape of individual capillary bridges is shown in Figure 3.4b. In

the samples shown in Figure 3.4, the BPO content was 15 mg/ml MMA and the polymerization time and temperature were 82 °C for 2.5 h. The particles are connected by the polymerized PMMA bridges, which are still located between the particles and still possess a pendular shape. Remarkably, these bridges are not a uniform block of PMMA, but appear to have an irregular texture. This may be due to the shrinkage of the material during the polymerization process. These SEM images also show that the hollow glass spheres have a wide size distribution. This may offer a tunable parameter to control the pore size and porosity of the produced samples [22].

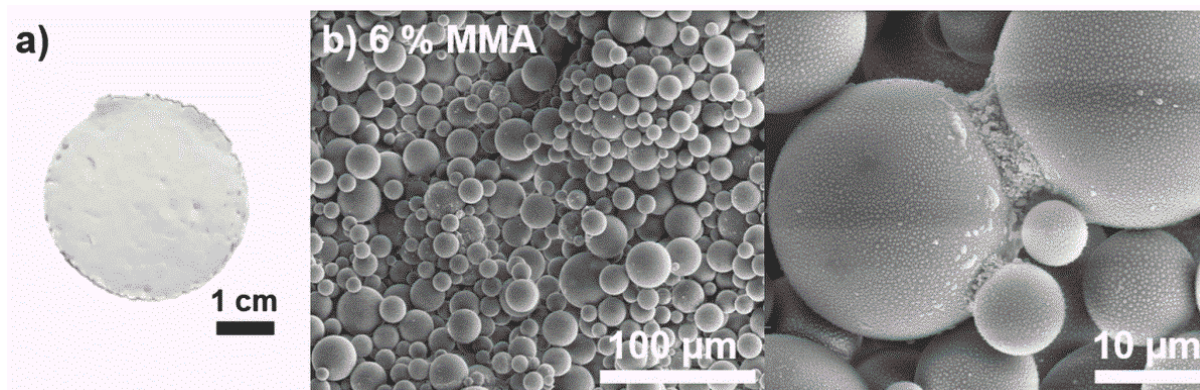


Figure 3.4 Image of a porous solid sample made from hydrophobic hollow glass spheres with PMMA bridges with 6 vol% MMA. b) Corresponding ESEM images of a fractured section of the body and the bridges. The samples were polymerized in water for 2.5 h at 82 °C and the BPO content was 15 mg/ml. Figure reprinted with permission from Springer (*Colloid and Polymer Science*), copyright 2017.

We also tested a second system using hydrophilic glass spheres in paraffin oil with HEMA as the secondary fluid. This system, with dyed HEMA, is shown in Figure 3.5. For this sample, both large clusters (Figure 3.5a) and binary pendular bridges (Figure 3.5b) are visible.

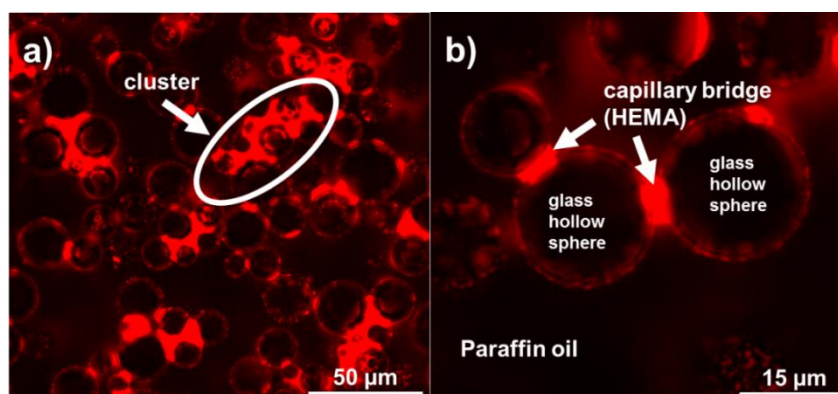


Figure 3.5 Confocal image slice for the hydrophilic hollow glass spheres in paraffin oil with 4 vol% added HEMA. The HEMA here is dyed (red) and the other components are undyed. Figure reprinted with permission from Springer (*Colloid and Polymer Science*), copyright 2017.

Polymerization also works well, if not better, in this system, as shown in Figure 3.6. These two systems demonstrate the versatility of this method where either hydrophilic or hydrophobic particles can be linked together with a judicious choice of the monomer and the bulk fluid. For the HEMA system, the bridges are smooth and clearly defined, though the particles are rough. The atomic composition of both the neck and the particle surface was investigated using Energy-dispersive X-ray spectroscopy (EDX) in the ESEM-mode (Figure S3.5). The bridges do not contain any silicon, just carbon and oxygen, suggesting that the bridges are made from polymer. EDX of the particle surface shows a

mixture of carbon, oxygen and silicon. Note the porosity of the solid bodies is equal to the fraction of bulk fluid in the samples. In contrast to porous sintering materials made from capillary suspensions no collapse of the particle network during drying and debinding or shrinkage during sintering does occur here, i.e. porosity is directly determined by particle concentration. However, for the samples with the highest particle loading a substantial amount of air was entrapped during paste preparation leading to an even higher porosity of the final dry specimen and additional larger pores $> 50 \mu\text{m}$, see μ -CT image in S3.3 (Supplementary information).

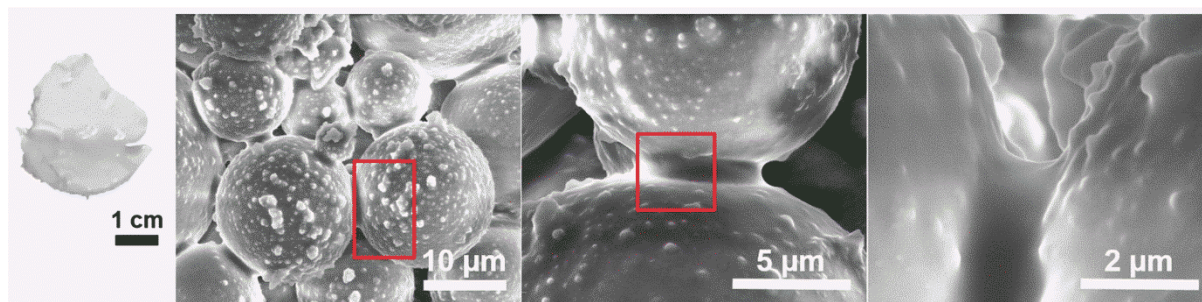


Figure 3.6 Image of a piece of porous solid samples made out of 40 vol% hydrophilic hollow glass spheres interconnected with poly(HEMA)-bridges with an amount of 4 vol% HEMA in the wet state (15 mg/ml BPO, polymerization in paraffin oil at 82 °C for 2.5 h) and corresponding ESEM images of a fractured section. The magnification of the ESEM images increase from left to right. Figure reprinted with permission from Springer (Colloid and Polymer Science), copyright 2017.

3.3.3 Chemical composition of polymeric bridges

Chemical composition of polymerized bridges has been analyzed using $^1\text{H-NMR}$ spectroscopy.

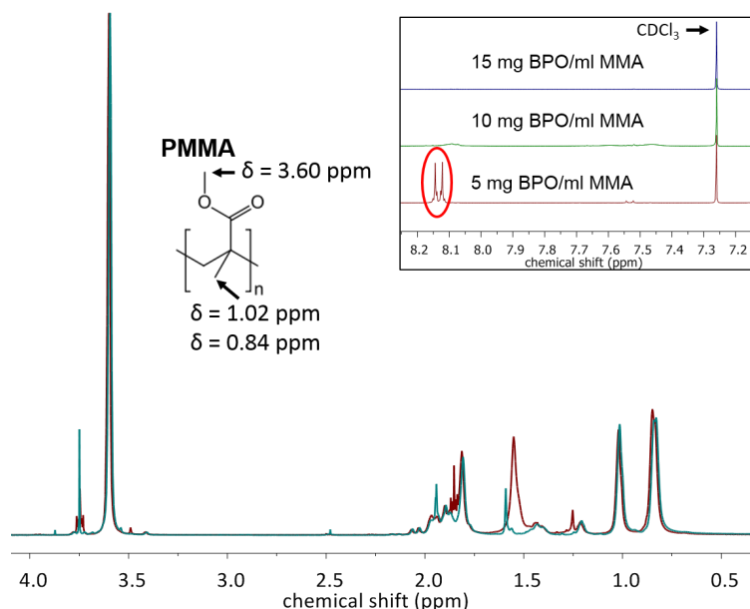
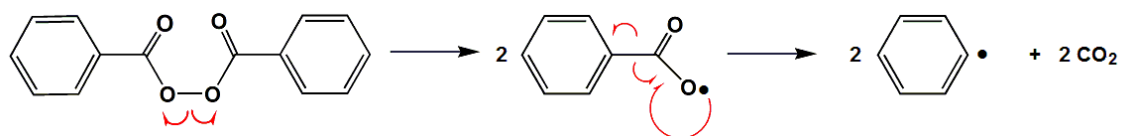


Figure 3.7 $^1\text{H-NMR}$ with the chemical shift for the relevant functional groups for PMMA in the reference sample (green) and the bridges (red). Peaks for PMMA at $\delta = 3.60 \text{ ppm}$, $\delta = 1.02 \text{ ppm}$ and $\delta = 0.84 \text{ ppm}$ are visible in both samples. The latter two peaks provide information about atactic and syndiotactic arrangement of the PMMA chains. The sum of their integral intensity equals that of the peak at $\delta = 3.60 \text{ ppm}$. The peaks in the region between $\delta = 2.2 \text{ ppm}$ and 1.3 ppm are significant for the CH_2 -group [85]. Differences between the bulk and capillary bridge samples occur in this δ -range, which are presumably due to impurities inferred from the preparation of the capillary suspension. Inset box: $^1\text{H-NMR}$ signals corresponding to initiator BPO and solvent CDCl_3 for capillary bridge samples with different initiator concentrations. The samples were prepared with 15 mg/ml BPO for 2.5 h at 87 °C and the spectra were normalized using the chemical shift at $\delta = 3.60 \text{ ppm}$. Figure reprinted with permission from Springer (Colloid and Polymer Science), copyright 2017.

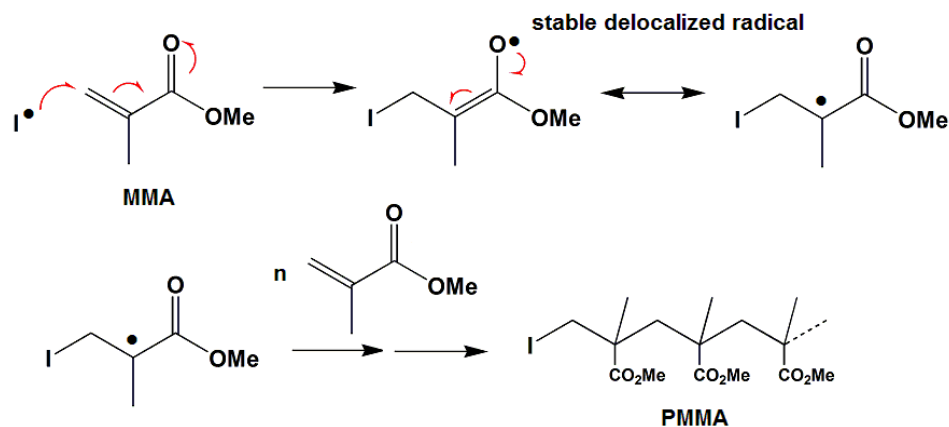
A comparison of the reference sample and material polymerized in the bridges (Figure 3.7) shows that their chemical composition is similar and the main expected signals for PMMA are present in each sample. The peak at 3.60 ppm corresponds to the methylester-group found in PMMA [85]. The peaks in the region between $\delta = 2.2$ ppm and 1.3 ppm are significant for the CH₂-group [86]. The peaks at $\delta = 1.2$ ppm and 0.84 ppm correspond to the cis- and trans-configurations of α -CH₃-group [86], and the sum of their integral intensities should be equal to the intensity of the peak at $\delta = 3.60$ ppm. This was confirmed for each measured spectrum. The insert in Figure 3.7 shows that additional peaks at $\delta = 8.14$ ppm and $\delta = 8.12$ ppm occur for the capillary bridge sample with the lowest initiator concentration of 5 mg BPO/ml MMA. This indicates that not all of the free radicals generated from the BPO initiate polymeric chain growth in this case, but immediate recombination occurs [87]. The pathways for decomposition of the initiator and corresponding polymeric chain growth are explored in the following section.

3.3.4 Degree of polymerization in capillary bridges

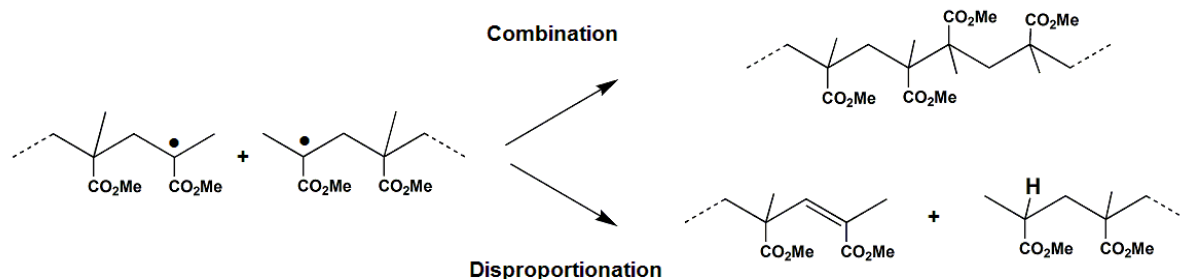
Conventional bulk polymerization is expected to take place in the monomer bridges between the particles. Since the monomeric bridges in the percolated network of particles have a characteristic size $\approx 1 \mu\text{m}$ and are surrounded by a bulk fluid, the anticipated chemical reaction can also be regarded as a type of suspension polymerization. To characterize the molecular weight and dispersity of the polymers synthesized in the bridges, we use the MMA system with hydrophobic glass particles and water as the bulk fluid. BPO was dissolved in MMA to induce a radical polymerization within the capillary monomer bridges. The initiation of polymerization consists of two steps. First, the BPO molecule is decomposed into two radicals, a process that is thermally triggered. Then, the MMA bonds to the initiating radical. This process is shown below. Red arrows with half-heads show where single electrons are shifted.



Either of the radicals, benzoyloxy or phenyl (showed in the following scheme as I: Initiator), can attach to a monomer unit and start a polymer chain. In the chain propagation phase, additional MMA molecules attach to the MMA radicals until chain termination takes place.



The termination is caused by the self-reaction of propagating radicals through combination and/or by disproportionation, where a free electron from a radical is transferred to another chain radical and a new double bond is created.



The kinetics of free radical polymerization lead to a polymerization rate k_d depending on the square root of the initiator concentration [40],

$$k_d \propto \sqrt{[I]} \quad (6)$$

where k_d is related to the initiator half-life $t_{1/2} = \ln 2/k_d$ is defined as the time needed to reduce the concentration of the initiator by half. The half-life for BPO depends on temperature and has a value of 7.3 h at 70 °C, 1.4 h at 85 °C and 20 min at 100 °C [88]. The number average degree of polymerization P_n of the macromolecules produced via free radical polymerization is proportional to the reciprocal square root of initiator concentration [89].

$$P_n \propto \frac{1}{\sqrt{[I]}} \quad (7)$$

Ergo, the molecular weight of the macromolecules obtained by free radical polymerization should decrease with increasing initiator concentration. We determined the dependence of BPO concentration on the resulting molecular weight and dispersity for the polymeric bridges and a reference sample using SEC. Both the reference and the bridges are subjected to identical conditions during polymerization. The dispersity \mathcal{D} is defined as ratio between the weight-averaged molecular mass M_w and the number-averaged molecular mass.

As can be seen in Figure 3.8, the average molecular weight M_w decreases with increasing BPO concentration caused by the increased number of free radicals that are able to simultaneously react with the MMA monomers. This reduction is consistent with the dependence on the initiator concentration, outlined above, where predictions using equation (7) are shown in Figure 3.8 as solid lines. An example molecular weight distribution for a bridge sample extracted after polymerization of a capillary suspension with 40 vol% solid fraction and 6 vol% MMA at 84 °C for 5 h with 15 mg/ml BPO, as obtained from SEC, is shown in Figure S3.4 (see section 3.8. Supplementary information). Similar molecular weight distributions were found for all other investigated samples. As shown in Figure 3.8, the mean molecular weight obtained in the polymerized bridges is, on average, 2.8 ± 0.15 times higher than the values for the corresponding reference PMMA samples. This is qualitatively expected for two reasons. First, the heat transfer in the small bridges, mediated by the surrounding water phase and hollow glass spheres, is lower than in the bulk and the mobility of polymer chains is inhibited due to gelation effects, i.e. the disproportionation is less probable [86]. Second, the high surface-to-volume ratio of the capillary bridges could result in a significant geometrical effect, which causes a mobility barrier for the polymer chains and macroradicals. It was shown in a previous work for sus-

pension polymerization that the molecular weight increases slightly with decreasing polymer particle size [90,91]. The mutual very low solubility could affect the volume of the bridge. On the basis of the confocal and SEM images in this publication, in which one recognizes both the still unpolymerized monomer bridge and the subsequently polymerized capillary bridge, this does not play a major role in this case. It has been found that trace amounts of water, usually by storage in a humid environment, cause the formation of carboxylate bonds at interfaces [92] and the tensile strength of PMMA reduces. For the present system, the changing solubility of water within the monomer and polymer can produce water-rich domains within PMMA, but the impact of these domains on molecular weight is considered unlikely since no change in dispersity was observed. The dispersity remains constant upon initiator variation within experimental uncertainty such that, in both the bridges and reference samples, $\bar{D} = 3 \pm 0.5$ is found.

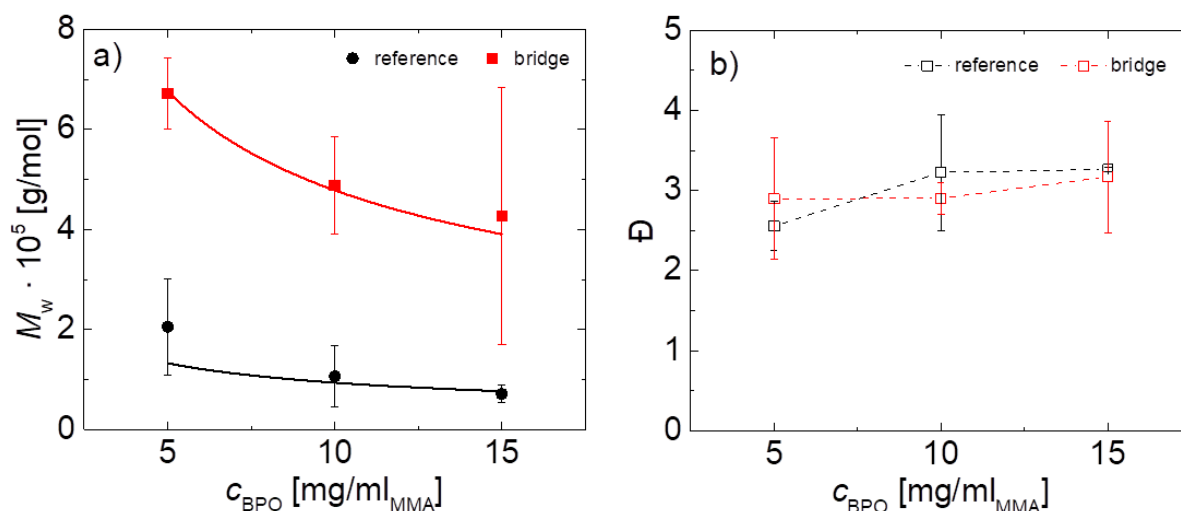


Figure 3.8 Dependence of BPO concentration on molecular weight M_w for polymeric bridges and reference PMMA samples. The solid lines represent the molecular weights predicted by equation (7), with proportionality constants of 15 (bridges) and 3 (reference). b) Dependence of BPO concentration on dispersity \bar{D} for polymeric bridges and reference PMMA samples. Lines are to guide the eye. Both parts show a capillary suspension with 40 vol% hydrophobic glass particles, 6 vol% MMA as secondary fluid and distilled water as the bulk fluid. The polymerization for both the bridges and reference sample occurred at 84°C for 2.5 h. Figure reprinted with permission from Springer (Colloid and Polymer Science), copyright 2017.

In another set of experiments, the effect of polymerization time on molecular weight distribution was investigated. The polymerization time has no significant influence on the average molecular weight M_w of the pure sample and the polymeric bridges at a single temperature of 84°C, but the dispersity seems to decrease slightly, as is shown in Figure 3.9. We can, therefore, use a time of 3.5 h, which is more than twice the half-life of the initiator, as a convenient polymerization time since the PMMA has a sufficiently high molecular weight and a dispersity index less than 3. Again, the average molecular weight of the capillary bridges is about three times higher than for the respective bulk samples. Because of the purification and separation steps needed to extract the polymeric material from the capillary suspension, yield measurements were not possible. Similar results regarding molecular weight distribution were obtained at other polymerization temperatures T in the range of 60 °C and 120 °C with a slight decrease with increasing T (at given BPO concentration and polymerization time) as expected due to the higher rate of initiator decomposition at higher temperatures [88]. According to the half-life $t_{1/2}$ of 7.3 h at 60 °C very long times > 15 h are required to complete polymerization.

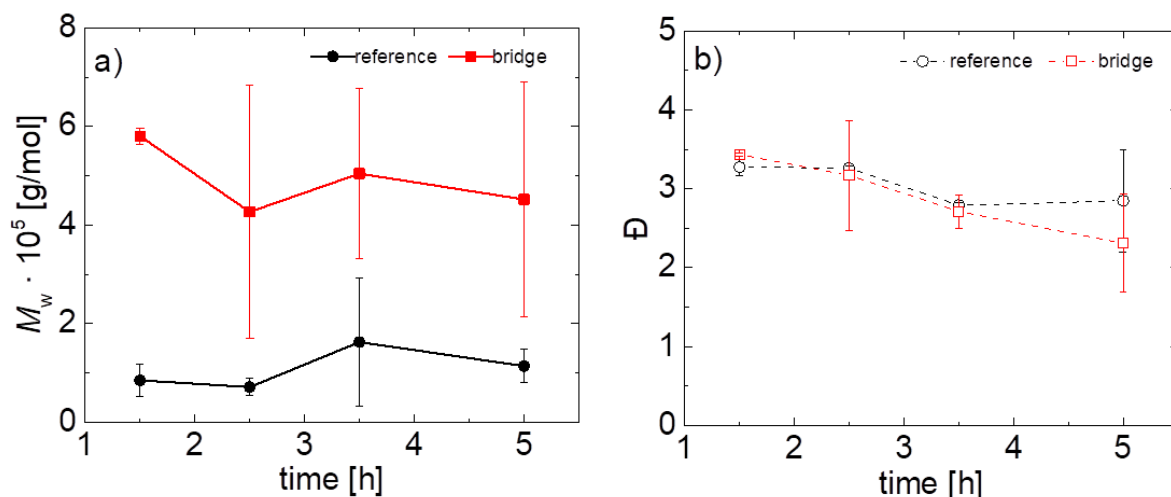


Figure 3.9 Dependence of polymerization time on molecular weight M_w for polymeric bridges and reference PMMA sample. b) Dependence of polymerization time on dispersity \mathcal{D} on polymerization time for polymeric bridges and reference PMMA sample. Lines in a) and b) are to guide the eye. The capillary suspensions were made of 40 vol% solid fraction and 6 vol% MMA with distilled water as the bulk fluid. Each measurement was carried out at 84°C for 2.5 h and with 15 mg/ml BPO. Figure reprinted with permission from Springer (Colloid and Polymer Science), copyright 2017.

With respect to the fabrication of porous solid materials based on capillary suspensions concept, we emphasize that PMMA bridges can be efficiently polymerized at temperatures below 100 °C and the concept can be used even for temperature sensitive particles that might melt or decompose at elevated temperatures.

3.4 Application routes

In addition to the model system with glass spheres, where a chemical reaction between the glass surface and the polymeric bridge can be excluded, we also tested other systems with potential technical relevance. These systems demonstrate both the versatility of this method and show how the properties are modified by the material choices. All of these systems are shown in Figure 3.10.

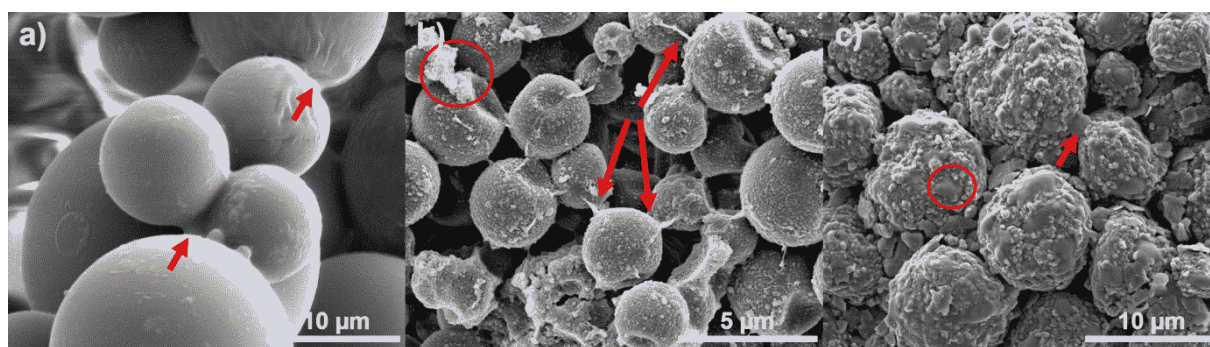


Figure 3.10 SEM images of porous solids made from capillary suspensions with polymerized bridges. Different particles and secondary fluids were used: a) 35 vol% PMMA particles, 3 vol% MMA. b) 35 vol% Micronal DS particles, 3 vol% MMA. c) 20 vol% graphite particles, 12 vol% HEMA. Polymerization was always done at 82 °C for 2.5 h with 15 mg/ml BPO as initiator. Figure reprinted with permission from Springer (Colloid and Polymer Science), copyright 2017.

The first system, shown in Figure 3.10a, is made from a capillary suspension including 35 vol% cross-linked PMMA particles and 3 vol% added MMA including 15 mg BPO/ml MMA as the secondary liquid. The confocal image S3.6 (Supplementary information) reveals that the dyed MMA completely coats the particles since it spreads extremely well on the PMMA surface. While it is not visible in the

confocal image, there remains some MMA that bridges the particles. These bridges are visible in the SEM image (Figure 3.10a), where polymerized bridges are located between the particles (as denoted by the arrows) and lead to a self-supporting membrane with flexural strength of 0.008 MPa at a given open porosity of 79%. We also fabricated porous bodies from micron-sized phase change material (PCM) particles coated with highly crosslinked PMMA. Porous materials made out of small encapsulated PCM particles may be applied as heat exchange materials offering superior heat transfer rates due to the large inner surface. Possible examples include thermally insulating paint or thin thermal interface layers in electrical devices. As shown in Figure S3.7, the dyed MMA coats these particles just as it does for the pure PMMA particles. In Figure 3.10b, string like structures (red arrows) are the polymeric connections between the particles. The red circled structure is likely due to additives as they are also observed on the samples without any added MMA as secondary phase. The stress at failure was measured to be 0.5 ± 0.1 MPa at an open porosity of $48.4 \pm 0.8\%$, which is in the expected range estimated for porous PMMA based on the Gibson-Ashby model for porous materials and mechanical strength data of pure PMMA [93]. A third system made from graphite particles ($\phi_{solid} = 20$ vol%) with HEMA (12 vol%) as secondary phase and paraffin oil as bulk fluid is shown in Figure 3.10c. The pure graphite particles are shown in Figure S3.8. The poly(HEMA) forms the bridges between graphite particles (arrow) and patches on the particles (circle). In this case, the poly(HEMA) is able to preserve a porosity of 60% in the graphite body. More importantly, this body is conductive with a value of 13 mS/cm. The pure powder ($\rho_{bulk} = 0.83$ g/cm³) has a conductivity of 30 mS/cm. If we consider the conductivity divided by the graphite mass in the samples, we can get almost the same conductivity per mass of 7.64 mS/(cm·g) for the graphite-poly(HEMA)-composite as for pure powder with 8.3 mS/(cm·g). This demonstrates that our polymerization strategy enables fabrication of porous hybrid membranes made out of graphite particles and polymeric bridges with high electrical and, presumably, good thermal conductivity.

3.5 Conclusions

Capillary suspensions in the pendular and funicular state can be used as a precursor for local adhesion of micron-sized particles. These solid-liquid-liquid systems are created when a small amount of a liquid, immiscible with the bulk, is added to a suspension. This secondary liquid creates capillary bridges between the particles and results in a strong, percolating network. This method offers a novel way to produce porous bodies by preserving the network structure during the transition from liquid capillary bridge, formed here by a monomer, to a solid polymeric bridge. This method can be realized at temperatures below 100 °C for times less than 5 hours, i.e. it is non-destructive to various kinds of particles. The material properties of the resulting porous sample can be controlled by choosing the particles and monomers as well as the bulk material. We used a model system made of glass spheres, monomer with initiator as secondary fluid, and a bulk fluid that is immiscible with the monomer. Hydrophobic and hydrophilic glass particles with methylmethacrylate (MMA) and hydroxyethylmethacrylate (HEMA), respectively, as capillary bridges were used for this proof of concept. This glass model system allows for a convenient imaging of capillary bridges and separation from the particles for further chemical characterization. The formation of a sample-spanning network was confirmed through yield stress measurements and also through direct imaging using a confocal microscope. The capillary suspensions were polymerized to solidify the capillary bridges and dried to produce solid porous bodies. These were imaged using SEM imaging with EDX analysis of the bridge material and the glass spheres. ¹H-NMR confirmed that polymerization took place and the MMA was successfully converted into polymer. The lowest concentration of 5 mg BPO per ml MMA may cause

incomplete conversion and residual BPO remains in the final polymer. SEC analysis shows that the average molecular weight in the bridges is 2.8 ± 0.15 times higher than the values for the bulk PMMA reference samples. This difference in molecular weight is attributed to the high heat transfer and the large surface-to-volume ratio of the small monomer fluid volumes surrounded by particles and bulk fluid. The molecular weight scales with the reciprocal square root of the initiator (BPO) concentration. This dependence allows the polymer molecular weight in the particle bridges and the corresponding bulk properties to be controlled. The molecular weight shows no dependence on the polymerization time and only a slight decrease with increasing temperature making this method fairly robust. The dispersity is not affected by BPO concentration nor by changes to the polymerization time and temperature. The applicability of the concept to particle systems with potential technical relevance was shown using PMMA particles, PMMA-coated PCM, and graphite particles. In all cases, we could show that the capillary suspensions with polymerizable liquid bridges could be used as precursor to make solid porous materials with customizable features. The solid made from PCM particles had a high porosity, aiding in rapid thermal exchange, and the graphite body was conductive. Possible other applications for this processing route are manifold; both polymeric filter media with defined porosity and chemical properties as well as bio-polymeric materials for medical applications such as soft matrix in the artificial tissue engineering or pharmaceutical processing of drugs could be two potential application routes. For direct application of this method in creating porous bodies, further research is needed to describe the microstructure and the mechanical properties of the polymeric bridges between the particles in order to adjust the physical properties for tailor-made porous materials. In particular, one must be able to control how well the bridge adheres to the particles.

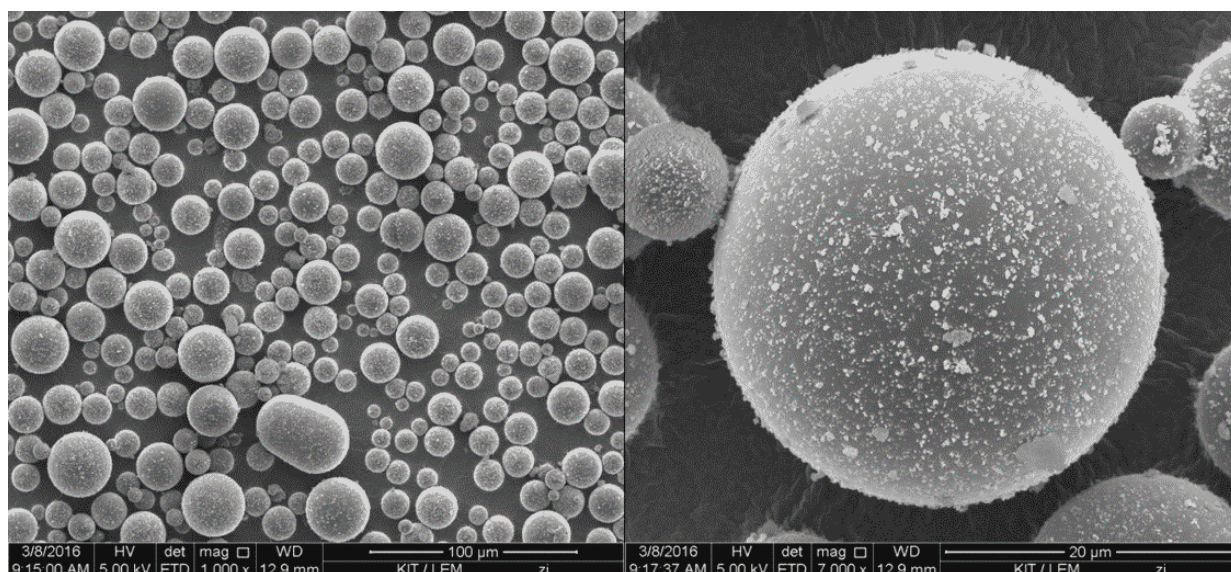
3.6 Acknowledgements

The authors would like to thank Jonas Keller and Christoph Pfeifer for fruitful discussions, as well as Carolyn Benner for contributing of physical properties of Micronal PCM materials and Frank Schultz and Stefanie Stadler from Freudenberg Technology Innovation SE for μ -Tomography images. Furthermore, we would like to thank Volker Zibat from LEM for SEM and 3M for providing glass hollow spheres iM16K, as well as BASF SE for providing the Micronal DS particles and Altuglas International for providing the PMMA particles. Additionally, we would like to acknowledge financial support from the European Research Council under the European Union's Seventh Framework Program (FP/2007-2013)/ERC Grant Agreement no. 335380.

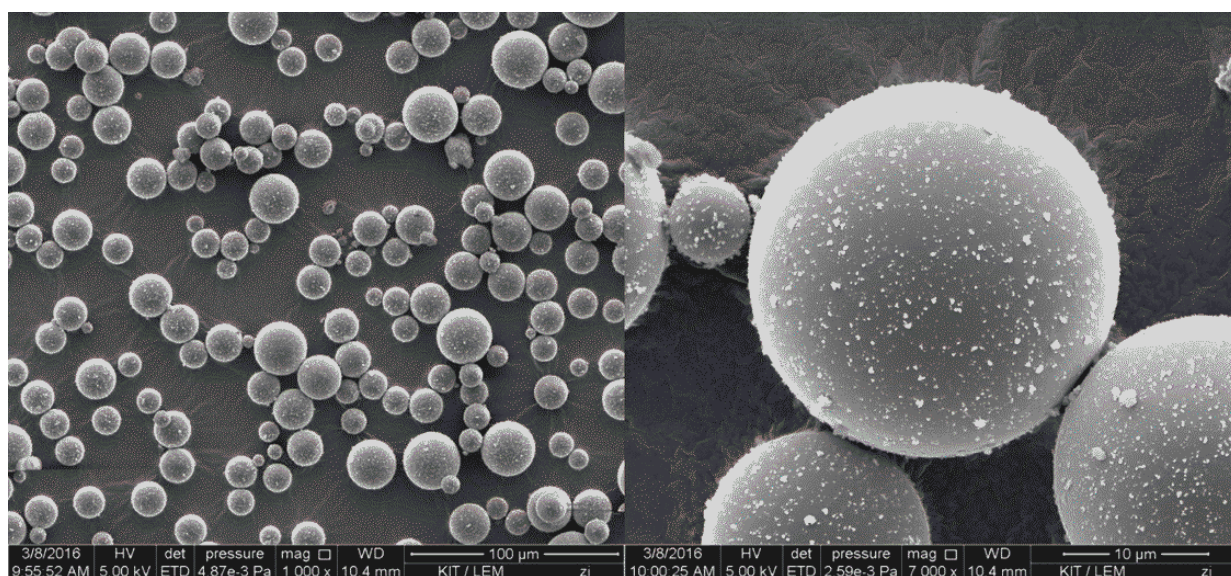
3.7 Conflict of interest

The authors declare no competing financial interests.

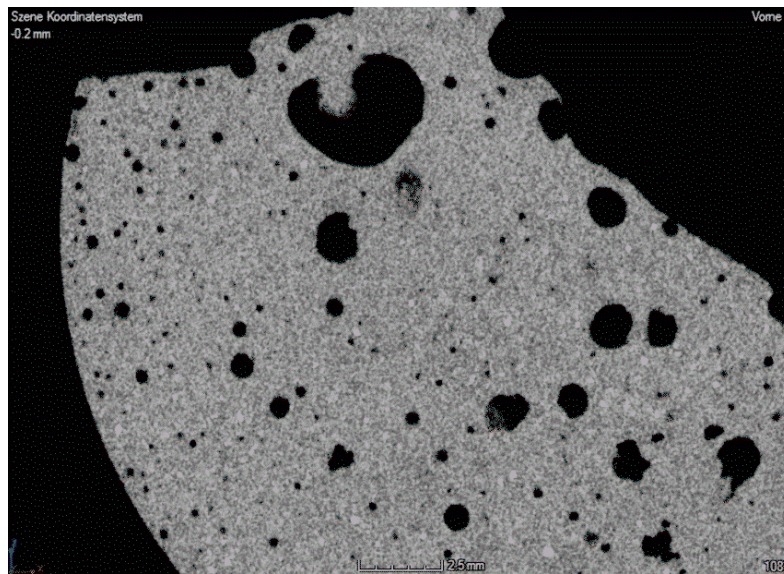
3.8 Supplementary Information



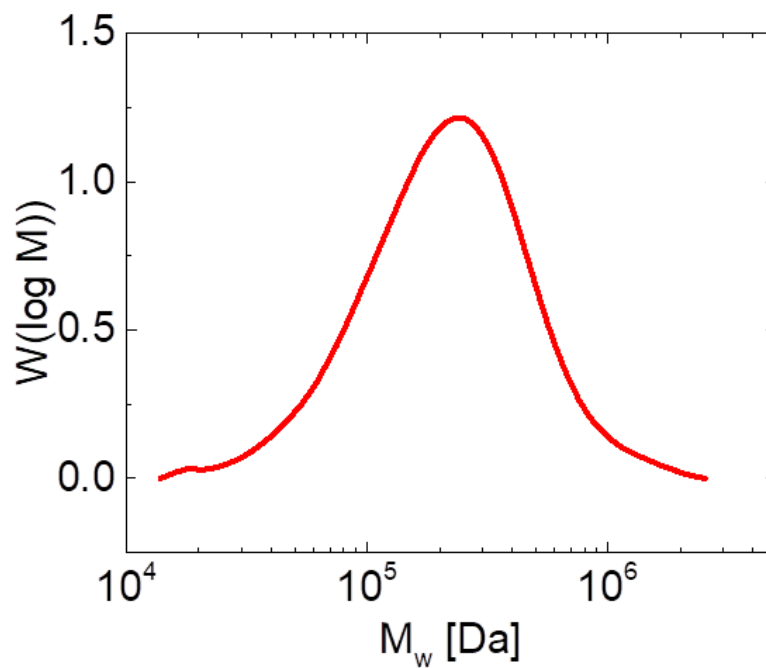
S3.1 Glass spheres iM16K OTES (hydrophobic) as received with attached nanoparticles. Figure reprinted with permission from Springer (Colloid and Polymer Science), copyright 2017.



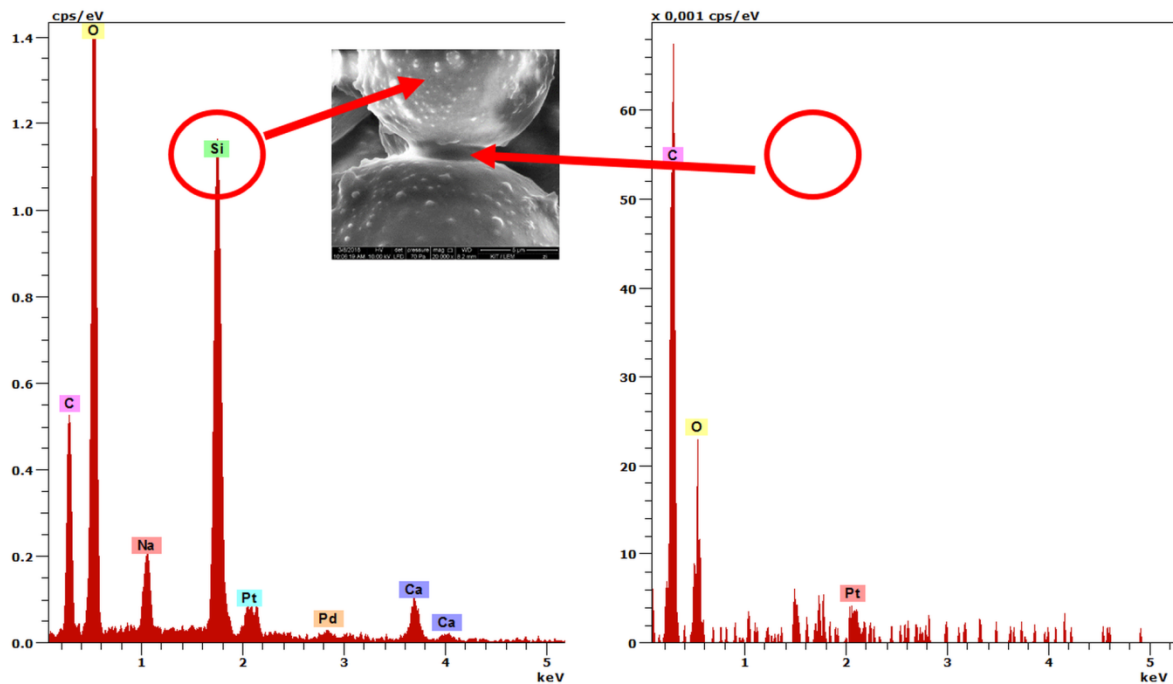
S3.2 Glass spheres iM16K (hydrophilic) as received with attached nanoparticles. Figure reprinted with permission from Springer (Colloid and Polymer Science), copyright 2017.



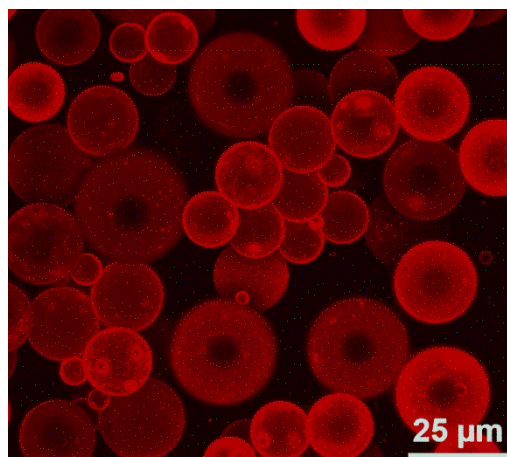
S3.3 μ -CT image of a solid porous sample made of 40 vol% hollow glass spheres with 6 vol% MMA at 82 °C for 2.5 h. Figure reprinted with permission from Springer (Colloid and Polymer Science), copyright 2017.



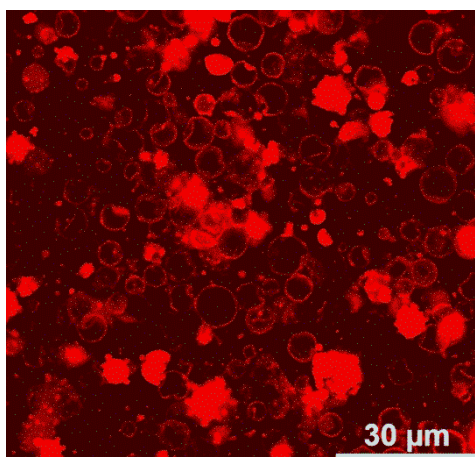
S3.4 Example for SEC analysis of the molecular weight distribution for a bridge sample extracted after polymerization of a capillary suspension with 40 vol% solid fraction and 6 vol% MMA at 84 °C for 5 h with 15 mg/ml BPO. Figure reprinted with permission from Springer (Colloid and Polymer Science), copyright 2017.



S3.5 The atomic composition of both the neck and the particle surface of porous materials made of hydrophilic glass spheres ($\phi_{solid} = 40 \text{ vol\%}$) and HEMA as secondary phase ($\phi_{HEMA} = 4 \text{ vol\%}$) using Energy-dispersive X-ray spectroscopy (EDX) in the ESEM-mode. The samples were polymerized in paraffin oil with 15 mg BPO/ml HEMA at 82 °C for 2.5 h and afterwards extracted with hexane. Figure reprinted with permission from Springer (Colloid and Polymer Science), copyright 2017.



S3.6 Confocal image of 35 vol% PMMA particles and 3 vol% MMA in glycerine-water-bulk (60/40 wt%). The confocal image is a flattened image with a depth of 25.1 μm. Figure reprinted with permission from Springer (Colloid and Polymer Science), copyright 2017.



S3.7 Confocal image of 35 vol% Micronal particles and 3 vol% MMA in glycerine-water-bulk (60/40 wt%). Figure reprinted with permission from Springer (Colloid and Polymer Science), copyright 2017.



S3.8 Graphite particles. Figure reprinted with permission from Springer (Colloid and Polymer Science), copyright 2017.

4. Measurement of adhesion and capillary forces between two microparticles

This chapter is written in the form of a scientific paper to be submitted. The main idea for the project came from Katharina Hauf-Hartung and Erin Koos, who did the investigation and methodology, the conceiving of the whole manuscript and wrote the manuscript. This work was completed with the cooperation of Richard Thelen and Hendrik Hölscher from the Institute of Microstructure Technology at Karlsruhe Institute of Technology. The contribution of Richard Thelen included the investigation and methodology, conceiving of the concept of the manuscript and writing and correcting regarding the technical setup. Hendrik Hölscher and Erin Koos contributed with the analysis and discussion of the data and results, the correction of the manuscript as long as the supervision in all parts of the paper. Norbert Willenbacher took part in the correction of the paper.

Preface

The goal of the work presented in this chapter was to observe and quantify the direct polymerization of a single capillary bridge between two microparticles in a liquid medium with an adapted AFM-setup. The results presented in this chapter are rather preliminary, because it was not possible to fully characterize the resulting bridging force for polymerized bridges.

Despite the limitations, the presented setup provides new and interesting insights into the measurement of contact angles of liquids in contact with spherical particles. The present design is very well suited for this goal and already provides valuable results that are important for understanding the microstructure of the particle networks.

Abstract

We demonstrate the direct visualization of force-distance measurements between two microparticles connected by a capillary bridge utilizing atomic force microscopy. This provides detailed insight in capillary bridge formation on the microscale and allows to observing the in-situ motion of the cantilever instead of common quasi blindfold measuring. The method is applicable for different types of microparticles under a variety of adjustable conditions. To demonstrate the experimental reliability of the presented approach, we show several measurements utilizing microspheres with an average diameter of 30 μm utilizing a side view camera determining the van der Waals forces between two microparticles in air and in glycerol. In this way, we visualize capillary bridges of glycerol between hydrophilic and hydrophobic glass spheres in ambient conditions allowing the determination of the contact angle of the capillary bridge. In addition, the time-dependent elongation process of the liquid bridge during retraction is recorded, as well as the breaking behavior of a polymerized epoxy bridge between two microparticles

4.1 Introduction

Capillary forces are well known from everyday phenomena like the capillary rise in narrow tubes, e.g. water transport in trees [94,95], as well as in sandcastles [96]. The study of materials with capillary bridges, wet granular media [10,11,45,47,97–100] and capillary suspensions [13,36,53], become of increasing importance. Recently, extensive investigations have been conducted on the interactions caused by liquid bridges between particles in order to understand the behavior of such materials [45,47,97–100]. The strength and appearance of the material is governed by the amount of liquid

volume and particles [98]. Capillary bridges between particles can appear in different shapes, which, depending on their wetting behavior, can be concave, convex, or even asymmetrical [101]. In most cases, they are regarded as being symmetrical, like in the studies of Bossler et al., where different bridge types and respective particle network formations were visualized [9,12,15].

In the recent years, a lot of research has been conducted in the field of measuring capillary forces between micron-sized particles via atomic force microscopy (AFM) to gain a quantitative insight into microscale forces [98,102–107]. These experimental measurements have been supplemented by theoretical calculations [10,108–110] and simulations [111]. Rumpf et al. and Schubert carried out extended research regarding the capillary bridging effects in wet granular media, where they investigated caused by the capillary pressure and wetting behavior and its influence on the tensile strength of the capillary bridges [10,11]. Tardos et al. presented a method to observe and measure capillary bridges of a binder solution to get insight in the solidification of the bridge regarding agglomeration processes [112–114]. Willett et al. measured capillary forces between particles with 2.4 mm diameter using different liquids to investigate the influence of surface tension on the wetting behavior [45]. They determined that the wetting hysteresis, which is caused by physical or chemical inhomogeneities on the particle surface resulting in energy barriers, has important consequences for the behavior of pendular liquid bridges [115,116].

Attractive capillary forces are particularly interesting for the research in the field of capillary suspensions where a sample-spanning network is created through bridging of particles [13,36,53]. A capillary suspension based processing route was used to produce porous solid materials using ceramics [22], glass [43], or composite materials as well as pastes like low-fat chocolate suspensions [33], battery slurries, and conductive materials [17,18]. The physical behavior of these suspensions has been typically characterized by measuring the rheological behavior or by probing the mechanical behavior of the solidified body, for example through compression tests. While these macroscale measurements are related to the strength of the individual bridges [36], the influence of specific parameters, like contact angle hysteresis, particle roughness, or other inhomogeneities, cannot be clearly probed. This problem is also true for other systems with particles and liquids, such as wet granular matter, Pickering emulsions [117,118] or bijels [119]. The influence of these complicating factors can be elucidated by directly observing the liquid bridges while measuring the force between two microparticles connected by this bridge.

In this work, we show how to modify an AFM setup that allows force-distance measurements with additional in situ visualization using a field of view of 270 x 400 μm . Its performance is demonstrated by the measurement of van-der-Waals forces in ambient conditions. Subsequently, the analysis of capillary bridges between two micron-sized spheres is presented. From the measured capillary force values, the contact angle is determined and compared to values obtained by other methods. A clear advantage of the presented setup is the in situ observation of the time dependent elongation process of the liquid bridge during ramping, providing insight into contact line pinning or the influence of extensional viscoelasticity. The presented setup is also applicable for measurements in a liquid cell and the investigation of solid bridges and their respective mechanical breaking force.

4.2 Experimental

For the correct modeling of a system consisting of two spheres connected by a capillary bridge, it is of major interest to measure force-distance curves as well as to depict and detect at the same time the shape changes of the capillary bridge until it breaks during retraction. The main component of

the setup is an AFM (Dimension Icon, Bruker Corporation, USA) equipped with an additional illumination, an elevated stage extension with an integrated heater and a camera, with a working distance of 22 mm and 400 μm wide field of view and the aperture of 0.5°, mounted on a lever connected to a micromanipulator with five degrees of freedom. The expanded setup of the AFM allows for precise determination of the minimum diameter of the meniscus of the bridge and the respective break force, simultaneously. Furthermore, the measured forces can be normalized by the bridge volume calculated from the pictures with a dedicated software script (MATLAB code for example). As every cantilever is individually calibrated, the error of each single measurement can be kept low. The setup is designed in a way that temperature, separation velocity and separation distance as well as delay time can be varied. This enables a software controlled systematic analysis choosing different parameters. A schematic of the utilized setup is shown in Figure 4.1.

Measurements can be performed in ambient conditions with a base sphere glued to a substrate, an upper sphere mounted on the AFM cantilever, and a capillary bridge between the two spheres as exemplary shown in Figure 4.1. Additionally, it is possible to carry out force-distance measurements within a liquid surrounding both spheres. This can be achieved with a liquid cell with embedded window in order to properly image the sphere-sphere interaction. The whole set-up contains mostly modular components so that all modules can be tested, operated and optimized independently.

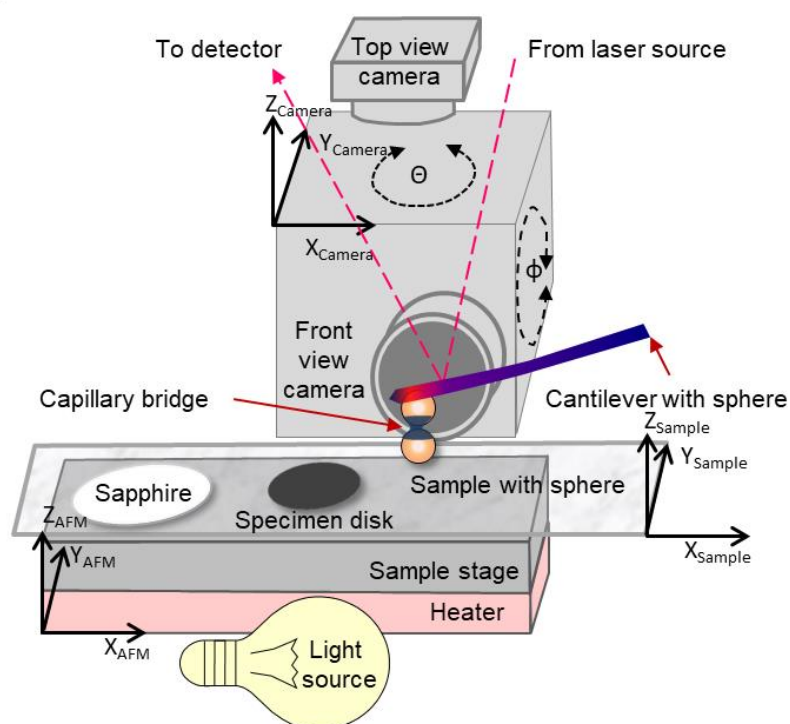


Figure 4.1 Schematic of the experimental measurement setup showing key components and all three adjustment axes. Spheres are glued to cantilever and glass slide, and imaged using two cameras (front and top view). The sapphire disk is used for calibration and the specimen disk serves as reservoir for the bridging fluid. The experimental challenge is to align all three coordinate systems in a way so that a proper depiction is attained during the recording of force distance data. This procedure is challenging and labor-intense because the additional camera is not mounted on the stage directly but on a 320 mm long lever connected to the AFM base to still allow for AFM stage motion.

4.2.1 Materials and sample preparation

Hollow borosilicate glass spheres (untreated hydrophilic iM16K and hydrophobically modified iM16K OTES, treated with octyltriethoxysilane) with a density of 0.46 g/cm^3 were obtained from 3M

Deutschland GmbH (Neuss, Germany). The spheres used in this study were approximately 30 μm in diameter. They had a hydrophilic (iM16K) or hydrophobic (iM16K OTES) surface. Glycerol with a surface tension of $\Gamma = 64 \pm 0.4 \text{ mN/m}$ and 98% purity (Carl Roth, Germany) was used as the bridging liquid. The surface tension was measured by the pendant drop method after DIN 55660 [120]. All items were used as received. The surface roughness R_a of the glass spheres, measured by AFM with a scan size of 2.5 μm by 2.5 μm , was $51 \pm 24 \text{ nm}$ on hydrophilic and $43 \pm 17 \text{ nm}$ on the hydrophobic particles after applying a spherical fit.

Tipless silicon cantilevers (All-in-one, BudgetSensors Ltd., Bulgaria) were manually equipped with particles on the bottom side of the cantilever with a micromanipulator using the protocol of Mak et al. [121]. The spring constant was determined for each prepared cantilever with the thermal tune function integrated in the AFM software (Force Volume Mode of Dimension Icon, Bruker Corporation). The deflection sensitivity was recorded on a hard sapphire specimen (Sapphire 12M, Bruker Corporation). Glass slides with particles on top were prepared by gluing the spheres with 2-K epoxy glue UHU Plus Endfest 300 (UHU GmbH & Co. KG Bühl, Germany). The glue was allowed to harden for at least 24 h in order to achieve maximum solidity. Small droplets of glycerol, to form liquid bridges, were dispensed on a metal specimen disc (Pelco 16219, Plano, Wetzlar, Germany) serving as reservoir. All components were placed on a common glass slide to ease handling.

4.2.2 Setup

To image the fine details of the examined microspheres, it is imperative to optimize the optical settings. Structures with a size of about 30 μm in diameter are easily depicted using an optical microscope with small working distances of a few millimeters using backlight illumination. Here, the sphere is glued to a micron-sized cantilever, mounted on a holder that is placed under the housing of a piezo tube with a diameter of 38 mm. Therefore, the working distance of the objective has to be larger than 21 mm (midway of the piezo tube plus a clearance of 2 mm for slight navigation freedom). If the measurements are done in liquid instead of air, the effective working distance increases further as the refractive index of practically all suitable liquids is larger than that of air.

The most critical and elaborate step is the alignment of all components relative to the given reference by the AFM setup to attain high quality depictions, which is a prerequisite for the subsequent analysis of experiments. Two cameras are used for that. The top view camera, mounted in the AFM housing, is placed and adjusted so that the focal plane matches the cantilever for adjustments and the sample underneath for measurements. The image of the front view camera is used to check if the heater stage is well adjusted relative to the angles ϕ_{camera} and Θ_{camera}

With manual “tip down” from motion control, the top sphere is moved down by steps of 1 μm until the top sphere touches the base sphere. The base sphere position is adjusted using the motion control of the AFM. The AFM is engaged using offset steps of 2 μm for x_{AFM} and y_{AFM} direction, until the top sphere touches at peak. This is verified by the top view camera. Additionally, the visible z-position shown by the front view camera is not exceeding the peak position, nor does the deflection depending detector voltage. This position is the zenith where the z_{AFM} position of the upper sphere reaches its maximum while still in contact with the lower one. The y_{camera} focus of the cantilever front view camera is adjusted using the micromanipulator.

The final step prior to the actual measurement is to pick up some liquid with the upper sphere glued to the cantilever. For that the scan head is lifted a secure distance of 1 mm above the specimen disk

level used as a reservoir for the liquid. Then the cantilever with the attached sphere is moved to the edge of the disk using the top view camera. After the cantilever touches the liquid reservoir, a change in the liquid surface reflection caused by a change of shape around the created meniscus is visible with the AFM top view camera. At this point, the sphere is immediately retracted from the liquid reservoir, and moved to the position the bottom sphere to be examined.

The complete measurement procedure is summarized in the following numbered list.

Measurement Procedure:

1. Microscope slide with bottom spheres, sapphire disk and fluid reservoir is mounted
2. Cantilever mounted with a sphere attached
3. Laser adjusted close to cantilever end at the tip position
4. Deflection sensitivity is calibrated using sapphire disk
5. Base sphere x_{sample} , y_{sample} , and z_{sample} position is recorded
6. Base sphere position is defined by zeroing x and y
7. First sphere-sphere contact is made to check for laser coupling
8. Precise zenith touching position is defined using AFM offset
9. Reservoir is approached and sphere brought into contact with liquid surface
10. Motion control is used to move to base sphere back into position
11. Focus is checked and corrected if necessary
12. Spheres are approached using false engage approximately 30 μm above bottom sphere
13. Final approach using tip down function with 1 μm step width until gap is smaller than 5 μm
14. Relative sphere position is adjusted for maximum visibility of gap/meniscus
15. Data file path is set
16. Ramp function parameters used to define a force distance curve are entered and executed
17. Force distance curve might be repeated to increase statistics validity
18. AFM head is withdrawn to secure position

The measurements of the force distance curves were recorded with the added front view camera, depicting the cantilever with sphere from the side. The cantilever was therefore moved down until it was about 5 μm above the bottom sphere. This step is conducted with the help of the AFM software (Nanoscope 8.15_SR8). The appropriate ramp size and surface delay of 10 seconds were set and the force distance measurement was started in a continuous mode with at least 10 measurements recorded at once.

4.3 Results and discussion

In this section, we present and discuss measurements of van-der-Waals forces between two micron-sized spherical particles in ambient conditions and measurements of capillary forces of glycerol bridges between two particles. The advantage of the presented setup is the visualization of the liquid bridge between the micron-sized spheres. This allows quantitative characterization of the bridge curvature, as well as the calculation of the liquid volume and contact angle and the in-situ observa-

tion of the force-distance measurements. For all sets of parameters at least three measurements were carried out ($N = 3$) and repeated with three different velocities in order to proof that a “quasi-stationary” state was achieved. All experiments were conducted at ambient conditions with a temperature of 25 ± 2 °C and a relative air humidity of 25 ± 3 %. While the data presented here is recorded in air the setup can also be applied with a cantilever in a liquid cell as long as the liquid medium is transparent.

4.3.1 Attractive forces between the particles in air and in glycerol

First, we present force-distance measurements between hydrophobic spheres at ambient conditions without any bridging fluid. Figure 4.2 shows an exemplary image taken during the experiment and the respective force distance curve. As the spheres are brought into contact (blue, dashed line), there is no detectable snap-in. The force then increases as the spheres are pushed against each other and the cantilever bends. The slope of trace and retrace curve (red, solid line) in this region depend mainly on the stiffness of the cantilever to which the upper sphere is attached.

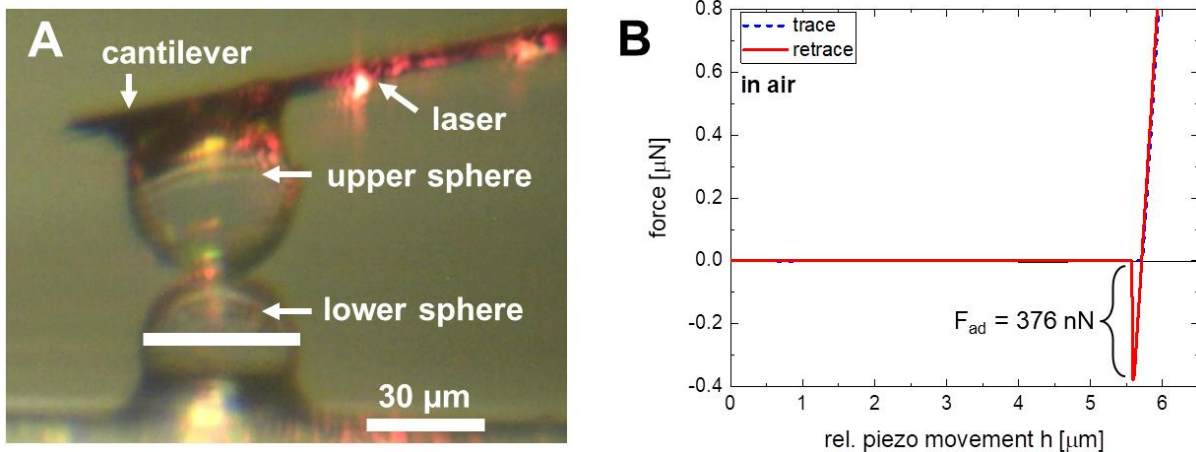


Figure 4.2 Front view taken during the measurement of force distance curve between hydrophobic microparticles in ambient conditions. (B) The respective force distance curve. The adhesion force during retraction is $F_{ad} = 376$ nN.

During further retraction the two spheres stay in contact due to their respective adhesion force (i.e., van-der-Waals force). However, the retraction force of the cantilever increases continuously till it becomes as large as the adhesion force, and the two spheres separate instantaneously [122]. This jump-off manifest as a sharp decrease in the force distance curve (see Figure 4.2B), which allow the easy determination of the adhesion force between the two particles. As the two spheres are hydrophobic we can neglect capillary forces by water. The lowest turning point corresponds to the adhesion force F_{ad} of 376 nN between the spheres. This is a reasonable value if compared to the theoretical value of the Hamaker force which can be calculated from [108,123]

$$F_{vdW} = \frac{A_H}{6h^2} R \quad (8)$$

where A_H is the Hamaker constant, $R = \frac{r_1 r_2}{r_1 + r_2}$ the reduced particle radius calculated from the respective radii r_1 and r_2 of the two spheres, and h is their separation distance. While the radii of the two spheres are well-known (21.4 μm and 19.9 μm) the Hamaker constant and the separation distance have to be estimated. The spheres are made from borosilicate glass (70 – 80% SiO_2), therefore, we assume the nominal Hamaker constant for glass $A_{H, \text{glass}} \approx 8.55 \cdot 10^{-20}$ J [124]. The largest uncer-

tainty is the separation distance. Here, a value between $h = 0.7$ nm and 0.4 nm, which is in the range of one silicon dioxide molecule, seems reasonable [125,126]. The adhesion force calculated with these values is between 290 nN and 888 nN and the measured value of 376 nN is well within this range.

Below in Figure 4.3, an example image is shown taken during the experiment in glycerol and the respective force distance curve is shown Figure 4.3.

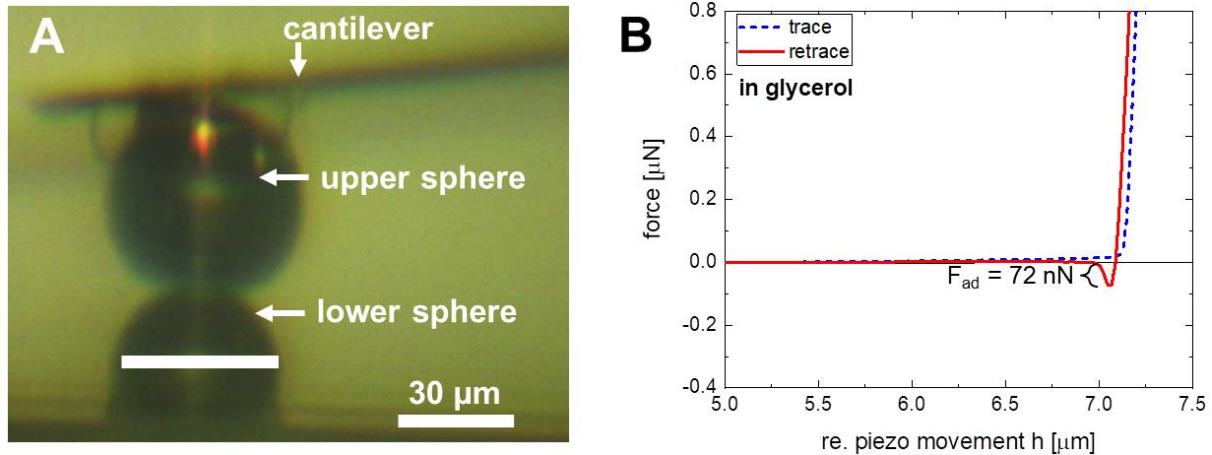


Figure 4.3 Front view taken during the measurement of force distance curve between hydrophobic microparticles in glycerol. (B) The respective force distance curve. The adhesion force during retraction is $F_{\text{ad}} = 72$ nN.

The Hamaker constant for glass in the glycerol medium can be calculated using the Good-Girifalco-Fowkes combining rule with $A_{\text{H,glycerol}} = 6.7 \cdot 10^{-20}$ J to be $1.13 \cdot 10^{-21}$ J [109]. The measured value was 72 nN for the van der Waals force in glycerol. The calculated was between 5 nN and 14 nN with the separation range of SiO_2 . Assuming $h = 2.3$ nm for the elongated octyltriethoxysilane molecule, the calculated force is 0.4 nN. A reason for the increased attractive force could be due to interactions between the long silane chains. The measurement in glycerol has to be optimized since the measured value is still a bit higher than the calculated. This can be realized using for example dense glass spheres without any attached silane molecules as well as a further optimization on the setup since other interactions can cause a deviation in the attractive force, which was observed in an increase during several measurements.

4.3.2 Capillary forces between two microparticles via AFM-measurement

As mentioned already, the most important feature of the modified AFM setup is the ability to study the capillary bridge force between two microparticles. A typical force distance curve of such a measurement is shown in Figure 4.4. Here, the cantilever approaches (blue, dash line) the fixed bottom sphere (image 1) until a snap-in takes place, as marked by the green circle. Then, the force increases due to the bending of the cantilever when the particles are in contact (image 2). Since the upper sphere was dipped in glycerol before the approach a capillary bridge is formed between the spheres. Since the two spheres touch each other mechanically, the force due to the cantilever bending should increase linearly (black dash-dotted) but a deviation is observed. This is mostly likely caused by a small relative movement of the particles in contact. The red dotted line corresponds to the retraction when the cantilever is moved upwards. It passes through the peak attractive force, the capillary force F_c , when the particles are just touching. It can be calculated from

$$F_{c_{h=0}} = 2\pi r_p \Gamma \cos \theta \quad (9)$$

where R is the reduced particle radius defined above, Γ the surface tension of the bridging fluid, and θ the contact angle [10,45,127]. Equation (9) assumes that the spheres are smooth and that the bridge volume is comparatively small with respect to the sphere size. The particle diameter was measured to be $16.5 \pm 0.5 \mu\text{m}$ ($N = 5$) utilizing ImageJ Fiji [128] with the cantilever length as a scale. Applying Eq. (9) it is straightforward to calculate the contact angle θ of the bridge between the two spheres from the measured capillary force at contact. This determination is an advantage of our set-up, especially for particulate multiphase-suspensions, since it is hard to accurately determine the contact angle with other methods. The established methods such as the sessile drop protocol or the microchannel confocal microscopy protocol of Bossler [9] suffer from problems caused by the particle curvature, contact angle pinning, or are limited regarding the optical properties of the suspension. For instance, a pressed powder is often employed for the sessile drop method since the particle surface treatment cannot be replicated, but such measurement is conducted on a greatly different length scale compared to the capillary force between particles, and often neglects the influence of roughness or fluid absorption.

After the particle-particle contact, the cantilever is retracted from the lower sphere and the glycerol bridge between the spheres elongates and thins (position 3 in Figure 4.4). Finally, a critical neck diameter is reached and the liquid bridge breaks. This point manifests as a sharp step in the force curve and is marked as F_{break} in Figure 4.4. Assuming a toroidal bridge the resulting capillary force can be calculated as a function of the bridge elongation h using equation (1) from chapter 2.4 [9,97]. Here, V_{bridge} is the volume of the liquid bridge and all other variables are defined as in Eq. (8) and (9).

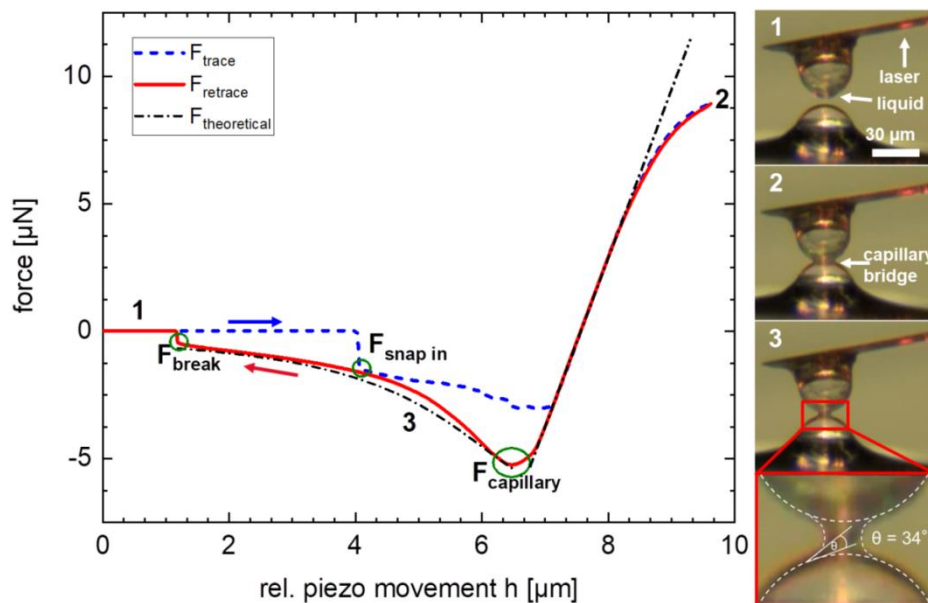


Figure 4.4 (left) Force distance measurement of a glycerol capillary bridge between two hydrophilic micron-sized glass spheres with (right) images respective to the measuring position 1, 2 and 3. The bridge is shown in the image inset with lines to guide the eye. The bridge volume was measured to be $V_{\text{bridge}} = 0.21 \pm 0.04 \text{ pL}$ and the upper sphere has a diameter of $16.5 \pm 0.25 \mu\text{m}$, respectively.

After the determination of the top particle radius $r_{\text{upper sphere}} = 16.5 \pm 0.25 \mu\text{m}$ and the bridge volume $V_{\text{bridge}} = 0.21 \pm 0.04 \text{ pL}$ from the images taken during the retraction, we fitted the retraction force (red dotted line) with Eq. (1). The radius of the upper sphere and the lower sphere are assumed being almost equal and therefore the radius of the upper sphere is used in Eq. (1). The average contact

angle θ was calculated via Eq. (9) and assumed to be nearly constant over the measured distance. The curves agree well, slight differences between the theoretical and experimental curves might be an indication that there is an influence from, e.g., the fluid viscosity and/or contact angle hysteresis. Therefore, the experiments were carried out at least 10 times with different velocities. However, the variation of the velocity of the cantilever movement (100, 765, 2000 nm/s) resulted in no detectable influence of this parameter on the measured force curves implying that velocities below 2000 nm/s can be considered as quasi-static. The good agreement of the theoretical fit and the experimental capillary force curve additionally confirms that the calculation of the contact angle via Eq. (9) is based on a reasonable description of the capillary forces.

A clear benefit of the presented approach is the possibility to visualize the liquid bridge between the two spheres in order to determine the volume V_{bridge} , which is required to compare experiment with theory, e.g., Eq. (1). The bridge shape can be extracted from the images, as shown in Figure 4.5. This step can be automated with the assumption of a toroidal curvature using a dedicated software script (Matlab code in our case). With such a procedure the liquid bridge volume was determined and we estimate an error of about 20% for two reasons. First, the spherical particles, which had to be used as scale, had blurry edges, and the shape of the liquid bridge was manually generated. Nonetheless, the contact angle can be calculated from such images, too. Figure 4.5B shows a plot of these contact angles as a function of the sphere distance during approach (advancing) and retraction (receding). In accordance to previous studies we observe clear differences between advancing and receding contact angles as well as a dependence on the separation distance h .

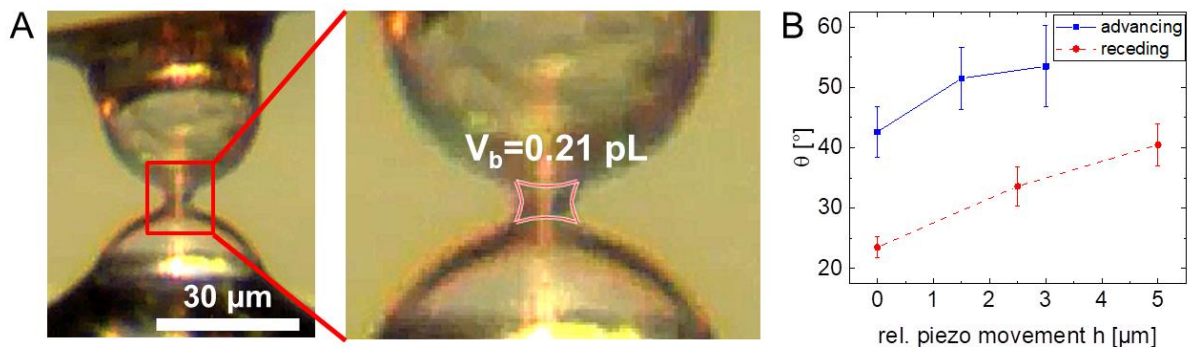


Figure 4.5 (A) Photos of the glycerol bridge between the two hydrophilic glass spheres used to calculate the bridge volume and contact angles. (B) Contact angles from the measurement shown in the insert 3 in Figure 4.4 were taken from the 4 edges of the curvature fit for three distance points.

4.3.3 Comparison between macroscopic and microscopic determined capillary forces

As discussed above the capillary forces between spheres are frequently calculated with Eq. (9) using a macroscopically determined contact angle. In the previous subsection, however, we demonstrated how the microscopic contact angle can be determined in an indirect (Eq. (9)) and direct way (Figure 4.5) via atomic force microscopy. In this subsection, we compare and discuss the differences between these macroscopy and microscopic approaches. The conventional macroscopic method to determine contact angles is the sessile drop method. Measurements of sessile drops on a pressed powder [128] surface made from the same spheres used in the AFM experiments result in $84 \pm 3^\circ$ for hydrophilic and $82 \pm 1^\circ$ for hydrophobic spheres. Using these values to calculate the capillary force with Eq. (9) gives $3.08 \mu\text{N}$ and $0.41 \mu\text{N}$. Measurements of the capillary force directly via AFM, however, result in $5.21 \pm 0.05 \mu\text{N}$ and $3.16 \pm 0.06 \mu\text{N}$. The reverse calculation of the respective contact angle gives values of $38 \pm 1^\circ$ and $67 \pm 1^\circ$. These values differ from the classical approach to determine

the contact angle of a pressed particle powder. The difference is even larger if we compare these results with contact angles determined from the analysis of the video images. In this case the microscopic contact angle is smaller for the hydrophilic ($24 \pm 2^\circ$) as well as for the hydrophobic ($42 \pm 2^\circ$) case. Consequently, the adhesion values are smaller, too. Table 2 compares the macroscopic and microscopic determined contact angles and adhesion force for the three discussed cases. The large differences between the values demonstrate that all methods have to be handled with care. Calculating bulk properties of bridged materials from them will lead to quite different results (and therefore, false predictions) depending on the actual method applied.

Table 2 Contact angles and capillary forces of a liquid bridge of glycerol between hydrophilic and hydrophobic glass spheres determined with three different methods. The transformation between capillary force and contact angle is calculated for $h = 0$ with Eq. (9) using $r_{1,2} = 16.5 \pm 0.25 \mu\text{m}$ and $\Gamma = 64 \text{ mN/m}$. The arrows indicate the direction of determination.

Method	hydrophilic spheres		hydrophobic spheres	
<u>Macroscopic:</u>	θ	$F_{\text{capillary}}$	θ	$F_{\text{capillary}}$
Sessile drop on pressed powder (Ref. [129])	$84 \pm 3^\circ \Rightarrow$	$3.08 \mu\text{N}$	$82 \pm 1^\circ \Rightarrow$	$0.41 \mu\text{N}$
<u>Microscopic:</u>				
AFM measurement of capillary force	$38 \pm 1^\circ \Leftarrow$	$5.21 \pm 0.05 \mu\text{N}$	$67 \pm 1^\circ \Leftarrow$	$3.16 \pm 0.06 \mu\text{N}$
Image analysis of receding capillary bridge at $h = 0$	$24 \pm 2^\circ \Rightarrow$	$6.06 \pm 0.10 \mu\text{N}$	$42 \pm 2^\circ \Rightarrow$	$4.93 \pm 0.15 \mu\text{N}$

4.3.4 Adhesion force for solidified bridges

This device is further suitable for the analysis of solid bridges, as shown by the example crosslinked epoxy bridge in Figure 4.6.

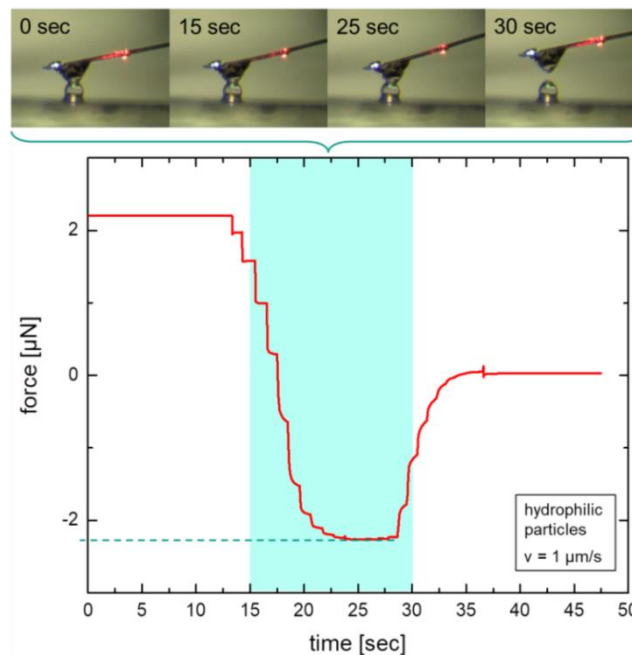


Figure 4.6 Example for force-time-measurement of epoxy between hydrophilic particles with $1 \mu\text{m/s}$ reverse velocity after polymerizing for 19 h at ambient conditions. The stepwise measurement is highlighted by the colored area and the bridge breaking point by the dashed line. (Scale: the upper particle is $32 \mu\text{m}$ in diameter)

For the adhesion measurement after polymerization of the liquid bridge into a solid bridge, the protocol was switched to manual retraction because the tunable ramp size of the AFM was too low. As a result, the curves in the highlighted area appear as steps. The initial force at the beginning of the measurement is caused by the preloading of the cantilever to ensure the particles are in contact before polymerization. The colored area is the effective measuring sequence, where the cantilever is retracted manually with a velocity of approximately 1 $\mu\text{m/s}$. As shown in Figure 4.6, the failure of the bridge occurs not under simple tension, but in horizontal direction that precedes the vertical. Despite this complex displacement, the thinnest point of the solidified epoxy bridge was the fracture point in all measurements. The adhesion between the epoxy and the glass seems to be stronger, as the contact area is larger, than the cohesion force within the epoxy bridge. A similar phenomenon was observed for the fracture of porous samples made from these glass hollow spheres connected by epoxy bridges [26]. In these samples, shown in Figure 5.3 (Chapter 5), SEM images show that bridge breaking rather than delamination of the epoxy from the particle surface.

4.3.5 Conclusion and outlook

With the presented AFM setup, it is possible to measure particle interactions in ambient conditions and potentially also in liquids. Force distance curves can be measured in a defined way between micrometer-sized spheres. When a capillary bridge is present, the setup also allows the simultaneous observation of the meniscus formed between the particles for precise determination of the bridge volume and the respective capillary force. The contact angle can be either determined by fitting the AFM curve with theory or directly from visual observation. While the resolution of a pixelated video limits the determination of the contact angle ($\pm 2^\circ$ in our case), continuous video monitoring allows the diagnoses of issues such as non-ideal bridge shapes and unwanted bridging effects.

One remaining problem that might be addressed in future experiments is the reliable application of extremely small amounts (femtoliters) of liquid between two spheres that are immersed in a second liquid. The procedure successfully applied in air - partially immersing the top sphere in a reservoir of the bridging fluid - failed to reproducibly dose the sphere in a liquid. We, therefore, examined an alternative utilizing a glass capillary with a conical shape. The capillary was mounted on a customized micromanipulator, which guided the liquid through tubes, connected to a cell-tram unit to the Eppendorf Femtotip II dispenser. This test was not successful as the tapered form of the microcapillary prevents the liquid from being dispensed due to the high force needed to overcome the capillary force and the pressure drop at the tip of the capillary. Furthermore, small tips were prone to undamped vibrations when moving into place. These problems were present for liquids being distributed via a tapered glass capillary with a final outer diameter of less than 3 μm and inner diameter of less than 0.5 μm . A dispensing system with capillaries with an inner diameter larger than 5 μm was able to reproducibly dispense the fluid when all interlocks were sealed by epoxy in addition to their mechanical connection. However, the minimal dosing volume for this comparable thick capillary is much larger than the tiny amount of liquids needed (some picoliters). A promising alternative to overcome the issue of reliable liquid dispense might be cantilevers with integrated liquid channels [130,131]. To navigate the delicate capillary, the system might be expanded by three additional components: a third camera for navigation, a dispensing unit, and a second micromanipulator. There is only a small space gap left between cantilever holder, AFM piezo tube housing, and camera optics to bring the capillary in close vicinity and finally in contact with the spheres seriously complicating such a procedure.

We also conducted some preliminary experiments showing that our approach is also suitable for the analysis of crosslinked epoxide bridges. The experimental procedure is similar to the aforementioned measurements of liquid bridges. But instead of stressing a liquid capillary bridge a solidified epoxy bridge is stressed until it breaks. That is attained using much stronger cantilevers with higher spring constant. The shape of the resulting solidified bridge is primarily determined by the surface forces of the not crosslinked epoxide.

Acknowledgements

We thank Frank Bossler for fruitful discussion and reading of the manuscript. This work was supported in part by the Karlsruhe Nano Micro Facility (KNMF, www.knmf.kit.edu), a Helmholtz Research Infrastructure at Karlsruhe Institute of Technology (KIT, www.kit.edu). Additional support was provided by the YIN Young Investigator Network. (KIT, www.yin.kit.edu).

5. Lightweight porous glass composite materials based on capillary suspensions

Full title: Lightweight Porous Glass Composite Materials Based on Capillary Suspensions

Authors: Katharina Hartung, Carolyn Benner, Norbert Willenbacher, Erin Koos

Status: published

Bibliographic data: Materials (2019) 12, 619. doi:10.3390/ma12040619

Copyright 2019 by the authors. This work is licensed under a Creative Commons Attribution License and is available at <https://doi.org/10.3390/ma12040619>. The text has been adapted in this thesis to change the citation and figure numbering. Additionally, some symbols have been modified to confirm with the other chapters.

Abstract

In this article, we present a simple, advanced method to produce lightweight tailor-made materials based on capillary suspensions that are made from locally bonded hollow glass spheres with a high total porosity in the range of 70% at apparent densities of 200 kg/m^3 , having a compressive strength of 0.6 MPa. The amount of added liquid and the particle surface treatment determine the network structure in the pastes and the resulting microstructure of the porous material in a straightforward manner. This structure has a strong impact on the porosity, pore size, and mechanical properties of the final body. The most promising porous materials were made of surface treated hollow glass spheres that create a sample-spanning network in the capillary state, where the added liquid wets the particles worse than the bulk fluid. These samples approach the density of natural balsa wood and they may find application in fields where either weight or structure are important, such as in insulation materials, filters, and membranes, as well as lightweight construction materials for automotive or aerospace engineering.

Keywords: porous materials; capillary suspensions; glass filters; thermal isolation; microparticles; capillary bridges



Figure 5.1 Graphical abstract. Copyright 2019.

5.1 Introduction

Porous materials are found in a broad field of applications, such as separation and filtering techniques, as well as thermal insulation materials or even catalytic materials [1], while the pore size is a key property. The pore size is categorized in macro- (>50 nm), meso- (50 nm–2 nm), and micro (<2 nm) porous structures [2]. Here, we focus on macroporous materials that are made from glass. Besides the pore size, the pore and inner structure of the material are also important, as they influence the mechanical properties along with the porosity. In the past few years, attention was focused on natural structure architectures, as these extraordinary structured materials evolve properties that are well-suited to specific environmental conditions. Examples include the plate-plate structure of sea shells with a compressive strength of up to 540 MPa [132], hierarchically porous structured bamboo with compressive strength up to 68 MPa at a density of 900 kg/m³ [133,134], and highly porous and strong balsa wood with compressive strength of around 40 MPa at densities of 100–250 kg/m³ [4,135,136]. Recent approaches have attempted to either directly mimic these natural structures using inorganic materials or to create other complex structures to surpass the material properties of these natural materials. Bauer and coworkers were able to create micron-sized cellular composite materials that are made of three-dimensional (3D) polymer trusses from laser lithography that were coated with alumina [137]. The samples had densities that were below 1000 kg/m³ and compressive strengths of up to a 280 MPa. Their micro-architecture, with size of 10 to 40 μm in all directions, is the benefit—and drawback—of these samples, since this method creates stable, but quite delicate, structures. Furthermore, these complex microstructures would be difficult to implement on a rapid, large scale for industrial processes where bodies that are larger than a few centimeters are required. A similar method was also established for pure ceramic materials on a larger scale. Minas et al. were able to produce cellular alumina scaffolds with a hierarchically-structured pore network and high porosity (67–77%) at a compressive strength between 9.5 and 29.3 MPa using three-dimensional (3D) printed Pickering emulsions and foams [138]. While ceramic materials often have superior strength, glass and glass composite materials are preferred in certain applications because of their resistance to chemicals, surface tunability, as well as easy cleaning and reuse. Maurath et al. used the capillary suspension concept, which will be described in the following paragraph, to produce sintered dense glass filters with porosities of up to 50% with a compressive strength of 14.7–21.4 MPa at an average sample density of 1375 kg/m³ [43]. Rincón et al. [139] were able to produce porous glass foam materials via alkali activation, gel casting, and sintering at 700–800 °C with porosities of 88–93%, densities from 2110–2660 kg/m³, and strengths from 0.5 up to 5 MPa. Qu and coworkers could produce even more efficient lightweight glass foams at equivalent sintering temperatures, but with lower densities of 129–229 kg/m³, higher porosities of 91–95%, and compressive strength of 0.85–5.92 MPa [140,141]. While there are advantages in the physical and mechanical properties of these products over traditional bulk manufacturing [142], the high sintering temperatures present clear drawbacks. Therefore, a simpler and more energy efficient processing route should be explored.

As mentioned above, further improvements on bulk forming methods are possible while using the capillary suspension processing route. Capillary suspensions are created by adding a small amount of an immiscible secondary fluid to a particulate suspension, thereby modifying rheological properties of the suspension [13,35]. The changes can be detected by, e.g., a strong increase of the yield stress, which is caused by a transition from fluid-like to gel-like behavior due to structure formation within the suspension. This small amount of secondary liquid phase is distributed as capillary bridges between the micron-sized particles, leading to a particle network due to the capillary attraction. This

percolating network of particles and capillary bridges was directly visualized using the confocal microscopy by Bossler and Koos [9]. They show the two extrema in the shape of the capillary bridges between the particles in the suspension, depending on the three-phase contact angle, where the secondary phase forms between the particles. The first case is the so-called capillary state for a three-phase-contact angle $\theta_{S,B} > 90^\circ$, where the secondary fluid (S) wets the particle surface worse than the surrounding bulk fluid (B). If the secondary fluid preferentially wets the particles ($\theta_{S,B} < 90^\circ$), then the particles are directly connected by capillary bridges and the system is in the pendular state. Both of the arrangements lead to a sample-spanning network, but they show significant differences in the overall structure. The pendular state is characterized by individual capillary bridges between the particles (binary interactions), while the capillary state often appears in multibody particle clusters [13,36,48,143]. Capillary suspensions in the pendular state have already been used to produce porous materials by either sintering or locally fusing the microparticles [23]. A proof of concept for direct polymerization within the capillary bridges was shown by Hauf et al. [8], where a simple method for direct polymerization in the bridges at temperatures below 100 °C, requiring less time and effort than existing methods, is presented. Hauf et al. investigated the chemistry, including the chemical composition and molecular weight distribution of poly(methyl methacrylate) (PMMA) capillary bridges between glass particles to demonstrate how the bridge structure and the resulting porous body properties could be tuned. Bitsch et al. were successful in using a reactive epoxy resin as the secondary fluid to connect plate shaped graphite particles, resulting in lightweight conductive open porous bodies ($\varepsilon = 60 - 75\%$), with a compressive strength of 0.1–1 MPa [23].

In this paper, we present an advanced method using capillary suspensions to create self-organized porous bodies with open porosities of up to 67% at an apparent density of only 200 kg/m³ and a compressive strength of 0.6 MPa. These samples are made of micron-sized hollow glass spheres that are locally connected by two-component epoxy bridges, which increases the compression strength of the produced samples compared with PMMA. The density of our glass-epoxy materials approach that of balsa wood and it is comparable with common insulation materials, like foamed poly(styrene), but they have superior resistance against chemicals, solvents, or thermal exposure, in addition to the easy surface modification. Furthermore, the process route is very simple, low cost, consumes little energy, and is environmentally friendly.

5.2 Experimental Section

5.2.1 Materials

Hollow, borosilicate glass spheres iM16k (untreated) and iM16k OTES (treated with octyltriethoxysilane) were provided by 3M Deutschland GmbH (Neuss, Germany) with a mean diameter $d_{50} = 20 \mu\text{m}$ and a density of 0.46 g/cm³, differing in surface treatment. Particles were used as received and are shown in the supplementary information Figures S5.1 and S5.2. As shown in the supporting information, the spheres have a rough surface consisting of small glass particles that were adsorbed onto the micro-particle surface. This roughness appears to be more pronounced for the treated particles than the untreated, but these nanoparticles can migrate during processing [8]. Glycerol (Carl Roth, Karlsruhe, Germany), with a density of 1.26 g/cm³, was used as the bulk phase and a two-component epoxy as the secondary phase. The epoxy base (Epoxydharz L) and curing agent (Härter L) were provided by Conrad Electronic SE (Hirschau, Germany). The interfacial tension between epoxy and glycerol was measured to be $\Gamma = 8 \text{ mN/m}$.

5.2.2 Sample Preparation

To prepare the capillary suspensions, the particles were dispersed in glycerol with a high-shear dissolver stirrer (35 mm diameter for rheological measurements and 60 mm diameter for the cured samples) at 1200 rpm for 10 min, with a solid volume fraction of 30 vol%. The two-component epoxy was premixed at a ratio of 10:4 by weight with a spatula and then added to the suspension while further mixing at 2000 rpm for 2 min. The amount of secondary fluid ϕ_{sec} was 0, 3, 4.5, 6, 7.5, or 9 vol%.

The prepared capillary suspensions were filled into silicone molds (35 mm diameter disks with 5 mm height for porosity measurements, bars of 48 mm × 12 mm × 5 mm for the mechanical experiments) and cured (crosslinking of the epoxy) in the mold for two days at ambient conditions. The glycerol was then removed from the cured samples by placing them on paper towels for at least three hours and then rinsing the samples twice with distilled water. Finally, they were dried overnight in a laboratory oven at 70 °C and 200 mbar.

5.2.3 Characterization

Yield stress measurements were performed with the stress controlled rheometer Haake RS 150 (Thermo Scientific, Karlsruhe, Germany) using a vane geometry (10 mm diameter) by increasing the stepwise shear stress in a range from 0.1 to 100 Pa for approximately 20 min. The temperature for all measurements was $T = 20 \pm 0.5$ °C. The yield stress was defined using the tangential method [23]. The values reported are for at least two unique measurements.

The three-phase contact angle between the glycerol and epoxy (without hardener) was determined by imaging particles at the interface between the two fluids using a microchannel and confocal microscope (Leica TCS SP8, Leica Microsystems, Wetzlar, Germany) [9]. The contact angle was determined to be $19 \pm 4^\circ$ for the untreated glass hollow spheres and $110 \pm 10^\circ$ for the treated particles. The interfacial tension between glycerol and the epoxy was determined using the pendent drop method with image analysis from Krüss (Krüss, Drop Shape Analysis, Hamburg, Germany).

The samples were also optically inspected after curing using an environmental scanning electron microscope (ESEM-mode at $p = 70$ Pa, Quanta 650 FEG, FEI, Hillsboro, OR, USA), where the images were taken from a fractured section of the solid samples. The samples were sputtered with a mixture of platinum and palladium prior to imaging.

The total porosity ε of the solid bodies was calculated using the ratio of the apparent (raw) density of the sample and the true (skeletal) density based on DIN EN 1936.

$$\varepsilon_{\text{total}} = 1 - \frac{\rho_{\text{apparent}}}{\rho_{\text{true}}} \quad (10)$$

Here, the apparent density of the sample was calculated as the ratio of sample weight and sample volume. The true density was measured using a multivolume gas pycnometer (Micromeritics GmbH, Aachen, Germany, Model MP 1305 with Helium) at 20 °C. Pore size measurements were carried out using the mercury porosimeter Autopore III 9420 (Micromeritics GmbH, Aachen, Germany) by detecting the intrusion volume at a mercury filling pressure of 3.9 kPa.

The compressive strength was measured using the texture analyzer TAX.T from Stable Micro Systems (Surrey, UK) in compression mode with an average sample size of 4 mm height, 7 mm length, and 7 mm depth for at least five samples at a constant laboratory temperature of 20 ± 1 °C. The flexural

strength was obtained from four-point bending tests using a custom-made device following DIN EN 843-1 that was mounted on the TAX.T.

5.3 Results and Discussion

Lightweight, strong, and highly porous glass bodies can be produced using hollow glass micro spheres that are locally interconnected with nano-sized epoxy bridges. The porous materials were made from capillary suspensions containing glass spheres, glycerol as bulk fluid, and an epoxy resin as secondary phase, inducing the formation of a strong sample-spanning network. High energy dispersing of a small amount of epoxy in this suspension ($\phi_{sec}/\phi_{solid} = 0.1$ to 0.3) leads to a break-up of the epoxy droplets and to the attachment of the resulting small droplets between the particles [14]. With the different surface treatment of the hollow glass spheres, the microstructure of the particulate network can be controlled due to the different wetting behavior of the epoxy on the particle surface. This effect is clear when comparing the SEM images displaying $\theta < 90^\circ$ for the untreated particles in Figure 5.2 and $\theta > 90^\circ$ for the treated particles in Figure 5.3.

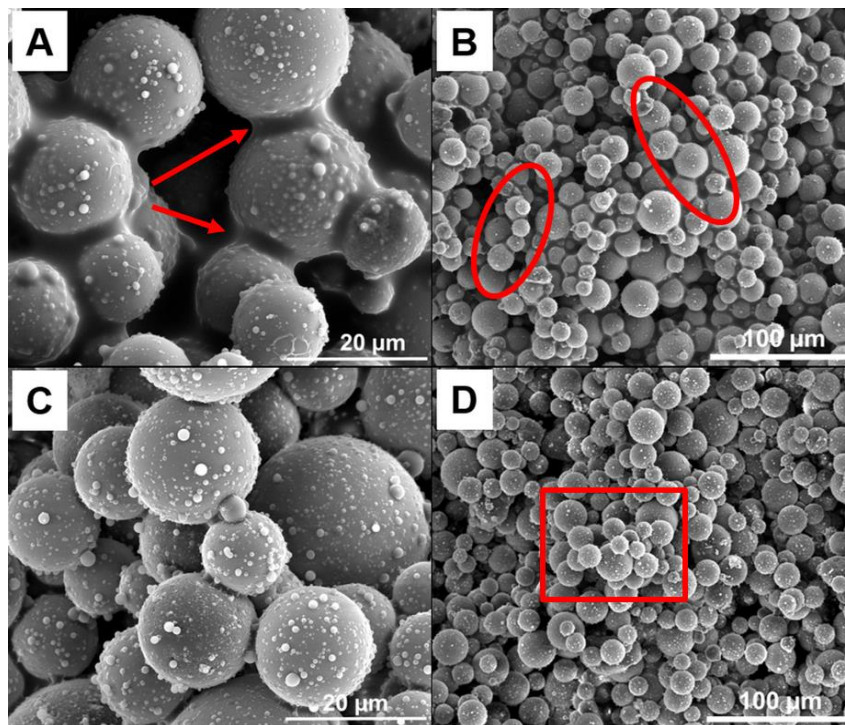


Figure 5.2 Images of fractured sections of the cured porous glass materials made from 30 vol% untreated hollow glass spheres and 3% (A,B) and 6% (C,D) epoxy. The samples were cured at ambient conditions for at least 24 h and the bulk phase was removed prior to imaging. Copyright 2019.

The contact angle of the cured samples is consistent with the three-phase contact angles ($19 \pm 4^\circ$ and $110 \pm 10^\circ$) that were measured in the liquids. The true contact angle, however, may differ because of the contact angle hysteresis (advancing vs. receding polar phase) as well as the contact line pinning that may occur during the mixing process [144]. The SEM images suggest a different bridging mechanism between the untreated and treated particles as well as a difference in the structure morphology as the amount of secondary liquid is varied. For the untreated particles that are shown in Figure 5.2, the epoxy creates concave capillary bridges (highlighted with arrows) between the untreated particles (Figure 5.2A) and a funicular network (highlighted with circles) is built with 3 vol% epoxy (Figure 5.2B). The funicular network, as described in Domenech and Velankar [38], and subsequently imaged in Bossler and Koos [9], consists of secondary fluid drops with low sphericity connecting several par-

ticles. The epoxy wets the particles very well, showing a low three-phase contact angle, which would facilitate the formation of a funicular network at low ϕ_{sec}/ϕ_{solid} [9]. At higher amounts in the secondary phase, here, 6%, the epoxy seems to partially flood the particle network forming agglomerates. Only small amounts of epoxy are visible in forming direct bridges between particles in the high magnification image (Figure 5.2C). Instead, a majority of the epoxy is on the inside of the large agglomerates (highlighted with squares), which are visible in Figure 5.2D. Domenech and Velankar observed a similar phenomenon while using silica particles to produce liquid-liquid-particle ternary blends containing two immiscible polymers [31]. They found several distinct morphologies upon varying the composition [31], and this image, Figure 5.2D, seems to resemble the capillary aggregates that they described. A different wetting behavior was observed on the surface of the treated particles in Figure 5.3. The epoxy connects multiple particles forming large, irregular agglomerates. The epoxy is also seen in Figure 5.3A forming sessile drops (highlighted with arrows) on the particle surface and connections between the larger micron-sized particles and the smaller, nanometer-sized particles on the particle surface. With an increasing amount of secondary liquid to 6% epoxy, the number and size of the sessile drops changes, but the agglomerate structure does not seem to vary significantly.

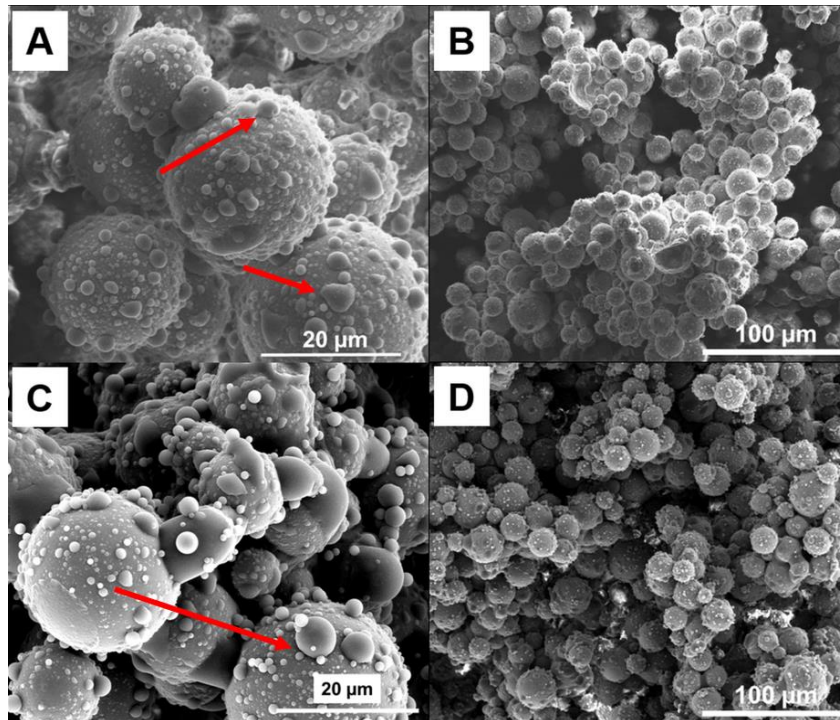


Figure 5.3 Images of fractured sections of the cured porous glass materials made with 30 vol% treated and 3% (A,B) and 6% (C,D) epoxy. The samples were cured at ambient conditions for at least 24 h and the bulk phase was removed prior to imaging. Copyright 2019.

The yield stress is closely related to the samples' microstructure [12]. The changes in structure following a variation of the amount of epoxy are manifested in measurements of the yield stress of the wet, uncured samples [12]. Thus, the network structure and bridge strength are indirectly detected by rheological measurements showing increasing yield stress with increasing amounts of epoxy, as seen in Figure 5.4.

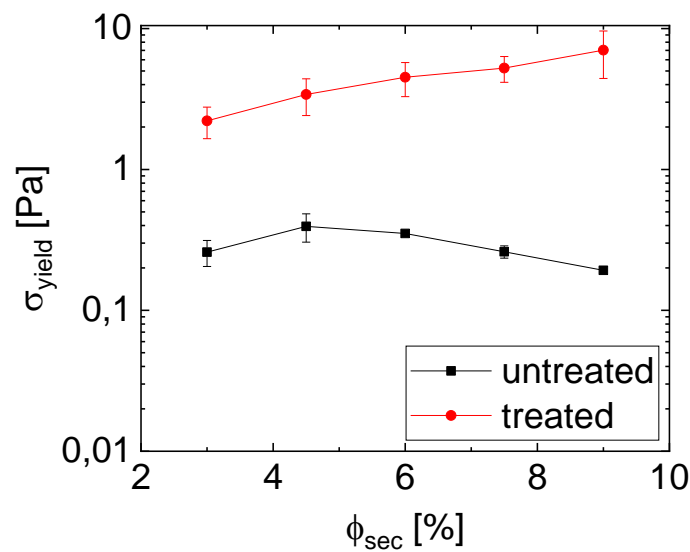


Figure 5.4 Yield stress of capillary suspensions made from untreated (black squares) and treated (red circles) glass spheres ($\phi_{\text{solid}}=30$ vol%) in glycerol with the epoxy base (without curing agent) as secondary phase. The value for the suspensions below 3 vol% epoxy could not be measured indicating a lack of structure formation. Lines are to guide the eye. Copyright 2019.

The measured yield stress values are relatively low in comparison to other capillary suspensions [9,43], which is likely because of the low interfacial tension ($\Gamma = 8$ mN/m) between epoxy and glycerol or the influence of the nanoparticles on the particle surface interfering with the wetting and bridging of the microparticles. The qualitative comparison between capillary suspensions with untreated and treated glass spheres shows that the particulate network using treated hollow glass spheres in glycerol with epoxy as secondary phase creates a stronger network than with untreated particles. This trend is the opposite to that demonstrated by Bossler and Koos [9], where the pendular state samples had a higher magnitude of the shear modulus than the capillary state samples. Subsequent experiments imply that this difference might be highly sensitive to the amount of added liquid; however, and the capillary state networks can indeed be stronger than the pendular state samples [12]. The rheological behavior of the capillary suspensions with treated glass spheres shows a slight, continuous increase in yield stress with an increasing amount of secondary phase, while the yield stress of the pastes with untreated particles shows a minor peak at 4.5% epoxy ($\phi_{\text{sec}}/\phi_{\text{solid}} = 0.15$) and then a decrease in strength. This is typical for a pendular to funicular transition—the transition from binary bridging interactions to coalesced bridges with multibody interactions—in pendular state (wetting) capillary suspensions, and typically occurs at $\phi_{\text{sec}}/\phi_{\text{solid}} = 0.1$ to 0.25, depending on the three phase contact angle and the mixing conditions [9,14,54]. The SEM images that are shown in Figure 5.2A and Figure 5.3B suggest that funicular clusters are already present at 3% epoxy ($\phi_{\text{sec}}/\phi_{\text{solid}} = 0.1$), implying that this may not be a pendular to funicular transition. Instead, we hypothesize that this transition denotes a microstructural transition to an agglomerated, capillary aggregate structure with either fewer or weaker bridging between the particle clusters. The steady increase in yield stress for the treated sample implies that no clear microstructural transition occurs in this range for the capillary state sample, and instead, either the strength or the number of bridging interactions steadily increases. SEM images in Figure 5.3 showing no clear change in structure between 3% and 6% epoxy confirm such an observation. The difference in σ_{yield} between the two different particle wetting types may be explained by the different network structures that are created by the secondary phase. Capillary state structures were observed on the treated particles (Figure

5.3). They are visible as convex drops between the particles and small droplets sitting on the particles surface. These drops between the particles (termed capillary state clusters, which are not to be confused with the capillary clusters for the untreated particles) also lead to the formation of a sample-spanning network [9], as shown in Figure 5.3B. With increased secondary liquid ($\phi_{sec} = 6\%$), the drops on the particle surface become larger and more numerous (Figure 5.3C). These drops may reinforce the connections between the particles.

The morphological changes also influence the porosity and the pore size distribution of the cured sample. The total porosity of the glass materials with treated particles was higher, by up to 10%, than that of the bodies that were made of untreated ones (Figure 5.5). The porosity drastically increases between 3 vol% to 4.5 vol% of added sec. fluid, from 59 to 69% for the treated particles and from 51 to 60% for the untreated particles. Further increasing the bridging phase for the treated samples does not significantly influence the porosity, but it may change the pore structure, as shown by the higher standard deviation between samples (error bars). The samples with the treated particles also have a higher volume of air bubbles that were entrapped during sample preparation, which may account for the higher porosity when compared to the samples that were made with untreated particles. For the untreated samples, the peak porosity occurred at a higher epoxy amount, which can be explained by the changing network structure that was caused by spherical agglomeration or by partial phase separation effects. The low yield stress of the precursor with untreated particles could be an indication of either possibility. A line (calculated by $100\% - \phi_{solid} - \phi_{epoxy}$), denoting the maximum theoretical open porosity if the glycerol (bulk fluid) is removed without phase separation or shrinkage, is also included in Figure 5.5.

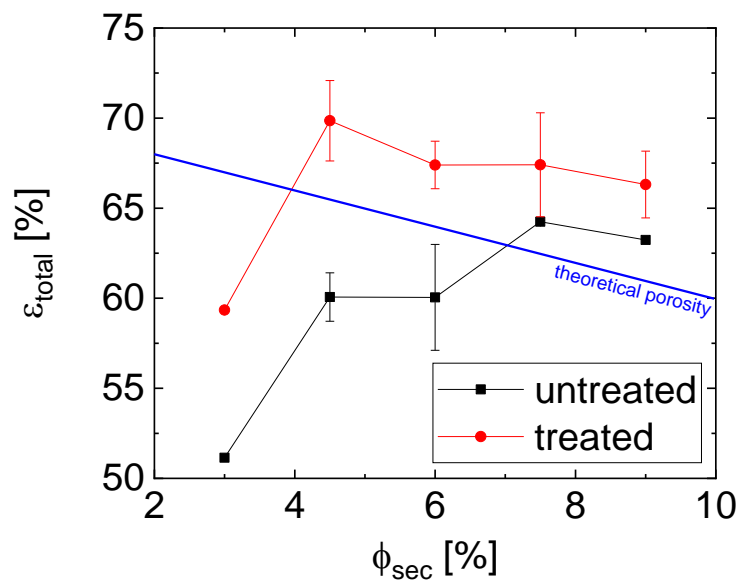


Figure 5.5 Influence of the amount of epoxy on the open porosity of the glass materials made of untreated particles (black squares) and treated (red circles). The values for the 0 vol% were not measured because there no self-supporting bodies could be produced. Lines are to guide the eye. The theoretical maximum open porosity line (blue) denotes the maximum porosity that is the volume of the bulk fluid, assuming there is no phase separation or shrinkage. Copyright 2019.

Due to the structural properties of capillary suspensions, we assume a predominantly open pore structure [50]. The points at low secondary fluid below this line comprise evidence for phase separation due to the weak yield. The contribution to the closed porosity from the hollow glass spheres is estimated to be 26.5% (as calculated using SEM images of broken particles showing a shell thickness

of 0.4 μm) and is constant for all samples. This could be the reason for porosity values above the theoretical open porosity line.

Structural differences between the samples become clear from average pore size measurements, as shown in Figure 5.6, where error bars represent the standard deviation of the pore size distribution. The 3% untreated sample has the lowest median pore size of 6 μm at a porosity of 51%, while the 6% sample has an average pore size of 8 μm and a porosity of 60%. This slight increase in the average pore size is caused both by the slight increase in the size of the small sized pores with size 8 μm as well as the development of a bimodal distribution with large pores of 90 μm . The bimodal distribution (as shown in the supplementary information in Figures S5.3 and S5.4) indicates agglomeration and the formation of the capillary aggregates, as was demonstrated for other systems [12,35]. The treated particles, on the other hand, show a similar porosity of 59%, like the untreated with 6% epoxy, but a larger pore size of 14 μm at 3% epoxy (supplementary information Figures S5.5 and S5.6). The average pore size stays approximately constant and the porosity increases up to 67% for the 6% treated sample with an increasing amount of epoxy.

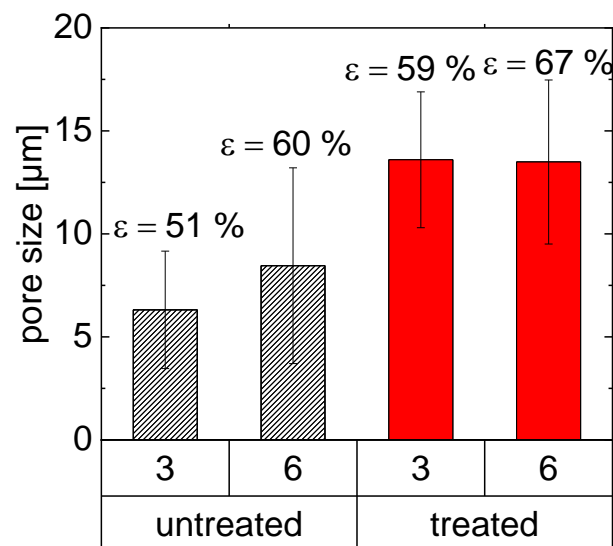


Figure 5.6 Pore size measurements of untreated and treated samples with 3 and 6 vol% epoxy. The pore size distributions were monomodal, with the exception of 6% untreated, which had a bimodal distribution with peaks at 8 μm and 90 μm (see supplementary information). The error bars denote the standard deviation as calculated from the pore size distribution. Copyright 2019.

The differences between the untreated and treated samples in porosity and pore size distribution can be explained by the difference in the density of the bodies. The average apparent and the true densities of the treated and untreated samples at all secondary fluid fractions are shown in Table 3. Here, higher densities for the samples from the untreated particles as compared with the treated particles can be observed. The apparent density is 15% and the true density 33% higher for the untreated particles. Therefore, the untreated samples are more compact than the treated ones, corresponding to a lower porosity in the solid bodies.

Table 3 Average apparent and true densities as well as the resulting porosity of porous samples made with untreated and treated particles as a function of the epoxy fraction ϕ_{sec} . The data are the average values from at least three samples. Copyright 2019.

Surface Treatment	Φ_{sec} [%]	$\rho_{apparent}$ [g/cm ³]	ρ_{true} [g/cm ³]	ϵ_{total} [%]
untreated	3.0	0.28 ± 0.00	0.72 ± 0.12	51.1 ± 0.00
	4.5	0.28 ± 0.01	0.70 ± 0.01	60.1 ± 1.34
	6.0	0.30 ± 0.10	0.65 ± 0.09	60.0 ± 2.94
	7.5	0.25 ± 0.06	0.65 ± 0.08	64.2 ± 0.07
	9.0	0.32 ± 0.12	0.71 ± 0.10	63.2 ± 0.00
treated	3.0	0.24 ± 0.06	0.62 ± 0.07	59.3 ± 0.09
	4.5	0.17 ± 0.02	0.57 ± 0.02	69.9 ± 2.18
	6.0	0.20 ± 0.02	0.59 ± 0.03	66.6 ± 3.35
	7.5	0.20 ± 0.02	0.62 ± 0.02	67.4 ± 2.89
	9.0	0.21 ± 0.02	0.64 ± 0.01	67.3 ± 1.16

The addition of the epoxy to the glass particles induces a sample-spanning network and, after curing, results in a self-supporting body. Changes in the pore structure as well as the size and number of bridges with changing amounts of epoxy should manifest in changes to the material strength, as is observed when using measurements of the flexural and compressive failure strength. Under flexural stress, the sample will crack, where this crack propagates through the weakest particle connections. Measurements of the four-point-bending failure strength are shown in Figure 5.7A as a function of ϕ_{sec} . The treated particle bodies show a much higher resistance against bending, with a maximum of 0.2 MPa for 7.5 vol%, while untreated materials had their maximum of 0.07 MPa with only 3% epoxy.

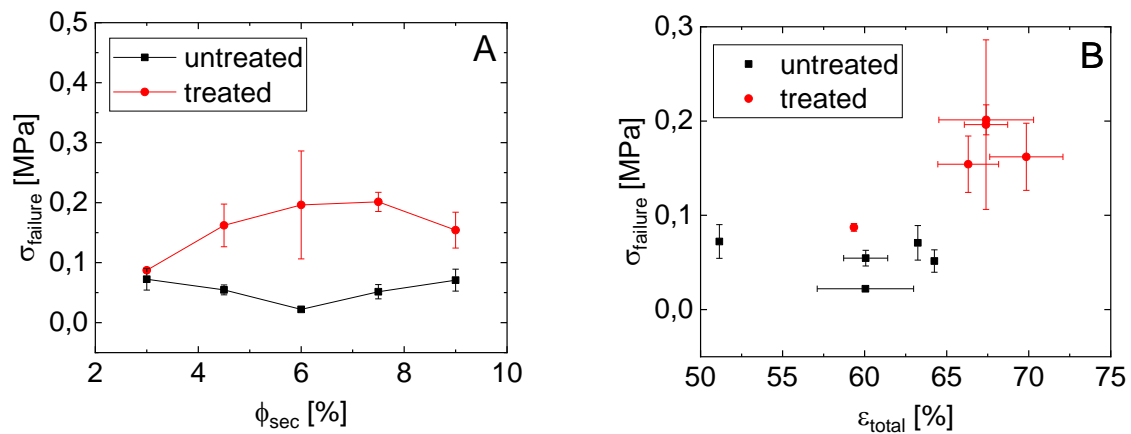


Figure 5.7 (A) Dependence of the four-point-bending failure strength on the secondary phase amount and (B) the correlation between the failure strength and the open porosity of the solid glass materials. Copyright 2019.

The failure stress, which is a measure of the strength of the network backbone, is higher for the treated particle samples at each ϕ_{sec} than for the untreated particles (Figure 5.7A). Remarkably, the treated particle samples show both higher porosity and strength (Figure 5.7B). While a capillary network is created through the use of treated particles with a small amount of epoxy, these bridges seem to become thicker and the contact area increases with higher secondary fluid fractions, thus causing increased adhesion between the particles. The small epoxy droplets that are shown in Figure 5.3 become larger with an increasing amount of epoxy and create a stronger cluster-network, which incorporates more epoxy volume [12]. Both the treated and untreated particle samples can be divid-

ed into two populations when comparing their failure strength to porosity (Figure 5.7B). The higher ϕ_{sec} samples form one group at higher porosity while the sample with the lowest epoxy fraction (3 vol%) clearly deviates. Interestingly, both the strength and porosity increase for the higher epoxy contents as compared to the $\phi_{sec} = 3\%$ sample for the treated particles. This clearly demonstrates the importance of the network backbone on the strength. However, it is worth noting that, besides the trend where the treated samples were stronger than the untreated, the dependence of the bending failure has little in common with the yield stress dependence. The treated sample bending failure has a peak or plateau beginning at 7.5 vol%, whereas the yield stress steadily increases over the measured range. For the untreated particles, the yield stress increases slightly, from 3% to 4.5% epoxy, and then weakens, while the failure strength is constantly weak during the entire range. These differences may arise due to the contribution of flexible bridges, which can break and reform in the wet state, or simply from the difference in the geometry of the applied force in these measurements.

A similar trend was observed for the compressive strength of the porous glass bodies, as shown in Figure 5.8. While the compressive strength for the untreated materials remains essentially in constant in the range from 0.1 to 0.04 MPa with increasing epoxy, the compressive strength of the treated samples increases from 0.18 to 0.62 MPa (Figure 5.8A). Once again, this strength is related to the structure and volume of the capillary bridges. The compressive failure decreases slightly with an increased porosity for the untreated samples, whereas the 3% epoxy treated sample had the lowest porosity and strength (Figure 5.5 and Figure 5.8B).

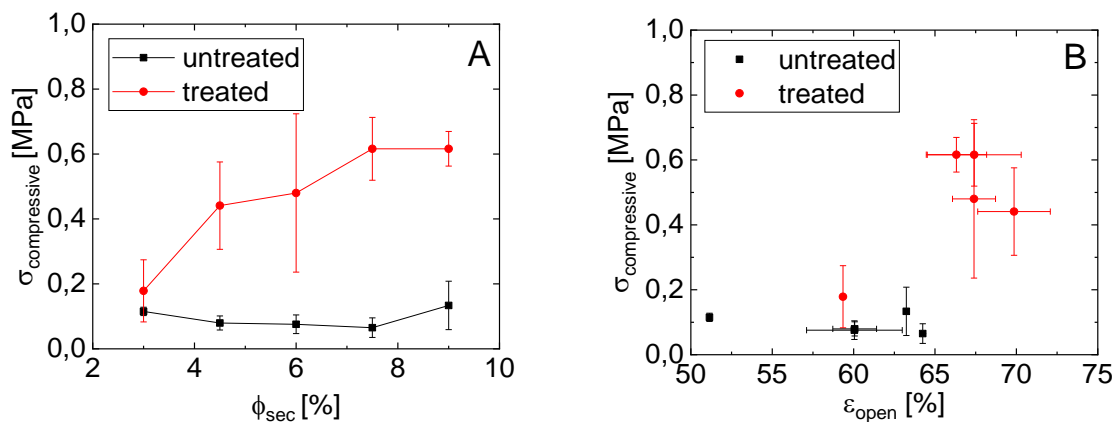


Figure 5.8 (A) Dependence of compressive strength on the secondary phase amount and (B) correlation between the compressive strength and the open porosity of the solid glass materials. Copyright 2019.

Thus, using the data from both the cured and uncured samples, we may construct the microstructural schemes, as shown in Figure 5.9. The untreated particles are wet by the epoxy secondary phase, which creates pendular and funicular bridges between the spheres. The largest contact area for adhesion occurs between 3–4.5% epoxy (highest σ_{yield}). The structure at this point is either a pendular or funicular structure, where each secondary fluid bridge connects a small number of particles. This structure changes upon the addition of more epoxy into a highly aggregated state. The epoxy wets the untreated particles very well and individual bridges will already start to coalesce at small ϕ_{sec}/ϕ_{solid} . These coalesced bridges will cover the particles, forming compact clusters [9]. This compact clustering causes the change in porosity and a bimodal pore size distribution was observed for the 6% sample (see Figure 5.6 and the supporting information). Some binary bridges remain in this

sample that connect the clusters [9]. These are the binary connections that will fracture. Thus, there is a large change in porosity between the funicular and spherical aggregate sample, Figure 5.7B, while the strength is only weakly affected. For the treated particles, the strength and number of the bridges increases slightly with increasing epoxy, but the general structure, as evidenced by the porosity and the pore size, remains unchanged.

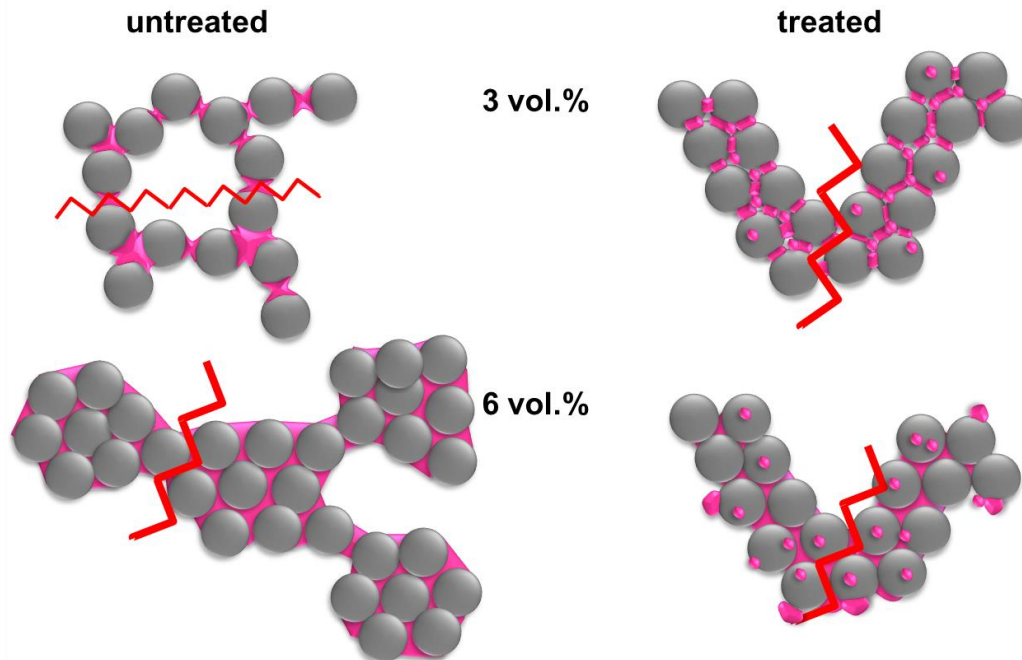


Figure 5.9 Schematic drawing of structure arrangement and corresponding failure mechanism in capillary suspensions with untreated and treated particles, at low and high secondary fluid contents. The zig-zag-lines show the location of mechanical failure. Copyright 2019.

The treated glass spheres create a capillary network upon the addition of small amounts of epoxy, which enables cured products that are highly porous, very lightweight, and nevertheless strong against bending and compression, as shown in Figure 5.10. The most promising material was made of 30 vol% treated hollow glass spheres ($d_{50} = 20 \mu\text{m}$) with 7.5 vol% epoxy ($\phi_{\text{sec}}/\phi_{\text{solid}} = 0.25$). At an apparent density of only 200 kg/m^3 , it had a failure strength of 0.2 MPa and a compressive resistance of 0.6 MPa at a porosity of 67.4%. The glass-epoxy materials favorably compare with the density of lightweight balsa wood [4,135,136]. This low density and reasonable strength is remarkable, having a porous material that is made of locally bonded hollow glass spheres without any sintering step. While the sintered glass materials showed stronger mechanical properties [43], the locally glued glass-epoxy-materials are 6.9 times lighter, with almost 18% higher porosity, with controllable pore shapes and without any shrinkage problems. Commercial glass frits (e.g., DURAN Group GmbH (Mainz, Germany), Heraeus Quarzglas GmbH & Co. KG (Kleinostheim, Germany)) were measured to have a porosity of 29% and a compressive strength of around 20 MPa, which is even less than for the sintered glass filters from capillary suspensions [43]. Hemmerle et al. [78], who used 55–2040 μm sized glass beads ($\rho_{\text{particle}} = 2460\text{--}2560 \text{ kg/m}^3$) with PDMS as the bridging phase, have shown similar values of 0.025–0.35 MPa compressive strength, but at much higher densities than the hollow glass samples that are shown here. When compared with the glass foams from Rincón et al. [139] and Qu and co-workers [140,141], our porous samples are in the same range of weight and mechanical properties and they have the advantage of a simple and environmentally friendly processing route.

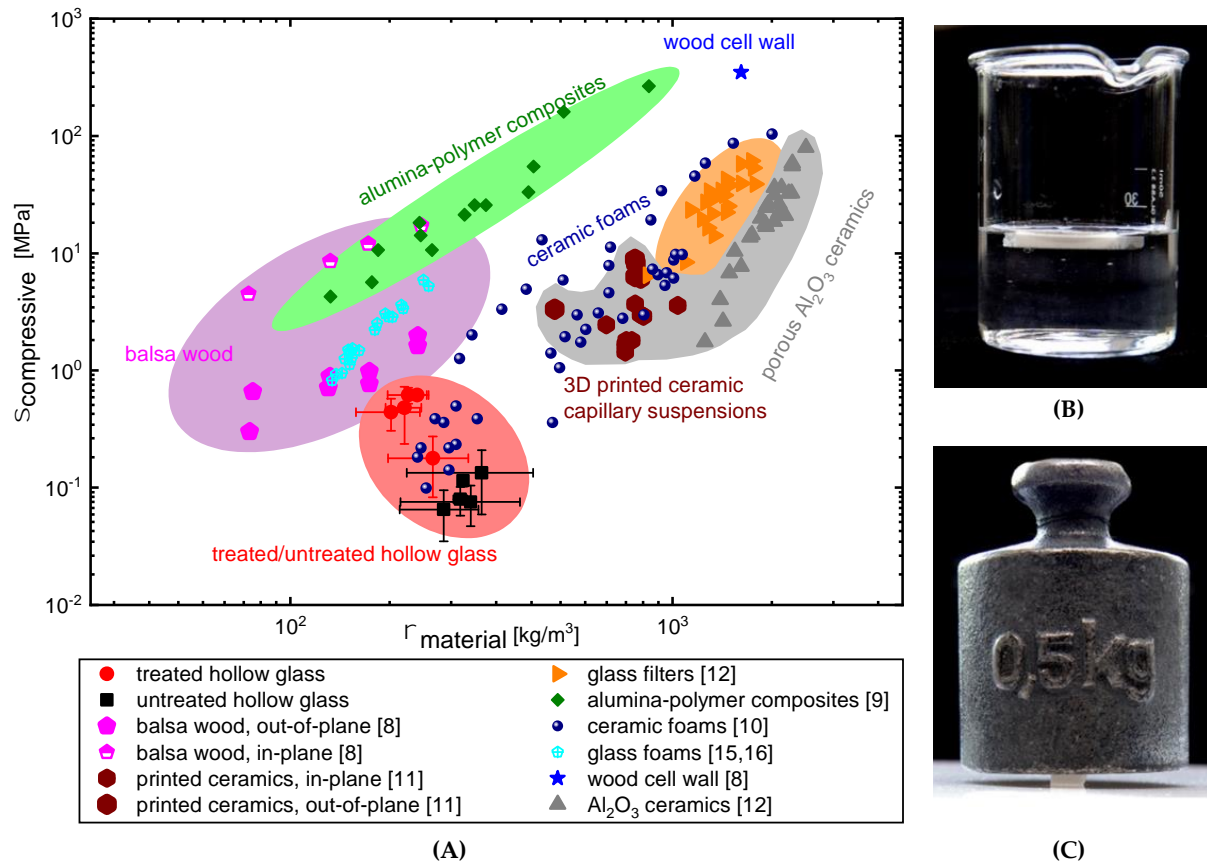


Figure 5.10 (A) Compressive strength as a function of density of the glass-epoxy samples, honeycomb-structured sintered ceramics [34] and polymers [9], sintered glass foams [13,14] and Balsa wood [8]. The produced treated glass-epoxy-materials are much lighter compared with sintered ceramics. (B,C) Images of samples, demonstrating their low density and high strength. (B) The image on top right shows a 50 mm × 20 mm × 5 mm bar floating in distilled water and (C) the right bottom image show a 48 mm × 12 mm × 5 mm bar supporting a 0.5 kg weight. Copyright 2019.

By soaking these bodies in ethanol, acetone and n-hexane for more than 30 h, the chemical resistance was tested. The thermal resistance was tested by heating up the samples in an evacuated laboratory oven at a temperature of 70 °C for 24 h. No fracturing or other degradation of the samples was observed during either treatment. This resistance depends on the chemical composition of the bridging material (epoxy in this case), and it can be modified to provide stability against thermal and chemical agents.

5.4 Conclusions

Our glass-epoxy-system demonstrates an advanced way to produce glass filters and other porous glass composite materials with tailor-made properties. The glass hollow spheres render the material lightweight, while also retaining the desired surface properties, allowing for capillary suspension networks to be formed and creating the desired pore structure. In this study, a commercial anaerobic two component epoxy was used. The processing route using capillary suspensions gives a variety of variables to control the pore network, the porosity, the mechanical properties, and even the chemical resistance of the resulting porous bodies. The low density and a reasonable compressive strength are in good agreement with the most lightweight materials, with the exception of state-of-the-art materials, like the high-sintering glass foams or 3D printed composite structures using more tedious lithographic printing methods. Our processing route, however, is much simpler and it can be easily transitioned to large-scale industrial processes. Possible applications for this porous material include separation and filtration, as well as lightweight construction for automotive and aerospace engineer-

ing, or insulation materials. These materials are made of hollow glass spheres that have a similar thermal conductivity of 0.05–0.25 W/mK, which is in the same range as foamed polystyrene (0.20–0.38 W/mK). The glass bodies are resistant to chemicals, solvents, or thermal exposure. Furthermore, the process route is very simple, low cost, consumes little energy, and is environmentally friendly.

Further research should be completed to improve the strength and further reduce the density. A possible approach to improve the strength can be to increase the adhesion between the glass spheres and the bridging phase by choosing a different epoxy or by modifying the particle treatment. The density could be lowered by 3D printed structured materials. The application of specific experiments should also be conducted, especially at different temperature and humidity ranges, where the strength of the glass and epoxy might vary. The strength of this material under tension should also be examined.

Supplementary Materials: The following are available online at <http://www.mdpi.com/1996-1944/12/4/619/s1>, Figure S5.1: SEM image of the untreated particles; Figure S5.2: SEM image of the treated particles; Figure S5.3: Pore size distribution of the untreated particles with 3% epoxy; Figure S5.4: Pore size distribution of the untreated particles with 6% epoxy; Figure S5.5: Pore size distribution of the treated particles with 3% epoxy; Figure S5.6: Pore size distribution of the treated particles with 6% epoxy.

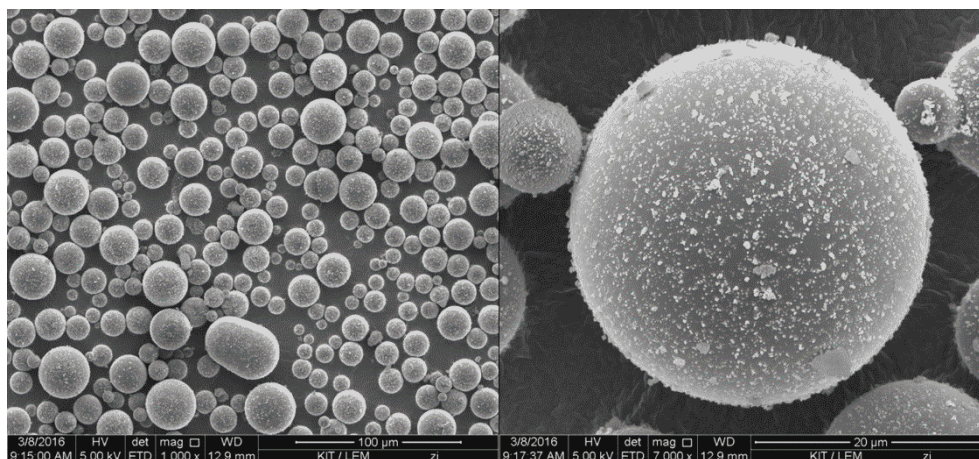
Author Contributions: Conceptualization, E.K.; Formal analysis, K.H. and E.K.; Funding acquisition, E.K.; Investigation, K.H. and C.B.; Methodology, K.H. and N.W.; Supervision, E.K. and N.W.; Writing—original draft, K.H.; Writing—review & editing, E.K. and N.W.

Funding: This research was funded by the European Research Council under the European Union’s Seventh Framework Program (FP/2007-2013)/ERC Grant Agreement No. 335380 and support from the Research Foundation Flanders (FWO) Odysseus Program (Grant agreement No. G0H9518N).

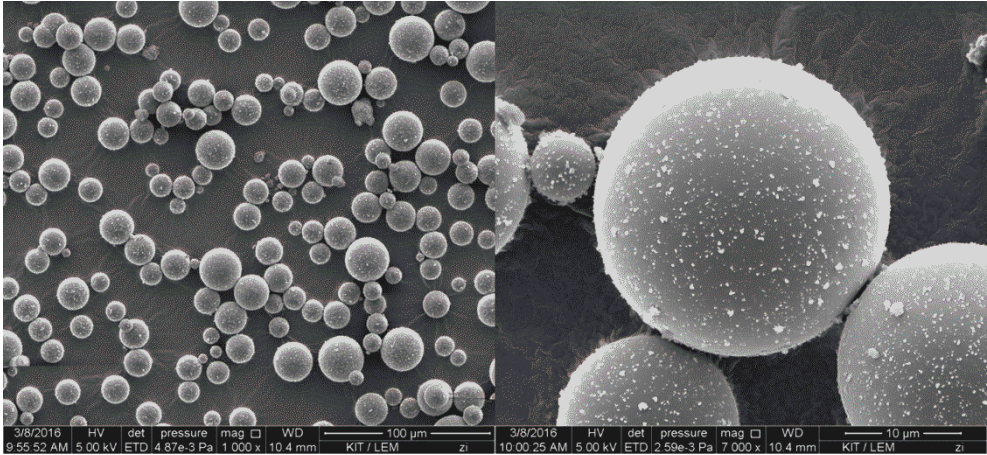
Acknowledgments: The authors would like to thank Petra Schlager from the IMB/MPA at KIT in Karlsruhe for contributing of physical properties of the glass materials and Volker Zibat from LEM for SEM. Special thanks to Frank Bossler for fruitful discussion and proof reading.

Conflicts of Interest: The authors declare no conflict of interest.

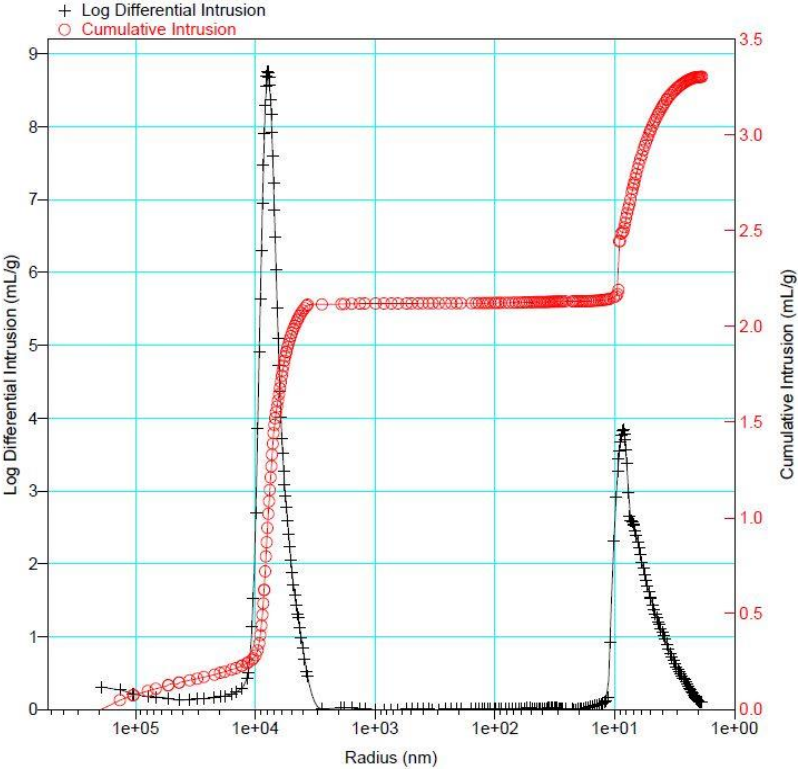
5.5 Supplementary Information



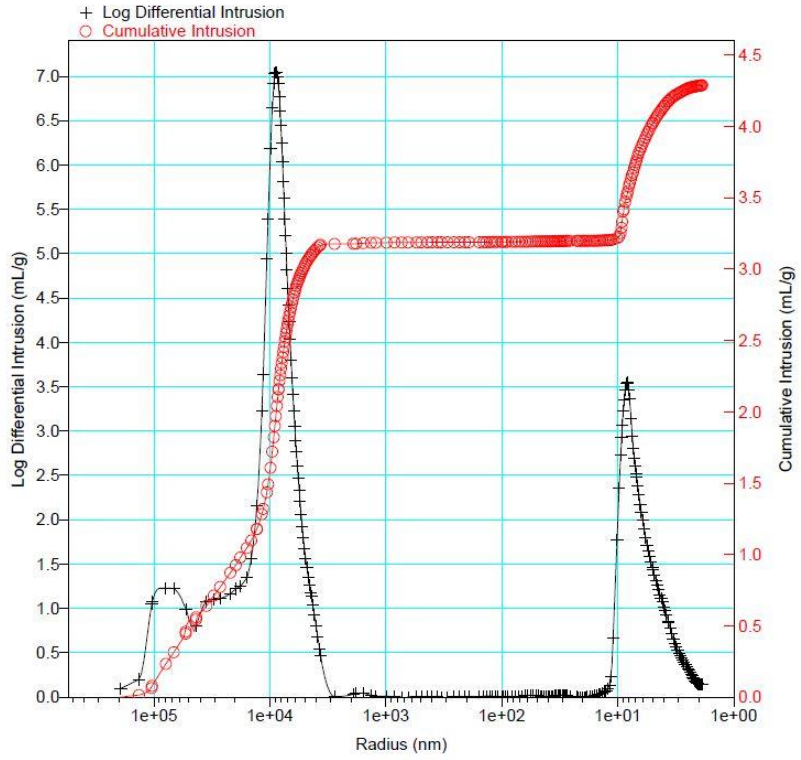
S5.1 SEM image of the untreated particles. Copyright 2019.



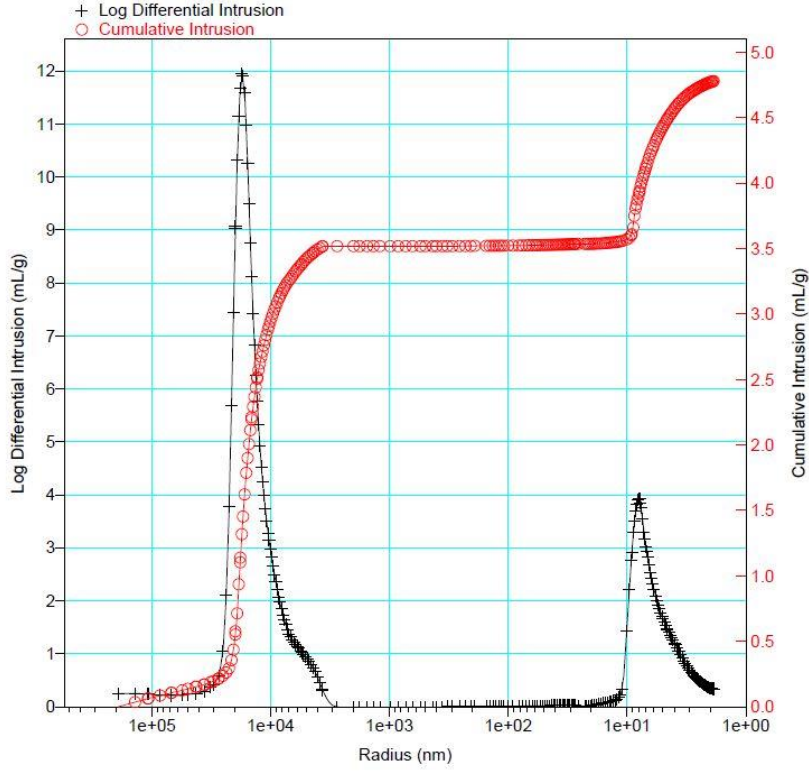
S5.2 SEM image of the treated particles. Copyright 2019.



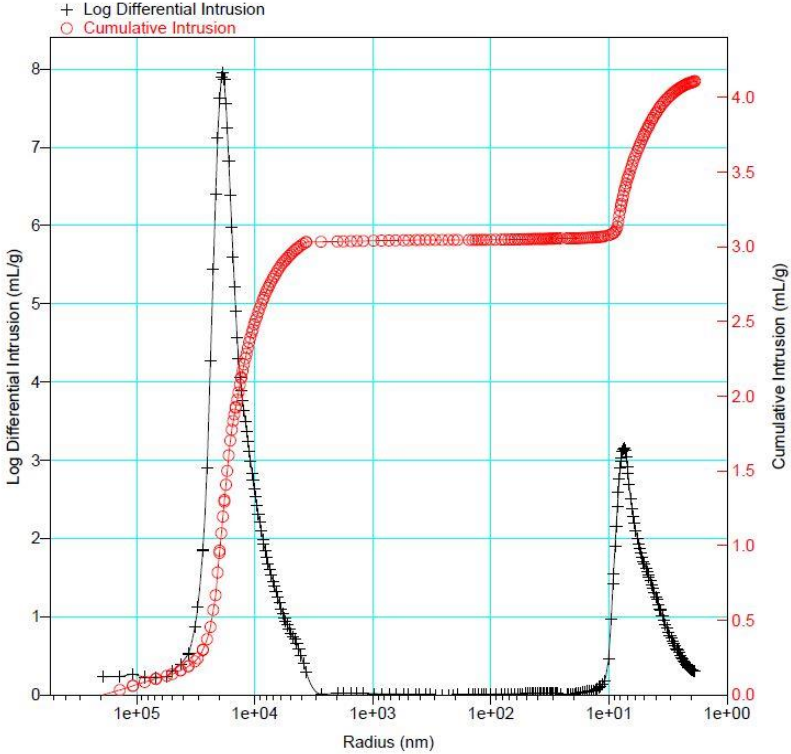
S5.3 Pore size distribution of the untreated particles with 3% epoxy. Copyright 2019.



S5.4 Pore size distribution of the untreated particles with 6% epoxy. Copyright 2019.



S5.5 Pore size distribution of the treated particles with 3% epoxy. Copyright 2019.



55.6 Pore size distribution of the treated particles with 6% epoxy. Copyright 2019.

6. Summary and outlook

The aim of this thesis was to find a way to create a particulate network with microporosity interconnected by nano-sized polymeric bridges via the capillary suspension theory. The requirements for this model were:

- Micron-sized particles with non-reactive surface properties
- A secondary liquid that is able to polymerize or crosslink without air
- A bulk fluid that is insoluble with the secondary liquid, does not modify the particles, and provides a sufficient droplet break-up of the secondary liquid to realize enough small droplets for the bridging phase between the particles

A study of the state of the art in the field was summarized **Paper 1**. “*Structure of capillary suspensions and their versatile applications in the creation of smart materials*” [25], where a review of similar research was presented. Starting from the investigative work on capillary suspensions from Bossler [9,14,50], the focus in this publication was on the different methods to bond particles. The work of Das and coworkers [37], where they used hydrogels as the bridging phase was highlighted along with the PDMS samples of Roh et al. [42]. Furthermore, various control and tuning parameters, known from the sintering technique of Dittmann and Maurath et al. [22,44,50] were presented.

The first model system meeting the aforementioned requirements was realized in **Paper 2**. “*Radical polymerization of capillary bridges between micron-sized particles in liquid bulk phase as a low-temperature route to produce porous solid materials*” [8]. Here, micron-sized glass hollow spheres were used in a suspension with water and a small amount of methyl methacrylate, which was radically polymerized with benzoyl peroxide under thermal treatment. The polymerized bridging phase was closely examined to determine the chemical composition and the molecular weight distribution as influenced by the amount of monomer, the concentration of the initiator as well as the experimental conditions, namely the polymerization temperature and time. It was shown that it is possible to place the monomer between the particles via the capillary suspension preparation method and to polymerize it in situ. This was possible at temperatures below 100 °C and at times less than 5 h. An unexpected result was the nearly 3x higher molecular weight of the bridge polymer compared to the bulk polymer. This was explained by the more efficient heat transfer and the large surface-to-volume-ratio of the small monomer bridges surrounded by glass and bulk fluid [8]. Additional to the chemical investigation, another model was presented with glass particles in paraffin oil with hydroxyethyl methacrylate and the application of other particles like graphite using this material system and processing route. This Paper demonstrated the versatility of placing and polymerizing a monomer droplet between particles to create a sample-spanning particle network that results in a porous material.

For better understanding of the inter-particulate forces created by the bridging phase between the particles, an advanced setup was developed combining an atomic force microscope (AFM) with additional cameras, presented in **chapter 4** in the form of a scientific paper to be submitted. With this arrangement, it is possible to transfer picoliters of a bridging fluid between two micron-sized spheres to determine the capillary forces of the unpolymerized bridges with simultaneously visual observation at every timestep. Special features of this system were shown to be the direct observation of the behavior of capillary bridges under the displacement as well as the easy calculation of the wetting contact angle between the liquid bridge and the spherical shaped particles from both the capillary

force data and the images. This device can also be used to determine the Hamaker constant between micron-sized glass particles via force-distance measurements in air and in glycerol, as well as for the investigation of the failure behavior of crosslinked epoxy bridges between two microparticles.

It was shown in Paper 2 that the bridging fluid could be used to create a porous material. The mechanical stability of porous materials made of glass hollow spheres bonded by polymers was examined in **Paper 4**. "*Lightweight porous glass composite materials based on capillary suspensions*", where a two-component epoxy was used as the bridging phase and glycerol as the bulk fluid. Using hydrophilic and hydrophobically modified glass hollow spheres, two different particle networks with different physical properties could be created. The contact angle determined the bridge shape between the particles as well as the resulting network. Polymerization in glycerol provided the preservation of the network structure from the wet into the solid state.

The benefits of porous materials made of interconnected particle networks provides a broad field of applications like materials for heat-exchange-interphases, flexible and conductive membranes for electronics, and a variety of filtering techniques. The processing route of creating porous bodies via capillary suspensions has various variables that can be tuned to influence the properties of the final product. These start with choosing the appropriate raw materials. The particles, the secondary phase (adhering material), and right bulk phase are chosen for appropriate handling and the desired rheological behavior for processing the paste. The material properties of the particles and the adhering phase defines the application. Examples include glass particles, heat exchange particles, graphite particles and stiff or flexible polymers, like epoxy glues or elastomers. The amount of particles, the particle size, as well as the class and amount of the secondary bridging phase determines the microstructure in the paste and, consequently, the physical properties, like porosity, pore size and mechanical strength. A selection of the material systems used in this thesis is presented in Table 4.

Capillary suspensions with polymeric bridges, where the chemical and physical characteristics can be tuned, provide an elegant method to produce customer-oriented materials. In addition to the filtering techniques presented in this work, the method is potentially applicable to other product segments like medical tissue engineering, food industries or pharmaceuticals. Each sector where a paste or a particulate network scaffold is needed, capillary suspensions with polymeric bridges could be used. Examples include bio-absorbable implant, such as bone or cartilage scaffolds where cells from the body can penetrate into degrade the implant. Capillary suspensions could also find an effective application for drug delivery in pills via the controlled solubility of their coating, which could be made of a fine particulate network of e.g. sugar particles interconnected by biopolymeric bridges. Here, the porosity the tunable solubility of the coating for digestion in the desired region of the body would be beneficial. These manifold application fields show the great ability of the capillary suspensions with polymeric bridges for the broad area of life sciences techniques.

Summary and outlook

Table 4 Different material combinations used in this thesis and the associated physical properties. For each combination, the amounts of particles and secondary phase were varied, but only the maximum values are presented here.

Material class	Glass						Micronal (PCM)	Graphite			
	hydrophobic (hollow)			hydrophilic (hollow)		hydrophilic (dense)	pure	plate-shaped		potato-shaped	
$d_{50, \text{particle}} [\mu\text{m}]$	20			20		5	5.2	18.3		7.8	
$\rho_{\text{material}} [\text{g}/\text{cm}^3]$	0.46			0.46		2.46	0.98	2.27		2.27	
Sec. phase	MMA	HEMA	Epoxy L	HEMA	Epoxy L	Silicone	MMA	HEMA	Epoxy L	HEMA	Epoxy L
$\theta [^\circ]$	0	0	< 57	0	< 50	< 22	0	0	< 26	0	< 28
$\sigma_{\text{yield}} [\text{Pa}]$	< 23	---	< 7	< 144	< 0.4	---	< 10	---	---	< 0.6	---
$\epsilon_{\text{open}} [\%]$	< 67	< 46	< 67	< 70	< 60	(< 48)	< 55	< 68	< 76	< 60	< 76
$d_{\text{pore}} [\mu\text{m}]$	0.5/75	---	14	---	8/90	---	< 67	---	---	---	---
$\sigma_{\text{compressive}} [\text{MPa}]$	< 0.09	< 0.25	< 0.6	< 0.1	< 0.1	< 4	< 0.7	< 0.01	< 0.02	< 0.02	< 0.4
$\sigma_{\text{failure}} [\text{MPa}]$	< 0.08	< 0.14	< 0.2	< 0.1	< 0.07	---	< 0.5	< 0.14	< 0.01	< 0.005	< 0.14
Possible applications	Insulation materials, filters					Flexible filters, interphase materials	Heat-exchange interphase materials	Conductive interphase materials (< 410 mS/cm)			

7. Bibliography

- (1) Schüth, F. Poröse Materialien Im Überblick. *Chemie-Ingenieur-Technik* **2010**, *82* (6), 769–777; DOI:10.1002/cite.201000063.
- (2) Sing, K. S. W. Reporting Physisorption Data for Gas/Solid Systems with Special Reference to the Determination of Surface Area and Porosity (Recommendations 1984). *Pure Appl. Chem.* **1985**, *57* (4), 603–619; DOI:10.1351/pac198557040603.
- (3) Heritage, E. MICROSEISMIC TESTS IN THE ANALYSIS AND CHARACTERIZATION OF. **1999**.
- (4) Da Silva, A.; Kyriakides, S. Compressive Response and Failure of Balsa Wood. *Int. J. Solids Struct.* **2007**, *44* (25–26), 8685–8717; DOI:10.1016/j.ijsolstr.2007.07.003.
- (5) Jacobs, L. J. M.; Kemmere, M. F.; Keurentjes, J. T. F. Sustainable Polymer Foaming Using High Pressure Carbon Dioxide: A Review on Fundamentals, Processes and Applications. *Green Chem.* **2008**, *10* (7), 731; DOI:10.1039/b801895b.
- (6) Torres-Rendon, J. G.; Femmer, T.; De Laporte, L.; Tigges, T.; Rahimi, K.; Gremse, F.; Zafarnia, S.; Lederle, W.; Ifuku, S.; Wessling, M.; et al. Bioactive Gyroid Scaffolds Formed by Sacrificial Templating of Nanocellulose and Nanochitin Hydrogels as Instructive Platforms for Biomimetic Tissue Engineering. *Adv. Mater.* **2015**, *27* (19), 2989–2995; DOI:10.1002/adma.201405873.
- (7) Jin, R. H.; Yuan, J. J. Fabrication of Silver Porous Frameworks Using Poly(Ethyleneimine) Hydrogel as a Soft Sacrificial Template. *J. Mater. Chem.* **2005**, *15* (42), 4513–4517; DOI:10.1039/b507125a.
- (8) Hauf, K.; Riaz, K.; Willenbacher, N.; Koos, E. Radical Polymerization of Capillary Bridges between Micron-Sized Particles in Liquid Bulk Phase as a Low-Temperature Route to Produce Porous Solid Materials. *Colloid Polym. Sci.* **2017**, *295* (10), 1773–1785; DOI:10.1007/s00396-017-4149-y.
- (9) Bossler, F.; Koos, E. Structure of Particle Networks in Capillary Suspensions with Wetting and Nonwetting Fluids. *Langmuir* **2016**, *32* (6), 1489–1501; DOI:10.1021/acs.langmuir.5b04246.
- (10) Pietsch, W.; Rumpf, H. Haftkraft, Kapillardruck, Flüssigkeitsvolumen Und Grenzwinkel Einer Flüssigkeitsbrücke Zwischen Zwei Kugeln. *Chemie Ing. Tech.* **1967**, *15*, 885–893; DOI:10.1002/cite.330391502.
- (11) Schubert, H. Kapillardruck Und Zugfestigkeit von Feuchten Haufwerken Aus Kornigen Stoffen *. **1973**, No. 6, 396–401.
- (12) Bossler, F. Structural Investigations of Capillary Suspensions Using Rheology and Confocal Microscopy. **2018**.
- (13) Koos, E.; Willenbacher, N. Capillary Forces in Suspension Rheology. *Science (80-.)*. **2011**, *331* (1994), 897–900; DOI:10.1126/science.1199243.
- (14) Bossler, F.; Weyrauch, L.; Schmidt, R.; Koos, E. Influence of Mixing Conditions on the Rheological Properties and Structure of Capillary Suspensions. 1–40; DOI:10.1016/j.colsurfa.2017.01.026.
- (15) Frank Bossler, Johannes Maurath, Katrin Dyhr, N. W. and E. K. Fractal Approaches to Capillary Suspension Structure Characterization Using Rheology and Confocal Microscopy. **2017**.
- (16) Wollgarten, S.; Yuce, C.; Koos, E.; Willenbacher, N. Tailoring Flow Behavior and Texture of Water Based Cocoa Suspensions. *Food Hydrocoll.* **2016**, *52*, 167–174;

DOI:10.1016/j.foodhyd.2015.06.010.

- (17) Bitsch, B.; Gallasch, T.; Schroeder, M.; Börner, M.; Winter, M.; Willenbacher, N. Capillary Suspensions as Beneficial Formulation Concept for High Energy Density Li-Ion Battery Electrodes. *J. Power Sources* **2016**, *328*, 114–123; DOI:10.1016/j.jpowsour.2016.07.102.
- (18) Bitsch, B.; Dittmann, J.; Schmitt, M.; Scharfer, P.; Schabel, W.; Willenbacher, N. A Novel Slurry Concept for the Fabrication of Lithium-Ion Battery Electrodes with Beneficial Properties. *J. Power Sources* **2014**, *265*, 81–90; DOI:10.1016/j.jpowsour.2014.04.115.
- (19) Schneider, M.; Maurath, J.; Fischer, S. B.; Weiß, M.; Willenbacher, N.; Koos, E. Suppressing Crack Formation in Particulate Systems by Utilizing Capillary Forces. *ACS Appl. Mater. Interfaces* **2017**, *9* (12), 11095–11105; DOI:10.1021/acsami.6b13624.
- (20) Jampolski, L.; Sängler, A.; Jakobs, T.; Guthausen, G.; Kolb, T.; Willenbacher, N. Improving the Processability of Coke Water Slurries for Entrained Flow Gasification. *Fuel* **2016**, *185*, 102–111; DOI:10.1016/j.fuel.2016.07.102.
- (21) Koos, E.; Dittmann, J.; Willenbacher, N. Kapillarkräfte in Suspensionen: Rheologische Eigenschaften Und Potenzielle Anwendungen. *Chemie-Ingenieur-Technik* **2011**, *83* (8), 1305–1309; DOI:10.1002/cite.201100059.
- (22) Dittmann, J.; Koos, E.; Willenbacher, N. Ceramic Capillary Suspensions: Novel Processing Route for Macroporous Ceramic Materials. *J. Am. Ceram. Soc.* **2013**, *96* (2), 391–397; DOI:10.1111/jace.12126.
- (23) Dittmann, J.; Maurath, J.; Bitsch, B.; Willenbacher, N. Highly Porous Materials with Unique Mechanical Properties from Smart Capillary Suspensions. *Adv. Mater.* **2016**, *28* (8), 1689–1696; DOI:10.1002/adma.201504910.
- (24) Maurath, J.; Willenbacher, N. 3D Printing of Open-Porous Cellular Ceramics with High Specific Strength. *J. Eur. Ceram. Soc.* **2017**, *37* (15), 4833–4842; DOI:10.1016/j.jeurceramsoc.2017.06.001.
- (25) Hauf, K.; Koos, E. Structure of Capillary Suspensions and Their Versatile Applications in the Creation of Smart Materials. *MRS Commun.* **2018**, 1–11; DOI:10.1557/mrc.2018.28.
- (26) Hartung, K.; Benner, C.; Willenbacher, N.; Koos, E. Lightweight Porous Glass Composite Materials Based on Capillary Suspensions. **2019**; DOI:10.3390/ma12040619.
- (27) Domenech, T.; Velankar, S. Capillary-Driven Percolating Networks in Ternary Blends of Immiscible Polymers and Silica Particles. *Rheol. Acta* **2014**, *53* (8), 593–605; DOI:10.1007/s00397-014-0776-0.
- (28) Yang, J.; Velankar, S. S. Preparation and Yielding Behavior of Pendular Network Suspensions. **2017**, *217*.
- (29) Xu, J.; Chen, L.; Choi, H.; Konish, H.; Li, X. Assembly of Metals and Nanoparticles into Novel Nanocomposite Superstructures. *Sci. Rep.* **2013**, *3*, 1–5; DOI:10.1038/srep01730.
- (30) Dunstan, T. S.; Das, A. A. K.; Starck, P.; Stoyanov, S. D.; Paunov, V. N. Capillary Structured Suspensions from *In Situ* Hydrophobized Calcium Carbonate Particles Suspended in a Polar Liquid Media. *Langmuir* **2017**, *acs.langmuir.7b03589*; DOI:10.1021/acs.langmuir.7b03589.
- (31) Domenech, T.; Velankar, S. S. Microstructure, Phase Inversion and Yielding in Immiscible Polymer Blends with Selectively Wetting Silica Particles. **2017**, *363*.
- (32) Danov, K. D.; Georgiev, M. T.; Kralchevsky, P. A.; Radulova, G. M. Hardening of Particle / Oil / Water Suspensions Due to Capillary Bridges : Experimental Yield Stress and Theoretical

Interpretation.

- (33) Hoffmann, S.; Koos, E.; Willenbacher, N. Using Capillary Bridges to Tune Stability and Flow Behavior of Food Suspensions. *Food Hydrocoll.* **2014**, *40*, 44–52; DOI:10.1016/j.foodhyd.2014.01.027.
- (34) Schneider, M.; Koos, E.; Willenbacher, N. Highly Conductive, Printable Pastes from Capillary Suspensions. *Sci. Rep.* **2016**, *6* (August), 1–10; DOI:10.1038/srep31367.
- (35) Dittmann, J.; Willenbacher, N. Micro Structural Investigations and Mechanical Properties of Macro Porous Ceramic Materials from Capillary Suspensions. *J. Am. Ceram. Soc.* **2014**, *97* (12), 3787–3792; DOI:10.1111/jace.13184.
- (36) Koos, E.; Willenbacher, N. Particle Configurations and Gelation in Capillary Suspensions. *Soft Matter* **2012**, *8*, 3988; DOI:10.1039/c2sm07347a.
- (37) Das, A. A. K.; Dunstan, T. S.; Stoyanov, S. D.; Starck, P.; Paunov, V. N. Thermally Responsive Capillary Suspensions. *ACS Appl. Mater. Interfaces* **2017**, acsami.7b11358; DOI:10.1021/acsami.7b11358.
- (38) Domenech, T.; Velankar, S. S. On the Rheology of Pendular Gels and Morphological Developments in Paste-like Ternary Systems Based on Capillary Attraction. *Soft Matter* **2015**, *11* (8), 1500–1516; DOI:10.1039/C4SM02053G.
- (39) Heidlebaugh, S. J.; Domenech, T.; Iasella, S. V.; Velankar, S. S. Aggregation and Separation in Ternary Particle/Oil/Water Systems with Fully Wettable Particles. *Langmuir* **2014**, *30* (1), 63–74; DOI:10.1021/la4039396.
- (40) Domenech, T.; Yang, J.; Heidlebaugh, S.; Velankar, S. S. Three Distinct Open-Pore Morphologies from a Single Particle-Filled Polymer Blend. *Phys. Chem. Chem. Phys.* **2016**, *18* (6), 4310–4315; DOI:10.1039/C5CP07576A.
- (41) Yang, J.; Roell, D.; Echavarria, M.; Velankar, S. S. A Microstructure-Composition Map of a Ternary Liquid/Liquid/Particle System with Partially-Wetting Particles. *Soft Matter* **2017**; DOI:10.1039/C7SM01571B.
- (42) Roh, S.; Parekh, D. P.; Bharti, B.; Stoyanov, S. D.; Velev, O. D. 3D Printing by Multiphase Silicone/Water Capillary Inks. *Adv. Mater.* **2017**, *29* (30), 1–7; DOI:10.1002/adma.201701554.
- (43) Maurath, J.; Dittmann, J.; Schultz, N.; Willenbacher, N. Fabrication of Highly Porous Glass Filters Using Capillary Suspension Processing. *Sep. Purif. Technol.* **2015**, *149*, 470–478; DOI:10.1016/j.seppur.2015.06.022.
- (44) Maurath, J.; Bitsch, B.; Schwegler, Y.; Willenbacher, N. Influence of Particle Shape on the Rheological Behavior of Three-Phase Non-Brownian Suspensions. *Colloids Surfaces A Physicochem. Eng. Asp.* **2016**, *497*, 316–326; DOI:10.1016/j.colsurfa.2016.03.006.
- (45) Willett, C. D.; Adams, M. J.; Johnson, S. A.; Seville, J. P. K. K. Capillary Bridges between Two Spherical Bodies. *Langmuir* **2000**, *16* (24), 9396–9405; DOI:10.1021/la000657y.
- (46) Pitois, O.; Moucheront, P.; Chateau, X. Rupture Energy of a Pendular Liquid Bridge. *Eur. Phys. J. B* **2001**, *23* (1), 79–86; DOI:10.1007/s100510170084.
- (47) Willett, C. D.; Adams, M. J.; Johnson, S. A.; Seville, J. P. K. Effects of Wetting Hysteresis on Pendular Liquid Bridges between Rigid Spheres. *Powder Technol.* **2003**, *130* (1–3), 63–69; DOI:10.1016/S0032-5910(02)00235-8.
- (48) Koos, E.; Johannsmeier, J.; Schwebler, L.; Willenbacher, N. Tuning Suspension Rheology Using Capillary Forces. *Soft Matter* **2012**, *8* (24), 6620; DOI:10.1039/c2sm25681a.

-
- (49) Flemmer, C. L. On the Regime Boundaries of Moisture in Granular Materials. *Powder Technol.* **1991**, *66* (2), 191–194; DOI:10.1016/0032-5910(91)80100-W.
- (50) Bossler, F.; Maurath, J.; Dyhr, K.; Willenbacher, N.; Koos, E. Fractal Approaches to Characterize the Structure of Capillary Suspensions Using Rheology and Confocal Microscopy. *J. Rheol. (N. Y. N. Y.)* **2018**, *62* (1), 183–196.
- (51) Piau, J.-M.; Dorget, M.; Palierne, J.-F.; Pouchelon, A. Shear Elasticity and Yield Stress of Silica–Silicone Physical Gels: Fractal Approach. *J. Rheol. (N. Y. N. Y.)* **1999**, *43* (2), 305–314; DOI:10.1122/1.550989.
- (52) Wu, H.; Morbidelli, M. Model Relating Structure of Colloidal Gels to Their Elastic Properties. *Langmuir* **2001**, *17* (4), 1030–1036; DOI:10.1021/la001121f.
- (53) Koos, E.; Kannowade, W.; Willenbacher, N. Restructuring and Aging in a Capillary Suspension. *Rheol. Acta* **2014**, *53* (12), 947–957; DOI:10.1007/s00397-014-0805-z.
- (54) Velankar, S. S. A Non-Equilibrium State Diagram for Liquid/Fluid/Particle Mixtures. *Soft Matter* **2015**, *11*, 8393–8403; DOI:10.1039/C5SM01901J.
- (55) Zhang, Y.; Allen, M. C.; Zhao, R.; Deheyn, D. D.; Behrens, S. H.; Meredith, J. C. Capillary Foams: Stabilization and Functionalization of Porous Liquids and Solids. *Langmuir* **2015**, *31* (9), 2669–2676; DOI:10.1021/la504784h.
- (56) Bharti, B.; Fameau, A. L.; Rubinstein, M.; Velev, O. D. Nanocapillarity-Mediated Magnetic Assembly of Nanoparticles into Ultraflexible Filaments and Reconfigurable Networks. *Nat. Mater.* **2015**, *14* (11), 1104–1109; DOI:10.1038/nmat4364.
- (57) Kumar, R.; Bhattacharjee, B. Porosity, Pore Size Distribution and In-Situ Strength of Concrete. *Cem. Concr. Res.* **2003**, *33* (1), 155–164; DOI:10.1016/S0008-8846(02)00942-0.
- (58) Babu, C. H. A.; Rao, M. P.; J, V. R. JPRHC Review Article. **2010**, *2* (1).
- (59) Tunón, Å.; Börjesson, E.; Frenning, G.; Alderborn, G. Drug Release from Reservoir Pellets Compacted with Some Excipients of Different Physical Properties. *Eur. J. Pharm. Sci.* **2003**, *20* (4–5), 469–479; DOI:10.1016/j.ejps.2003.09.009.
- (60) Tunón, Å.; Gråsjö, J.; Alderborn, G. Effect of Intragranular Porosity on Compression Behaviour of and Drug Release from Reservoir Pellets. *Eur. J. Pharm. Sci.* **2003**, *19* (5), 333–344; DOI:10.1016/S0928-0987(03)00106-4.
- (61) Ulbricht, M. Advanced Functional Polymer Membranes. *Polymer (Guildf)*. **2006**, *47* (7), 2217–2262; DOI:10.1016/j.polymer.2006.01.084.
- (62) Lee, M.; Park, J. K.; Lee, H. S.; Lane, O.; Moore, R. B.; McGrath, J. E.; Baird, D. G. Effects of Block Length and Solution-Casting Conditions on the Final Morphology and Properties of Disulfonated Poly(Arylene Ether Sulfone) Multiblock Copolymer Films for Proton Exchange Membranes. *Polymer (Guildf)*. **2009**, *50* (25), 6129–6138; DOI:10.1016/j.polymer.2009.10.023.
- (63) Vankelecom, I. F. J. Polymeric Membranes in Catalytic Reactors. **2002**.
- (64) Tabatabaei, S. H.; Carreau, P. J.; Ajji, A. Microporous Membranes Obtained from Polypropylene Blend Films by Stretching. *J. Memb. Sci.* **2008**, *325* (2), 772–782; DOI:10.1016/j.memsci.2008.09.001.
- (65) Lee, S. Y.; Park, S. Y.; Song, H. S. Lamellar Crystalline Structure of Hard Elastic HDPE Films and Its Influence on Microporous Membrane Formation. *Polymer (Guildf)*. **2006**, *47* (10), 3540–3547; DOI:10.1016/j.polymer.2006.03.070.

-
- (66) Tabatabaei, S. H.; Carreau, P. J.; Ajjji, A. Microporous Membranes Obtained from PP/HDPE Multilayer Films by Stretching. *J. Memb. Sci.* **2009**, *345* (1–2), 148–159; DOI:10.1016/j.memsci.2009.08.038.
- (67) Stropnik, C.; Germic, L.; Zerjal, B. Morphology Variety and Formation Mechanisms of Polymeric Membranes Prepared by Wet Phase Inversion. *J. Appl. Polym. Sci.* **1996**, *61* (10), 1821–1830; DOI:10.1002/(SICI)1097-4628(19960906)61:10<1821::AID-APP24>3.0.CO;2-3.
- (68) Wienk, I. M.; Boom, R. M.; Beerlage, M. A. M.; Bulte, A. M. W.; Smolders, C. A.; Strathmann, H. Recent Advances in the Formation of Phase Inversion Membranes Made from Amorphous or Semi-Crystalline Polymers. *J. Memb. Sci.* **1996**, *113* (2), 361–371; DOI:10.1016/0376-7388(95)00256-1.
- (69) Pinnau, I.; Freeman, B. D. Formation and Modification of Polymeric Membranes: Overview. *Membr. Form. Modif.* **1999**, *744*, 1; DOI:doi:10.1021/bk-2000-0744.ch001.
- (70) Li, D.; Chung, T. S.; Wang, R. Morphological Aspects and Structure Control of Dual-Layer Asymmetric Hollow Fiber Membranes Formed by a Simultaneous Co-Extrusion Approach. *J. Memb. Sci.* **2004**, *243* (1–2), 155–175; DOI:10.1016/j.memsci.2004.06.014.
- (71) Jeong, B. H.; Hoek, E. M. V.; Yan, Y.; Subramani, A.; Huang, X.; Hurwitz, G.; Ghosh, A. K.; Jawor, A. Interfacial Polymerization of Thin Film Nanocomposites: A New Concept for Reverse Osmosis Membranes. *J. Memb. Sci.* **2007**, *294* (1–2), 1–7; DOI:10.1016/j.memsci.2007.02.025.
- (72) Song, Y.; Sun, P.; Henry, L. L.; Sun, B. Mechanisms of Structure and Performance Controlled Thin Film Composite Membrane Formation via Interfacial Polymerization Process. *J. Memb. Sci.* **2005**, *251* (1–2), 67–79; DOI:10.1016/j.memsci.2004.10.042.
- (73) Freger, V. Nanoscale Heterogeneity of Polyamide Membranes Formed by Interfacial Polymerization. *Langmuir* **2003**, *19* (11), 4791–4797; DOI:10.1021/la020920q.
- (74) Zou, L.; Vidalis, I.; Steele, D.; Michelmore, A.; Low, S. P.; Verberk, J. Q. J. C. Surface Hydrophilic Modification of RO Membranes by Plasma Polymerization for Low Organic Fouling. *J. Memb. Sci.* **2011**, *369* (1–2), 420–428; DOI:10.1016/j.memsci.2010.12.023.
- (75) Silverstein, M. S. Emulsion-Templated Porous Polymers: A Retrospective Perspective. *Polym. (United Kingdom)* **2014**, *55* (1), 304–320; DOI:10.1016/j.polymer.2013.08.068.
- (76) Studart, A. R.; Gonzenbach, U. T.; Akartuna, I.; Tervoort, E.; Gauckler, L. J. Materials from Foams and Emulsions Stabilized by Colloidal Particles. *J. Mater. Chem.* **2007**, *17* (31), 3283; DOI:10.1039/b703255b.
- (77) Yan, F.; Goedel, W. A. A Simple and Effective Method for the Preparation of Porous Membranes with Three-Dimensionally Arranged Pores. *Adv. Mater.* **2004**, *16* (11), 911–915; DOI:10.1002/adma.200306419.
- (78) Hemmerle, A.; Schröter, M.; Goehring, L. A Tunable Cohesive Granular Material. **2016**, 1–12.
- (79) Kiesow, I.; Marczewski, D.; Reinhardt, L.; Mühlmann, M.; Possiwan, M.; Goedel, W. A. Bicontinuous Zeolite Polymer Composite Membranes Prepared via Float Casting. *J. Am. Chem. Soc.* **2013**, *135* (11), 4380–4388; DOI:10.1021/ja311785f.
- (80) Uemura, T.; Kitagawa, S. Polymerization in Confined Geometries. In *Materials Science and Technology*; Wiley-VCH Verlag GmbH & Co. KGaA, 2006; DOI:10.1002/9783527603978.mst0442.
- (81) Petrie, R. J. et al. *Polymerization in Confined Geometries*; 2006.
- (82) Dittmann, J. Verwendung von Kapillarsuspensionen Als Precursor Für Die Herstellung

-
- Hochporöser Sinterwerkstoffe; KIT, Karlsruhe: Karlsruhe, **2015**.
- (83) de Rooij, R.; Potanin, a a; van den Ende, D.; Mellema, J. Steady Shear Viscosity of Weakly Aggregating Polystyrene Latex Dispersions. *J. Chem. Phys.* **1993**, *99* (11), 9213; DOI:10.1063/1.465537.
- (84) Zhang, J.; Zhao, H.; Li, W.; Xu, M.; Liu, H. Multiple Effects of the Second Fluid on Suspension Viscosity. *Sci. Rep.* **2015**, *5* (130), 16058; DOI:10.1038/srep16058.
- (85) Bovey, F. A.; Jelinski, L.; Mirau, P. A. *NMR Spectroscopy.Pdf*, Second Edi.; ACADEMIC PRESS, INC., 1988.
- (86) Smith, L. M.; Coote, M. L. Effect of Temperature and Solvent on Polymer Tacticity in the Free-Radical Polymerization of Styrene and Methyl Methacrylate. *J. Polym. Sci. Part A Polym. Chem.* **2013**, *51* (16), 3351–3358; DOI:10.1002/pola.26745.
- (87) Matyjaszewski, K. Radical Polymerization. **2010**.
- (88) Odian, G. Principles of Polymerization; 2004; Vol. 58; DOI:10.1002/047147875X.ch3.
- (89) Moad, G. Radical Polymerization; Elsevier B.V., 2012; Vol. 3; DOI:10.1016/B978-0-444-53349-4.00063-7.
- (90) Ober, C. K.; Lok, K. P. Formation of Large Monodisperse Copolymer Particles by Dispersion Polymerization. *Macromolecules* **1987**, *20* (2), 268–273; DOI:10.1021/ma00168a007.
- (91) Paine, A. J.; Luymes, W.; McNulty, J. Dispersion Polymerization of Styrene in Polar Solvents. 6. Influence of Reaction Parameters on Particle Size and Molecular Weight in Poly(N-Vinylpyrrolidone)-Stabilized Reactions. *Macromolecules* **1990**, *23* (12), 3104–3109; DOI:10.1021/ma00214a012.
- (92) Pletincx, S.; Marcoen, K.; Trotochaud, L.; Fockaert, L.; Mol, J. M. C.; Head, A. R.; Karslioglu, O.; Bluhm, H.; Terryn, H.; Hauffman, T. Unravelling the Chemical Influence of Water on the PMMA / Aluminum Oxide Hybrid Interface In Situ. **2017**, No. July, 1–11; DOI:10.1038/s41598-017-13549-z.
- (93) Gibson, L. J.; Ashby, M. F. *Cellular Solids: Structure and Properties*; 1997; Vol. 7.
- (94) van den Honert, T. H. Water Transport in Plants as a Catenary Process. *Discuss. Faraday Soc.* **1948**, *3* (146), 146; DOI:10.1039/DF9480300146.
- (95) Zimmermann, U.; Haase, A.; Langbein, D.; Meinzer, F. Mechanisms of Long-Distance Water Transport in Plants: A Re-Examination of Some Paradigms in the Light of New Evidence. *Philos. Trans. R. Soc. B Biol. Sci.* **1993**, *341* (1295), 19–31; DOI:10.1098/rstb.1993.0087.
- (96) Seemann, R.; Brinkmann, M.; Herminghaus, S. Auf Sand Gebaut. *Phys. J.* **2009**, *8* (11), 31–36.
- (97) Strauch, S.; Herminghaus, S. Wet Granular Matter: A Truly Complex Fluid. *Soft Matter* **2012**, *8* (32), 8271–8280; DOI:10.1039/c2sm25883h.
- (98) Zitzler, L.; Herminghaus, S.; Mugele, F. Capillary Forces in Tapping Mode Atomic Force Microscopy. *Phys. Rev. B* **2002**, *66* (15), 1–8; DOI:10.1103/PhysRevB.66.155436.
- (99) Scheel, M.; Seemann, R.; Fingerle, A.; Roeller, K.; Fournier, Z.; Geromichalos, D.; Herminghaus, S.; Kohonen, M. M.; Mugele, F.; Scheel, M.; et al. Mechanical Properties of Wet Granular Materials. *J. Phys. Condens. Matter* **2005**, *17* (9); DOI:10.1088/0953-8984/17/9/013.
- (100) Scheel, M.; Seemann, R.; Brinkmann, M.; Di Michiel, M.; Sheppard, A.; Breidenbach, B.; Herminghaus, S. Morphological Clues to Wet Granular Pile Stability. *Nat. Mater.* **2008**, *7* (3), 189–193; DOI:10.1038/nmat2117.

-
- (101) Farmer, T. P.; Bird, J. C. Asymmetric Capillary Bridges between Contacting Spheres. *J. Colloid Interface Sci.* **2015**, *454*, 192–199; DOI:10.1016/j.jcis.2015.04.045.
- (102) Gandyra, D.; Walheim, S.; Gorb, S.; Barthlott, W.; Schimmel, T. The Capillary Adhesion Technique: A Versatile Method for Determining the Liquid Adhesion Force and Sample Stiffness. *Beilstein J. Nanotechnol.* **2015**, *6* (1), 11–18; DOI:10.3762/bjnano.6.2.
- (103) Wang, J. P.; Gallo, E.; François, B.; Gabrieli, F.; Lambert, P. Capillary Force and Rupture of Funicular Liquid Bridges between Three Spherical Bodies. *Powder Technol.* **2017**, *305*, 89–98; DOI:10.1016/j.powtec.2016.09.060.
- (104) Noy, A.; Frisbie, C. D.; Rozsnyai, L. F.; Wrighton, M. S.; Lieber, C. M. Chemical Force Microscopy - Exploiting Chemically-Modified Tips To Quantify Adhesion, Friction, and Functional-Group Distributions in Molecular Assemblies. *J. Am. Chem. Soc.* **1995**, *117* (30), 7943–7951; DOI:10.1021/ja00135a012.
- (105) Göttinger, M.; Peukert, W. Dispersive Forces of Particle-Surface Interactions: Direct AFM Measurements and Modelling. *Powder Technol.* **2003**, *130* (1–3), 102–109; DOI:10.1016/S0032-5910(02)00234-6.
- (106) Sprakel, J.; Bartscherer, E.; Hoffmann, G.; Cohen Stuart, M. A.; Van Der Gucht, J. Dynamics of Polymer Bridge Formation and Disruption. *Phys. Rev. E - Stat. Nonlinear, Soft Matter Phys.* **2008**, *78* (4), 2–5; DOI:10.1103/PhysRevE.78.040802.
- (107) Ouyang, Q.; Ishida, K.; Okada, K. Investigation of Micro-Adhesion by Atomic Force Microscopy. *Appl. Surf. Sci.* **2001**, *169–170* (July 1999), 644–648; DOI:10.1016/S0169-4332(00)00804-7.
- (108) Hamaker, H. C. The London-van Der Waals Attraction between Spherical Particles. *Physica* **1937**, *4* (10), 1058–1072; DOI:10.1016/S0031-8914(37)80203-7.
- (109) van Oss, C. J.; Chaudhury, M. K.; Good, R. J. Interfacial Lifshitz—van Der Waals and Polar Interactions in Macroscopic Systems. *Chem. Rev.* **1988**, *88* (6), 927–941; DOI:10.1021/cr00088a006.
- (110) Mastrangelo, C. H. C. H.; Hsu, C. H. H. Mechanical Stability and Adhesion of Microstructures under Capillary Forces. II. Experiments. *J. Microelectromechanical Syst.* **1993**, *2* (1), 33–43; DOI:10.1109/84.232594.
- (111) Hwang, K. S.; German, R. M.; Lenel, F. V. Capillary Forces between Spheres during Agglomeration and Liquid Phase Sintering. *Metall. Trans. A* **1987**, *18* (January), 11–17; DOI:10.1007/BF02646216.
- (112) Tardos, G. I.; Khan, M. I.; Mort, P. R. Critical Parameters and Limiting Conditions in Binder Granulation of Fine Powders. *Powder Technol.* **1997**, *94* (3), 245–258; DOI:10.1016/S0032-5910(97)03321-4.
- (113) Tardos, G. I.; Gupta, R. Forces Generated in Solidifying Liquid Bridges between Two Small Particles. *Powder Technol.* **1996**, *87* (2), 175–180; DOI:10.1016/0032-5910(95)03074-3.
- (114) Bika, D.; Tardos, G. I.; Panmai, S.; Farber, L.; Michaels, J. Strength and Morphology of Solid Bridges in Dry Granules of Pharmaceutical Powders. *Powder Technol.* **2005**, *150* (2 SPEC. ISS.), 104–116; DOI:10.1016/j.powtec.2004.11.024.
- (115) Marmur, A. Soft Contact: Measurement and Interpretation of Contact Angles. *Soft Matter* **2006**, *2* (1), 12–17; DOI:10.1039/b514811c.
- (116) Tadmor, R. Line Energy and the Relation between Advancing, Receding, and Young Contact Angles. *Langmuir* **2004**, *20* (18), 7659–7664; DOI:10.1021/la049410h.

-
- (117) Pickering, S. U. Cxcvi.—Emulsions. *J. Chem. Soc. Trans.* **1907**, *91*, 2001–2021.
- (118) Lee, M. N.; Chan, H. K.; Mohraz, A. Characteristics of Pickering Emulsion Gels Formed by Droplet Bridging. *Langmuir* **2011**, *26* (6), 3085–3091; DOI:10.1021/la203384f.
- (119) Tavacoli, J. W.; Thijssen, J. H. J.; Schofi, A. B.; Clegg, P. S. Novel , Robust , and Versatile Bijels of Nitromethane , Ethanediol , and Colloidal Silica : Capsules , Sub-Ten- Micrometer Domains , and Mechanical Properties. *Adv. Funct. Mater.* **2011**, *21* (11), 2020–2027; DOI:10.1002/adfm.201002562.
- (120) Thomsen, F. Standardized Measurement of Wetting and Adhesion. *Adhes. Adhes.* **2013**, *10* (4), 12–15.
- (121) Mak, L. H.; Knoll, M.; Weiner, D.; Gorschlüter, A.; Schirmeisen, A.; Fuchs, H. Reproducible Attachment of Micrometer Sized Particles to Atomic Force Microscopy Cantilevers. *Rev. Sci. Instrum.* **2006**, *77* (4), 2006–2008; DOI:10.1063/1.2190068.
- (122) Burnham, N. A.; Colton, R. J.; Burnham, N. A.; Colton, R. J. Measuring the Nanomechanical Properties and Surface Forces of Materials Using an Atomic Force Microscope Measuring the Nanomechanical Properties and Surface Forces of Materials Using an Atomic Force Microscope. *J. Vac. Sci. Technol. A* **1989**, *7* (2906); DOI:10.1116/1.576168.
- (123) Butt, H. J.; Cappella, B.; Kappl, M. Force Measurements with the Atomic Force Microscope: Technique, Interpretation and Applications. *Surf. Sci. Rep.* **2005**, *59* (1–6), 1–152; DOI:10.1016/j.surfrep.2005.08.003.
- (124) Fujita, T.; Ito, R.; Tokoro, C.; Sadaki, J.; Dodbiba, G. Classification of Submicron Ni Particles by Heterocoagulation. **2007**, *173*, 19–28; DOI:10.1016/j.powtec.2006.10.033.
- (125) Hartmüller, J.; Ripperger, S. Die Haftung von Partikeln an Bauteiloberflächen Teil 2 : Theoretische Abschätzung von Haftkräften Aufgrund von Flüssigkeitsbrücken. **2014**, *28* (5), 274–277.
- (126) Martin Göttinger, W. P. Haftkraftverteilungen von Rauhen Haftsystemen Am Beispiel Kugel-Platte. *Chemie Ing. ...* **2003**, No. 12, 1848–1851; DOI:10.1002/cite.
- (127) Herminghaus, S. The Dynamics of Wet Granular Matter. *Adv. Phys.* **2005**, *54*(3), 221–261; DOI:10.1080/00018730500167855.
- (128) Schindelin, J.; Arganda-carreras, I.; Frise, E.; Kaynig, V.; Longair, M.; Pietzsch, T.; Preibisch, S.; Rueden, C.; Saalfeld, S.; Schmid, B.; et al. Fiji : An Open-Source Platform for Biological-Image Analysis. **2019**, *9* (7); DOI:10.1038/nmeth.2019.
- (129) Palzer, S. Anreichern Und Benetzen von Pulverförmigen Lebensmitteln Mit Flüssigkeiten in Diskontinuierlichen Mischaggregaten, Technische Universität München, 2000.
- (130) van Oorschot, R.; Perez Garza, H. H.; Derks, R. J. S.; Staufer, U.; Ghatkesar, M. K.; Oorschot, R. Van; Hugo, H.; Garza, P.; Derks, R. J. S.; Staufer, U.; et al. A Microfluidic AFM Cantilever Based Dispensing and Aspiration Platform. *EPJ Tech. Instrum.* **2015**, *2* (1), 4; DOI:10.1140/epjti/s40485-014-0012-4.
- (131) Hirt, L.; Ihle, S.; Pan, Z.; Dorwling-Carter, L.; Reiser, A.; Wheeler, J. M.; Spolenak, R.; Vörös, J.; Zambelli, T. Template-Free 3D Microprinting of Metals Using a Force-Controlled Nanopipette for Layer-by-Layer Electrodeposition. *Adv. Mater.* **2016**, *28* (12), 2311–2315; DOI:10.1002/adma.201504967.
- (132) Lin, A. Y. M.; Meyers, M. A.; Vecchio, K. S. Mechanical Properties and Structure of Strombus Gigas, Tridacna Gigas, and Haliotis Rufescens Sea Shells: A Comparative Study. *Mater. Sci. Eng.*

-
- C **2006**, 26 (8), 1380–1389; DOI:10.1016/j.msec.2005.08.016.
- (133) Lakkad, S. C.; Patel, J. M. Mechanical Properties of Bamboo, a Natural Composite. *Fibre Sci. Technol.* **1981**, 14 (4), 319–322; DOI:10.1016/0015-0568(81)90023-3.
- (134) Lo, T. Y.; Cui, H. Z.; Leung, H. C. The Effect of Fiber Density on Strength Capacity of Bamboo. *Mater. Lett.* **2004**, 58 (21), 2595–2598; DOI:10.1016/j.matlet.2004.03.029.
- (135) Borrega, M.; Gibson, L. J. Mechanics of Balsa (*Ochroma Pyramidale*) Wood. *Mech. Mater.* **2015**, 84, 75–90; DOI:10.1016/j.mechmat.2015.01.014.
- (136) Compton, B. G.; Lewis, J. A. 3D-Printing of Lightweight Cellular Composites. *Adv. Mater.* **2014**, 26 (34), 5930–5935; DOI:10.1002/adma.201401804.
- (137) Bauer, J.; Hengsbach, S.; Tesari, I.; Schwaiger, R.; Kraft, O. High-Strength Cellular Ceramic Composites with 3D Microarchitecture. *Proc. Natl. Acad. Sci.* **2014**, 111 (7), 2453–2458; DOI:10.1073/pnas.1315147111.
- (138) Minas, C.; Carnelli, D.; Tervoort, E.; Studart, A. R. 3D Printing of Emulsions and Foams into Hierarchical Porous Ceramics. *Adv. Mater.* **2016**, 28 (45), 9993–9999; DOI:10.1002/adma.201603390.
- (139) Rincón, A.; Giacomello, G.; Pasetto, M.; Bernardo, E. Novel ‘Inorganic Gel Casting’ Process for the Manufacturing of Glass Foams. *J. Eur. Ceram. Soc.* **2017**, 37 (5), 2227–2234; DOI:10.1016/j.jeurceramsoc.2017.01.012.
- (140) Qu, Y. N.; Xu, J.; Su, Z. G.; Ma, N.; Zhang, X. Y.; Xi, X. Q.; Yang, J. L. Lightweight and High-Strength Glass Foams Prepared by a Novel Green Spheres Hollowing Technique. *Ceram. Int.* **2016**, 42 (2), 2370–2377; DOI:10.1016/j.ceramint.2015.10.034.
- (141) Qu, Y. N.; Su, Z. G.; Xu, J.; Huo, W. L.; Song, K. C.; Wang, Y. L.; Yang, J. L. Preparation of Ultralight Glass Foams via Vacuum-Assisted Foaming. *Mater. Lett.* **2016**, 166, 35–38; DOI:10.1016/j.matlet.2015.12.027.
- (142) Gonzenbach, U. T.; Studart, A. R.; Tervoort, E.; Gauckler, L. J. Stabilization of Foams with Inorganic Colloidal Particles. *Langmuir* **2006**, 22 (26), 10983–10988; DOI:10.1021/la061825a.
- (143) Koos, E. Capillary Suspensions: Particle Networks Formed through the Capillary Force. *Curr. Opin. Colloid Interface Sci.* **2014**, 19 (6), 575–584; DOI:10.1016/j.cocis.2014.10.004.
- (144) Papadopoulos, P.; Deng, X.; Mammen, L.; Drotlef, D. M.; Battagliarin, G.; Li, C.; Müllen, K.; Landfester, K.; Del Campo, A.; Butt, H. J.; et al. Wetting on the Microscale: Shape of a Liquid Drop on a Microstructured Surface at Different Length Scales. *Langmuir* **2012**, 28 (22), 8392–8398; DOI:10.1021/la300379u.